FEASIBILITY STUDY OF JET PROPULSION FOR REMOTE OPERATED UNDERWATER VEHICLES

SATHYA NARAYAN GANGADHARAN

FEASIBILITY STUDY OF JET PROPULSION FOR REMOTE OPERATED UNDERWATER VEHICLES

BY

© G. SATHYA NARAYAN, B. Eng. (Hons.)

© A thesis submitted to the School of Graduate Studies in partial fulfillment of the requirements for the degree of Master of Engineering

Faculty of Engineering and Applied Science
Memorial University of Newfoundland

July 1986

St.John's Newfoundland Canada

TO

MY SISTER

ABSTRACT

This thesis is a feasibility study of jet propulsion for remote operated vehicles (ROV's). The concept of using a tilting type nozzle for improved maneuverability is discussed. Though the propulsion efficiency of jets is less compared to that of the propellers for the velocity ranges usually encountered in ROV movements, the implementation of jet propulsion is considered in view of the advantages in improving maneuvering qualities. Also, the simplicity of the system and less complexity in pressure compensation adds to its advantages.This study concentrates on the selection of an optimum nozzle configuration for ROV's.

An experimental set-up was designed and fabricated for this investigation. Ten different plexi-glass conical nozzles were used for five different circular disk shaped drag plates, simulating the drag of the ROV motion under water. Energy losses were determined both experimentally and theoretically. Wall-effects encountered in the experimental tank were compensated by towing the model in an open water wave tank for the same range of speeds. It was found that the propulsion efficiency is maximum for one particular nozzle over a wide range of flow rates encountered in the experiments. Finally, a feasible design of a jet propelled ROV with tilting type nozzles is presented. This design could be fabricated and tested for commercial production.

ACKNOWLEDGEMENTS

This thesis was completed at the Faculty of Engineering, Memorial University of Newfoundland and partially funded by the National Research Council of Canada. The receipt of Memorial University fellowship and graduate supplement by the author during the period of study is gratefully acknowledged.

The author is greatly indebted to Dr. H.L. Krein, Associate professor of Ocean Engineering for his excellent guidance, understanding, cooperation, continuous support and careful review of the manuscript. Thanks are due to Dr. D.A. Aldrich, Dean of Graduate Studies, Dr. G.R. Peters, Dean of Engineering, and Dr. T.R. Chari, Associate Dean of Engineering, for the facilities provided and to the various professors for their valuable advice and suggestions.

Thanks are also due to the Technical staff at the fluids lab, instrumentation lab, workshop and draftsmen, who made their services readily available at every stage of this project. Finally special thanks are due to many of my fellow students for their valuable suggestions and advice during the course of this thesis.

TABLE OF CONTENTS

LIST OF FIGURES

LIST OF TABLES

LIST OF SYMBOLS

A_j	Area of jet
$C1$	Figure of Merit
d	Characteristic length (diameter) under consideration
f	Friction factor
g	Acceleration due to gravity
H_p	Total head at the inlet to the nozzle
H_P	Head developed by the pump
H_l	Head loss in the system
H_L	Energy loss in the nozzle
H_R	Total head recovered by inlet
H_S	Static head rise from inlet to discharge
K	Loss coefficient
K_T	Thrust coefficient
L	Length of the nozzle
$N1$	Nozzle 1 (exit dia. 16 mm)
$N2$	Nozzle 2 (exit dia. 22 mm)
$N3$	Nozzle 3 (exit dia. 30 mm)
$N4$	Nozzle 4 (exit dia. 36 mm)
$N5$	Nozzle 5 (exit dia. 44 mm)
$N6$	Nozzle 6 (exit dia. 48 mm)
$N7$	Nozzle 7 (exit dia. 52.8 mm)

$N8$	Nozzle 8 (exit dia. 57 mm)
$N9$	Nozzle 9 (exit dia. 61 mm)
$N10$	Nozzle 10 (exit dia. 64 mm)
N_E	Experimental results for the nozzle under consideration
N_T	Theoretical results for the nozzle under consideration
P	Power input
Q	Flow rate through the nozzle
R_e	Reynolds number $\left(\frac{V_a\ d}{\nu}\right)$
T	Thrust of the nozzle
V_a	Velocity under consideration
V_j	Velocity of the jet
V_v	Linear velocity of the vehicle
η_0	Overall efficiency of the system
η_p	Propulsion efficiency of the nozzle
η_{pump}	Efficiency of the pump
$\overline{\eta}$	Overall efficiency neglecting the pump efficiency
ρ	Mass density of water
ω	Angular velocity of the vehicle
μ	Absolute viscosity of water
ν	Kinematic viscosity of water

CHAPTER 1

INTRODUCTION

1.1 GENERAL:

The high cost of employing commercial divers for underwater exploration and inspection of pipelines, platforms, and other marine installations, has led to the development of remotely operated underwater vehicles (ROV's). Although these vehicles are small and slow-moving, they reach depths far beyond diver's capabilities [14]. Generally, divers reach to depths like 1500 feet whereas, the ROV's go down anywhere between 6000 to 20,000 feet depending on the degree of sophistication of the vehicle [15], to perform complex operations as underwater mining.

A number of systems are available for underwater exploration. The major systems include:

- Wet diving such as scuba, bounce and saturation diving.
- One atmosphere manned vehicles, with manipulators and cameras, either tethered or autonomous.
- Remotely operated vehicles (ROV's), with manipulators and/or cameras, either tethered or untethered.

Of the above mentioned systems, remotely operated vehicles (ROV's) have emerged in the last five years as a dominant tool for observation and exploration

of sub-ocean resources [19],[21]. The following propulsion systems are presently in use:

Propellers [4] driven by

a) one atmosphere electric motor.

b) pressure compensated, fluid filled electric motors.

c) pressure compensated hydraulic pumps and motors.

Water jets fascinated man for a long time as a means of propulsion of sea crafts. However, it is only during the last two decades that it has received serious consideration in its potentials and limitations as a means of propulsion. Water jets were studied by various authors for the propulsion of surface marine crafts in such areas as the performance analysis [20], hydrodynamic design principles [29], application to high speed vessels [1],[2], component study [23] and, experimental and theoretical investigation [5],[7],[10],[11]. The state-of-the-art [3],[26] and its practical considerations [7],[8],[9] were also dealt with in other studies.

There are circumstances under which water jets are decidedly preferred over propellers. These include: operation in shallow water, high speed crafts, low noise levels, easy maneuverability and, weed and ice infested areas. Current reasons for water jet propulsion not being adopted more frequently are: low overall efficiency, high cost of the unit, weight, and space penalties. By proper matching of the water jet propulsion unit to a given application, higher efficiencies are feasible.

1.2 SCOPE OF THIS INVESTIGATION:

Though jets were used for propulsion of marine vehicles, its application to ROV propulsion was not tried before. This study is an outcome of the previous lack of experimental results on and immediate interest in the feasibility of using a jet propulsion system for small, slow-moving ROV's which use ambient fluid for its movements.

The experimental study in this investigation is aimed at studying the effect of different nozzle profiles on the propulsion performance and arriving at the optimum nozzle. The experimental set-up is designed and fabricated, taking into account the purpose of this investigation. Ten different nozzles of various conical profiles are used and for each nozzle, the thrust, the vehicle velocity and head at inlet and exit are measured for different flow rates through the nozzle. Also, for each nozzle, these parameters are measured for different drag plates simulating the drag of the moving vehicle under water.

The wall effects of the experimental tank are compensated by towing the model in the wave tank. Also, a design of a jet propelled ROV with tilting type nozzles is presented in this study.

1.3 ORGANIZATION OF THE THESIS:

In Chapter 2 of this thesis, a review of the jet propulsion system is presented. An expression is derived for optimum efficiency of propulsion, neglect-

ing the inlet head recovery.

Chapter 3 explains the various parameters and an insight into the terms involved in evaluating the performance.

Chapter 4 describes the experimental organization of the thesis. Details of experimental set-up, test procedures and instrumentation are presented in this chapter.

In Chapter 5, the results of the experiments, the discussion and a comparison with the theoretical solutions are presented.

In Chapter 6, a feasible design of an ROV with tilting type nozzles is put-forth.

Finally, the summary and conclusions of this investigation are presented in Chapter 7.

CHAPTER 2

STATE-OF-THE-ART AND LITERATURE REVIEW

2.1 GENERAL:

Only during the last two decades jet propulsion was given considerable importance and its application was primarily towards surface vessels. With the advent of ROV's (Fig.1), jet system was thought of as a means of propulsion and maneuverability. A brief description of the basic elements involved in the jet system is presented. Merits and demerits of jet system are discussed. An expression is derived for propulsion efficiency neglecting the inlet head recovery.

2.2 STATE-OF-THE-ART:

Most water-jet propulsion systems as emphasized in literature [3],[26], have three basic elements (fig.2). These are,

(i) an intake duct which inducts fluid from outside the craft,

(ii) a pump for transmitting energy to this fluid,

(iii) an exhaust duct and nozzle which guide the jet of fluid outside.

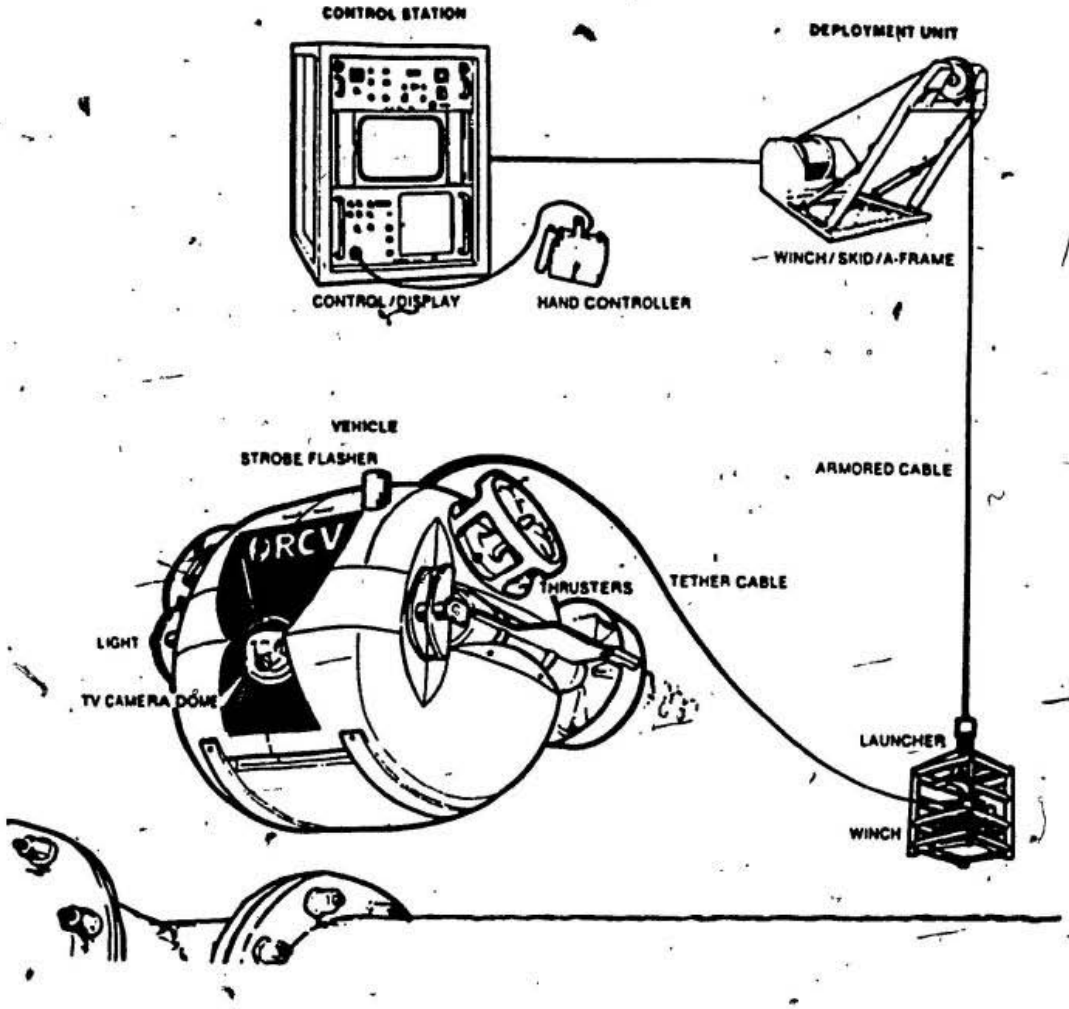

Fig. 1 Schematic of a ROV system [30]

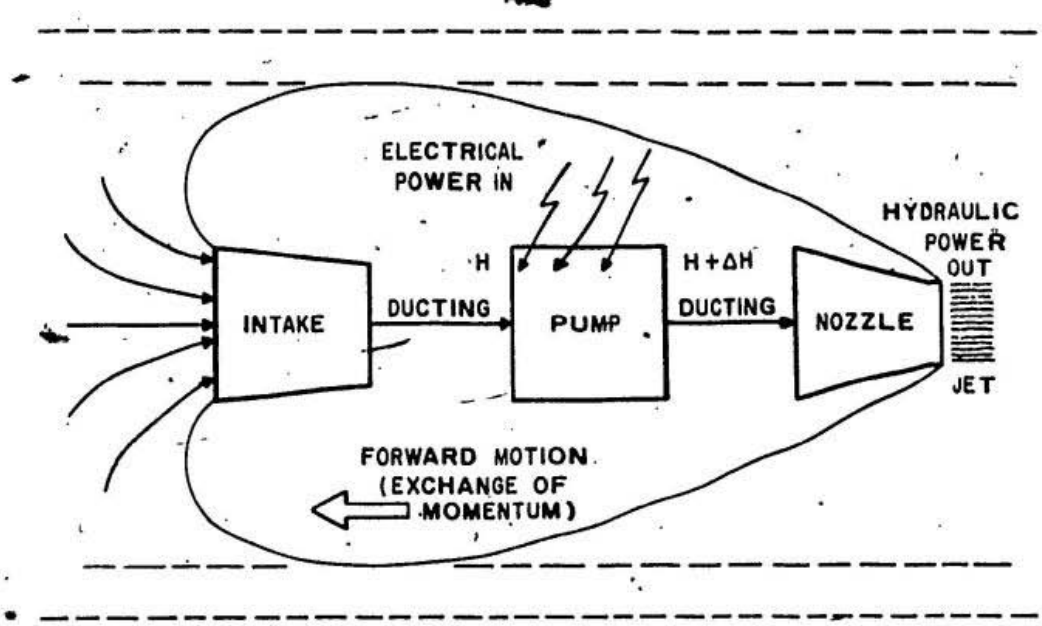

Fig. 2 Schematic of Water-Jet Propulsion System for ROV's

Evaluation of performance characteristics are to be carried out depending on the particular application [12].

2.2.1 INLET:

The inlet or scoop location depends on the hull and water-jet propulsion system configuration [5]. The major design location considerations are in keeping the vertical distances (which produce elevation losses) short, keeping the inlet immersed in water to prevent aeration, providing sufficient water flow to the pumps to produce the required thrust, and preventing or delaying the inception of cavitation. Good inlet system design requires low internal losses and high resistance to cavitation during the take-off mode and low external drag during cruise [22]. The scoop must capture the free stream flow efficiently under a range of operating conditions between take-off and cruise.

The net effect of cavitation, in and around the inlet, is two fold:

(i) cavitation can produce significant erosion of the inlet material,

(ii) cavitation can degrade the pump performance due to excessive inlet/diffuser head loss and, ultimately, complete choking of the flow which starves the pump.

Definitive evaluation of inlet performance [16] involves the determination of how efficiently the water can be 'captured', over what range of velocities inlet cavitation will not significantly degrade this capturing, and how much the hull drag is affected by the presence of the inlet. It is possible that some inlet designs could be low in internal loss but have high external drag effects. An inlet with

poor flow will experience a large energy or head loss. A wire mesh to screen off the debris is desirable in some applications.

2.2.2 DUCTING:

In a water-jet propulsion system, a certain amount of ducting must be installed [22] to move the water from the hull inlet to the pump and from the pump to the exhaust nozzle. The function of the duct is to deliver the correct quantity of water to the entrance of the impeller efficiently (with minimum pressure loss) and with reasonably uniform velocity distribution, and to exhaust the water efficiently. The efficiency of the ducting system depends on the length of the pipe, number and type of transitions, and pipe roughness.

In general, a duct system should be light-weight (including the weight of water), have low vibration levels and low hydrodynamic loss. The lightness and vibration levels depend on the material property. The hydrodynamic losses include friction losses at internal ducting walls, mixing losses (pressure loss and friction loss) in areas of transitions such as enlargements, contractions, etc., and velocity profiles at sections approaching the impellers and stator vanes.

2.2.3 WATER-JET PUMP:

The function of the pump in a water-jet system is to accelerate the surrounding fluid medium or increase the energy of flow, thereby producing thrust. A pump with high mass flow rate and low head performance is a major

requirement for efficient operation. However, a high-speed pump will keep the duct size and weight of the waterjet system small.

The types of pumps utilised by various propulsion system designers include:

(i) centrifugal (radial flow) - high head and low specific speed,

(ii) mixed flow (inclined flow) - medium head and medium specific speed,

(iii) axial flow (propeller) - low head and high specific speed.

In ROV applications, a single stage axial/mixed flow pump of suitable capacity is used to minimize the size and weight of the vehicle and increase the payload capacity.

2.2.4 NOZZLE:

Nozzles play a vital role in jet propulsion as a thrust unit by converting potential energy into kinetic energy. A good design of a nozzle depending on its application [24], will increase the propulsion efficiency of the jet considerably. The first aspect is to determine the optimum area ratio for the desired speed and then streamlining the nozzle to have a minimum loss. In certain cases, a variable area nozzle is found to be useful for a large range of speeds from take-off to cruise. Hence testing of a nozzle for a particular application is considered essential.

2.3 ADVANTAGES AND DISADVANTAGES OF JET SYSTEM:

2.3.1 ADVANTAGES:

(1) For ROV applications with a jet system, less pressure compensation is required. Only the electric pump-motor needs to be pressure compensated.

(2) The jet system is much simpler than the propeller system.

(3) Direct steering and maneuvering control from the propulsor is possible.

(4) For weed and ice infested areas and for places of debris, a jet system is the only alternative.

(5) With a waterjet, it is possible to eliminate external underwater appendages.

(6) A wider choice of location of the propulsion machinery than is normally found.

(7) Elimination of complex transmission machinery where right-angle drives are required, such as in hydrofoil craft strut propeller applications.

(8) Possible alleviation of underwater radiated propeller cavitation noise through more control over cavitation, and removal of the propeller from the main body of water.

(9) Detrimental effects of propeller vibration may possibly be alleviated due to control of the impeller inflow characteristics over that of an open propeller.

(10) For towing (removal of debris from underwater), the waterjets can produce greater tow-rope pulls than an open propeller; however, a Kort nozzle, in this regard, will be more efficient.

2.3.2 DISADVANTAGES:

(1) In general, a waterjet system will not be as efficient as a propeller system, i.e., more horsepower will be required to perform a particular function with a waterjet system.

(2) The possibility of cavitation at the inlet system can adversely affect performance. This means that there are several sources of cavitation to be considered.

(3) Impeller access compared with conventional propeller designs is poor, making inspection, repair, or removal of debris difficult.

2.4 PRINCIPLES OF DESIGN

2.4.1 THRUST:

From momentum principles, the thrust of a waterjet is given by

$$T = \rho\, Q\, (V_j - V_v) = \rho\, A_j\, V_j^2 \left[1 - \left(\frac{V_v}{V_j}\right)\right] \qquad (1)$$

where,

Q = flowrate $= A_j\, V_j$

T = thrust produced

ρ = density of the fluid

A_j = area of the jet

V_j = velocity of the jet

V_v = velocity of the vehicle

2.4.2 ENERGY BALANCE:

The energy balance is obtained by writing Bernoulli's equation for a streamline passing through the pump

$$H_R + H_P - H_l - H_S = \frac{V_j^2}{2g} \qquad (2)$$

where,

H_P = head developed by the pump

H_l = energy losses in the system $= K \frac{V_j^2}{2g}$

H_R = dynamic head recovered at inlet = 0 (negligible for slow speed)

$H_S = 0$ (since inlet and discharge are at the same level)

K = loss coefficient

g = acceleration due to gravity

Thus (2) reduces to

$$H_P - K \frac{V_j^2}{2g} = \frac{V_j^2}{2g} \qquad (2a)$$

Hence

$$H_P = (1 + K) \frac{V_j^2}{2g} \qquad (2b)$$

2.4.3 OVERALL EFFICIENCY:

The overall efficiency of the water jet system is defined as

$$\eta_0 = \frac{T V_e}{\rho g Q H_P} \eta_{pump} \qquad (3)$$

where,

η_0 = overall efficiency of the system

η_{pump} = efficiency of the pump

Substituting for 'T' and 'H' from equation (1) and (2b) respectively, we get

$$\overline{\eta} = \frac{\eta_0}{\eta_{pump}} = \frac{2\left(1 - \frac{V_s}{V_j}\right) V_s}{(1 + K)\, V_j} \tag{4}$$

where,

$\overline{\eta}$ = overall efficiency of the system neglecting the pump efficiency

Differentiating equation (4) with respect to $(\frac{V_s}{V_j})$ and equating it to zero, gives

$$\frac{V_s}{V_j} = \frac{1}{2} \tag{5}$$

Substituting this value of V_s / V_j into equation (4), the optimum efficiency becomes

$$\eta_{optimum} = \frac{1}{2(1 + K)} \tag{6}$$

(neglecting the effect of inlet head recovery). This shows that the optimum efficiency can be only about 50% if head recovery at inlet is neglected. Also, the lower the loss coefficient K, the higher the efficiency of propulsion will be.

2.5 OBJECTIVES OF PRESENT INVESTIGATION:

(i) To find the optimum nozzle configuration for slow moving ROV applications.

(ii) To provide experimental results on jet propulsion of small, slow- moving ROV's, the velocities not exceeding 4 knots (Fig.3).

(iii) To arrive at the energy loss in the nozzle by experimental and analytical means.

(iv) To provide a feasible design of a jet propelled ROV with tilting type nozzles which could be used for commercial production.

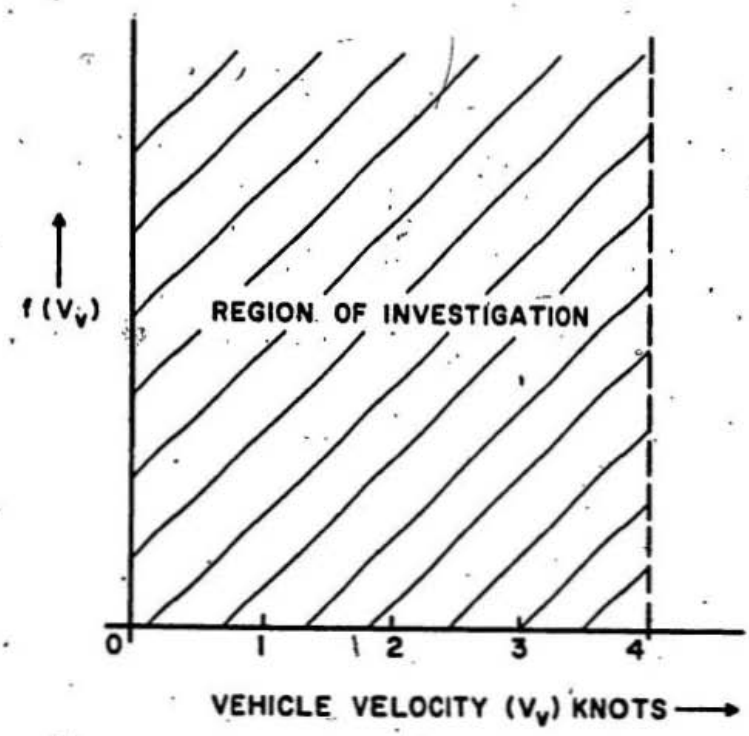

Fig. 3 Schematic Showing the Region of Experimental Investigation

CHAPTER 3

REVIEW OF PERFORMANCE PARAMETERS

3.1 GENERAL:

The objective of this chapter is to show an insight into the various performance parameters related to this investigation. Also the terms involved are explained and defined. A supporting documentation for the energy losses in the nozzle is provided.

3.2 DEFINITIONS OF PERFORMANCE PARAMETERS:

3.2.1 OVERALL EFFICIENCY:

The overall efficiency of the waterjet system is defined as

$$\eta_0 = \frac{T\ V_v}{\rho g Q H_P}\ \eta_{pump} \qquad (7)$$

where,

η_0 = Overall efficiency of the jet system

T = Thrust produced

V_v = Vehicle velocity

ρ = Mass density of the fluid (water) $= 1000 Kg/m^3$

g = Acceleration due to gravity $= 9.81 m/s^2$

Q = Flow rate

H_P = Head developed by the pump

η_{pump} = efficiency of the pump $= 85\%(assumed)$

However in the experiment, since the head developed was measured at the entry to the nozzle, a term called propulsion efficiency of the nozzle η_p is introduced. Hence,

$$\eta_p = \frac{T\ V_j}{\rho g Q H_p}\ \eta_{pump} \qquad (8)$$

where,

H_p = Head developed at the entry to the nozzle.

A term $\bar{\eta}$, which defines the overall efficiency neglecting the pump efficiency, is taken for ideal case considering that the pump has 100% efficiency. This term is not used for as performance parameter in this work.

3.2.2 THRUST COEFFICIENT;

The performance characteristics of water jets should be presented in dimensionless quantities. Thrust coefficient is one such parameter which is the ratio of the actual thrust measured to the thrust which would be produced for the flow through the nozzle. It is defined as

$$K_T = \frac{T}{\rho\ A_j\ V_j^2} \qquad (9)$$

where,

K_T = Thrust coefficient

ρ = Mass density of the fluid

A_j = Exit area of the nozzle

V_j = Velocity of the jet

3.2.3 FIGURE OF MERIT:

Figure of merit is another non-dimensional performance parameter, obtained by combining the thrust/horsepower and the jet velocity as represented by $\sqrt{\frac{T}{\rho A}}$. This is independent of V_j and the pump rpm and for a given configuration, is essentially independent of the absolute value of the thrust produced. If geometrical changes are made in the model, such as the variations in the jet area, the static performance is compared on the basis of the figure of merit. The optimum configuration will produce the maximum value of figure of merit regardless of the magnitude of the thrust produced. The figure of merit is defined by the equation

$$C_1 = \left(\frac{T}{P}\right)\left[\sqrt{\frac{T}{\rho A_j}}\right] \qquad (10)$$

where,

C_1 = Figure of merit

P = Power input

which reduces to

$$C_1 = \left[\frac{T^{3/2}}{(\rho A_j)^{1/2} P} \right] \tag{10a}$$

3.2.4 VELOCITY RATIO:

Velocity ratio is another non-dimensional parameter which is used for comparison of performance between the nozzles. It is normally used for the plotting of performance curves. The value of the velocity ratio merely shows a relationship between the velocity of the vehicle to the velocity of the jet and since it is a ratio, the performance of the nozzles could be compared by the use of this parameter. The velocity of the vehicle is measured experimentally and the velocity of the jet is obtained by knowing the flow rate and the exit area of the nozzle from the relationship $V_j = \frac{Q}{A_j}$.

3.2.5 REYNOLDS NUMBER:

Reynolds number is a non-dimensional number which is a ratio of the inertia forces to the viscous forces. It is defined by

$$R_e = \frac{V_j \; d_e \; \rho}{\mu} \tag{11}$$

where,

R_e = Reynolds number at exit of nozzle

d_e = Exit diameter of the nozzle

ρ = Mass density of water = 1000 Kg/m^3

μ = Absolute viscosity of water at 15 Celsius = 1.139×10^{-3} $Kg/m\text{-}s$

Taking $\nu = \mu/\rho$, the reynolds number becomes

$$R_e = \frac{V_j \, d_e}{\nu} \qquad (11a)$$

where,

ν = Kinematic viscosity of water at 15 Celsius = 1.139×10^{-6} m^2/s

3.3 PARAMETERS INVOLVED IN ENERGY LOSSES:

3.3.1 HEAD LOSS IN THE NOZZLE:

The head loss in the nozzle are due to various factors like friction. The head loss necessarily occurs when there is a flow through the nozzle, which converts the potential energy into the kinetic energy. The head loss due to friction is given by the 'Darcy-Weisbach' equation

$$H_L = f \, \frac{L \, V_e^2}{2 \, g \, d} \qquad (12)$$

where,

H_L = Head loss in the nozzle

f = Friction factor depends on surface roughness and reynolds number

L = Length of the nozzle

V_e = Velocity under consideration

d = diameter of the nozzle under consideration

3.3.2 LOSS COEFFICIENT:

The loss coefficient is a non-dimensional parameter and is a ratio of the energy loss to the velocity head at the exit of the nozzle. It is defined by

$$K = \frac{H_L}{V_j^2/2\,g} \tag{13}$$

where,

K = Loss coefficient

H_L = Energy loss in the nozzle

$V_j^2/2\,g$ = Velocity head at the exit of the nozzle

3.4 DETERMINATION OF THEORETICAL LOSSES:

The theoretical losses in the nozzle are determined by using 'Darcy-Weisbach' equation (12) by integration of cylindrical strips across the length of the nozzle. The nozzle is divided into strips and each strip is approximated to a cylinder by taking the average diameter over the small length. The velocity is obtained by knowing the flow rate and the average diameter of the strip under consideration. Assuming the surface roughness (ϵ=0.001) for the machining

operation undertaken with polishing, and from the average diameter of the strip, the relative roughness ϵ/d is calculated. Also the reynolds number is calculated for each strip and from the moody's chart, the friction factor for a strip is found and then the 'Darcy-Weisbach' formula is applied for each strip to get the energy loss for the strip. Finally, summation of these energy losses in these strips gives the overall energy loss in the nozzle under consideration.

A computer program (program 1 in appendix A) is written to find out the energy losses in the nozzle by integration of the losses in the strips and program 2 (in appendix A) gives the calculation of the loss coefficients from the theoretical loss in the nozzle.

3.5 DETERMINATION OF EXPERIMENTAL LOSSES:

The experimental losses are determined by finding the total head at the inlet and at the exit of the nozzle and then taking the difference between the total head at the inlet and the total head at the exit, Piezo- electric pressure transducers connected to the pitot tube assembly are used to find the total head accurately until repeatability is obtained. Program 4 (in appendix A) gives the calculation for the energy losses from the measured data obtained from the piezo-electric pressure transducers.

CHAPTER 4

EXPERIMENTAL ORGANISATION AND TEST PROCEDURE

4.1 GENERAL:

The experimental program was designed with the objective of investigating the use of water-jet propulsion for ROV applications. The influence of the various parameters relating to the performance is recognised and reported in literature [3],[8],[21]. The experimental set-up was designed (Fig.10) and successfully used to determine the performance parameters.

4.2 EXPERIMENTAL SET-UP:

4.2.1 TEST SET-UP:

The test set-up consists of a rectangular tank of dimensions 183cm x 183cm x 190cm (Figs.4 and 5). A high flow rate centrifugal pump and two rotameters in parallel (calibrated for the experiment) are used to measure the flow with two gate valves, one below each rotameter, to vary the flow rate. A rotating water-tight joint located at the bottom of the fixed vertical pipe (Fig.6), and a nozzle at the back end of the lever arm are used. The pump draws water from the tank and discharges it, into the same tank through the submerged nozzle, thereby

rotating the whole leyer arm assembly about the rotating joint. In the front end of the lever arm, there is a provision to put different drag plates to simulate the drag of the vehicle under water. There is a provision for replacing the nozzle by means of a screw assembly (Fig.7). There are two cylindrical buoyant floats beneath the nozzle to compensate for the weight of the lever arm to avoid uneven weight transmitted to the rotating joint.

4.2.2 THRUST PLATE ASSEMBLY:

The thrust plates are held from the top of the experimental tank by means of a fixture and clamps. The fixture houses two beams running across the length of the tank. In one of the beams, two holes are drilled alligning the holes in the thrust plates to fix the thrust plates by means of bolts without any play. Clamps are used as an auxiliary means of support.

4.2.3 THRUST MEASUREMENT SET-UP:

The thrust plate assembly resembles a cantilever beam and the thrust being applied to the end of the cantilever beam. The deflection experienced by the thrust plates are sensed by strain gages mounted on the surface of these plates. These gages are given a water proof coating and connected by a full-bridge circuit (Fig.11)so that there is minimum error due to temperature difference between these gages and sensitivity is increased. The strain gages are connected to an amplifier and in turn to a multimeter and an oscilloscope. The previous

calibration of the strain gages in terms of load and strain directly gives the unknown thrust, knowing the strain developed.

4.2.4 TOTAL HEAD MEASUREMENT SET-UP:

A pitot-tube assembly (Fig.12) is used for the measurement of total head at the inlet and exit of the nozzle. A fixture slides over the nozzle and grips it when stationary. A rod which holds the pitot-tube assembly can be moved along parallel to the axis of the nozzle. This facility makes the measurement of the total head at the inlet and exit of the nozzle along the centre-line possible. The pitot-tube assembly is connected to a piezo-electric pressure transducer, which in turn, is connected to an amplifier, a multimeter and an oscilloscope. Previous calibration of the pressure transducer in terms of the pressure and voltage directly gives the unknown total head, knowing the voltage produced.

4.2.5 MATERIALS:

The rotating joint and the lever arm assembly are made of aluminium. The pipe connections upto the fixed vertical pipe holding the rotating joint are made of 2" PVC pipes. The fixed vertical 2" pipe is made of steel. The drag plates and buoyant floats are made of wood (Fig.8) and PVC, respectively. The nozzles are made of transparent plexi-glass because of its advantages to observe flow on cavitation, in easy machinability, and minimum surface roughness.

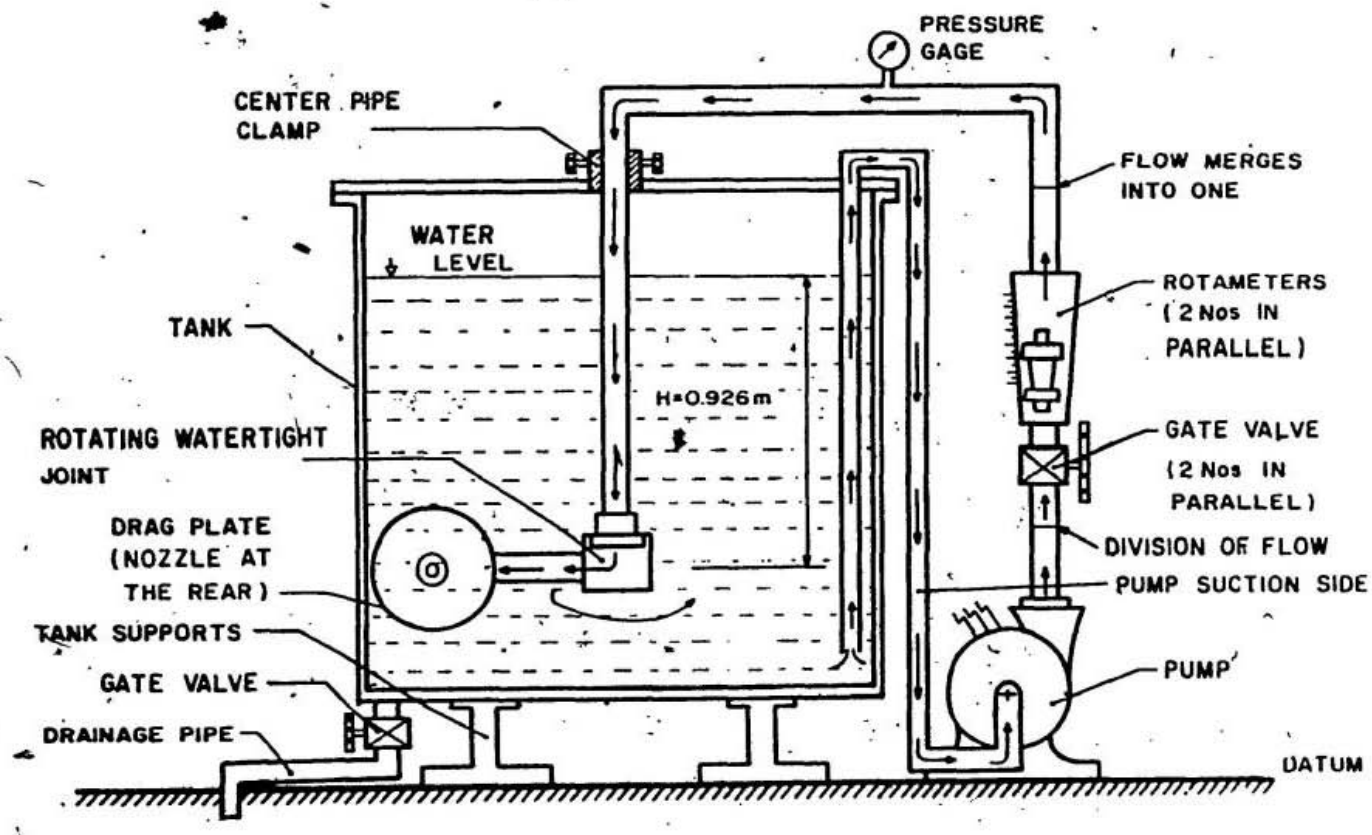

Fig. 4 Elevation-View of the Experimental Set-Up

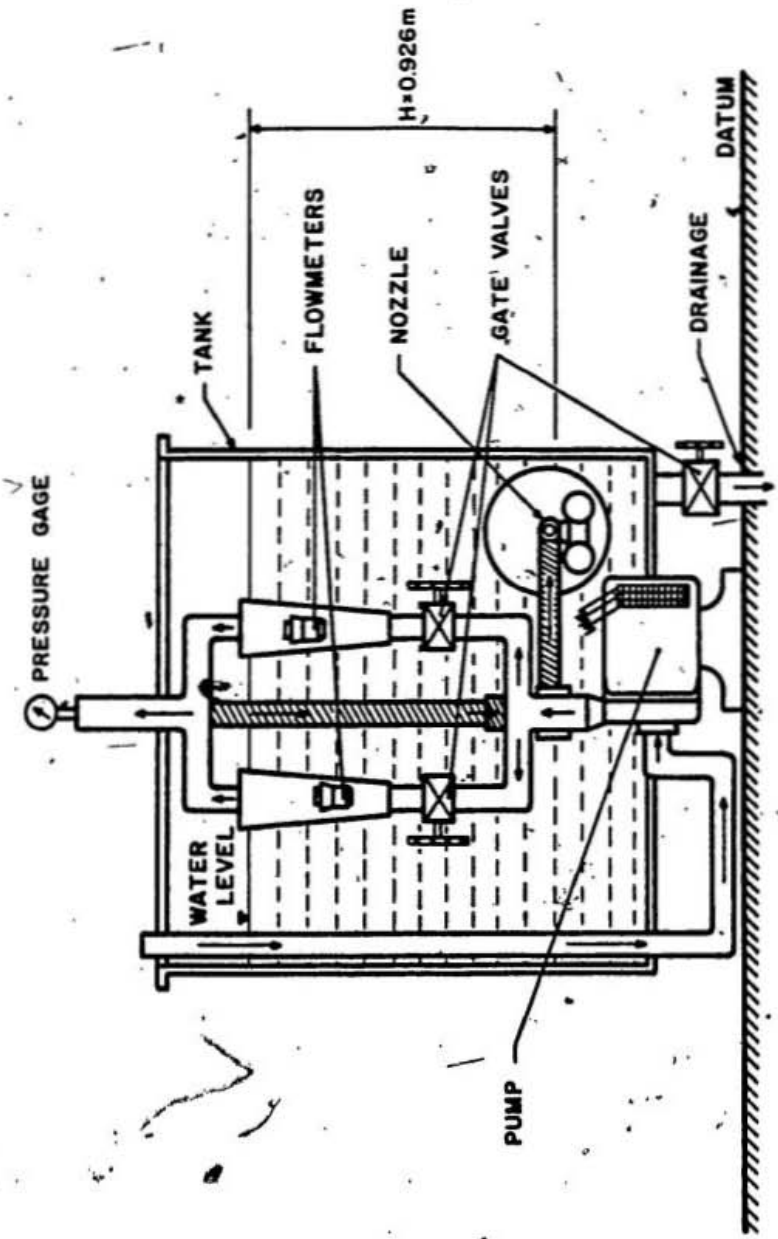

Fig. 5 End-View of the Experimental Set-Up

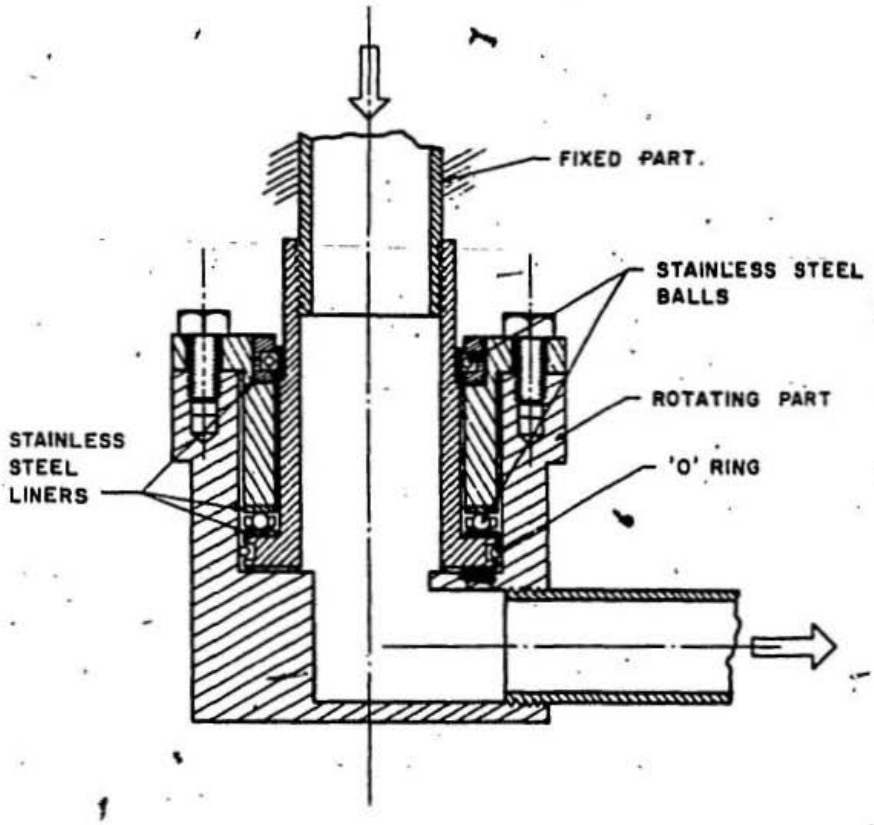

Fig. 6 Water-Tight Rotating Joint

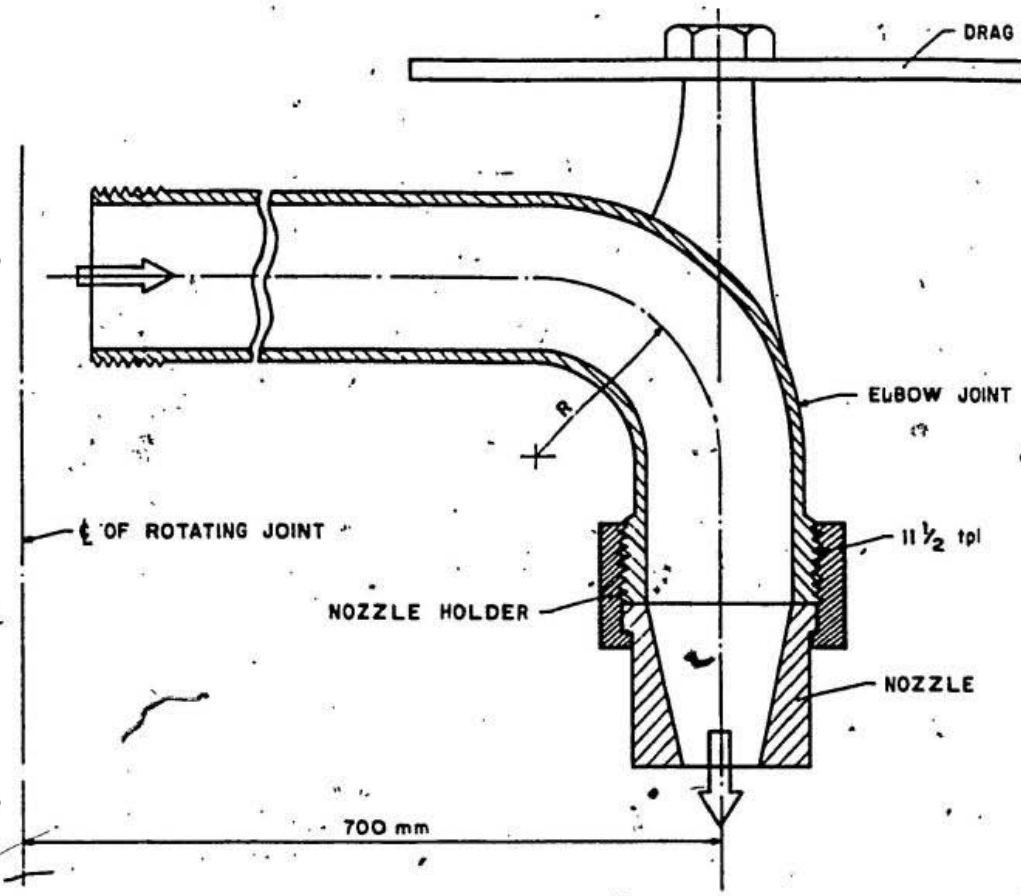

Fig. 7 Sectional Plan of Lever Arm Assembly

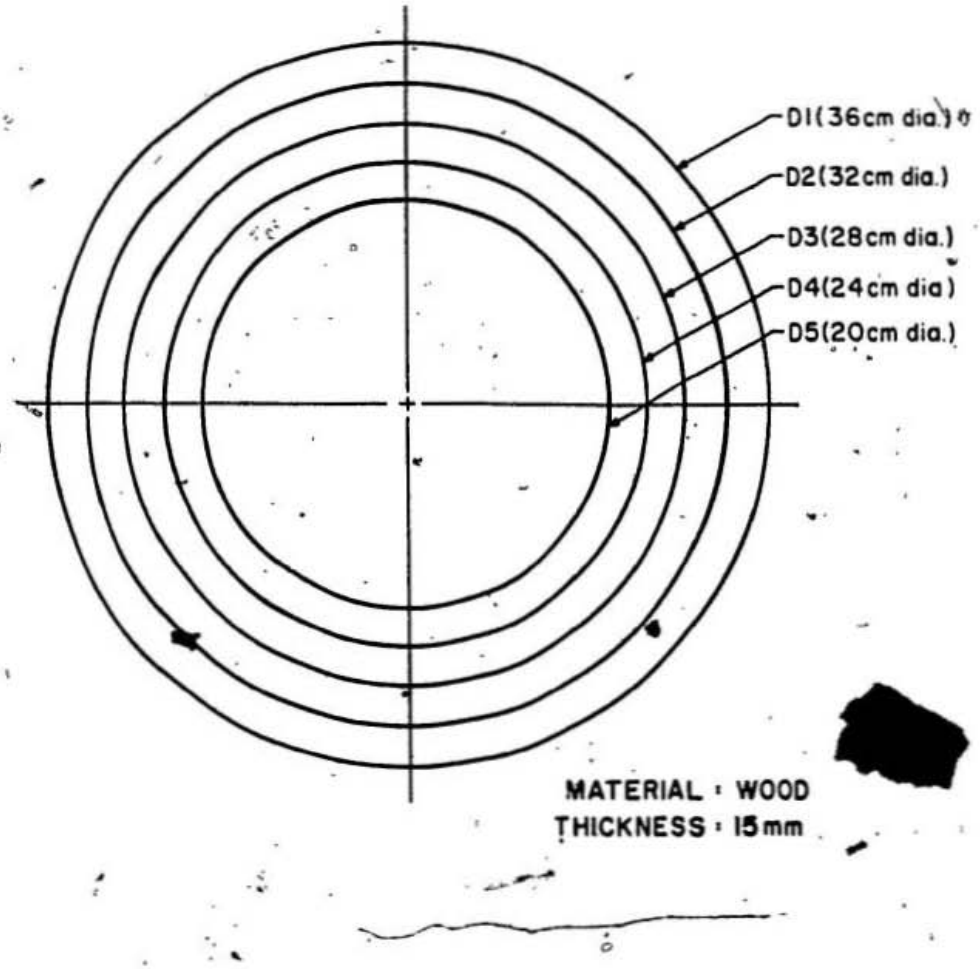

Fig. 8 Drag Plates Used in the Investigation

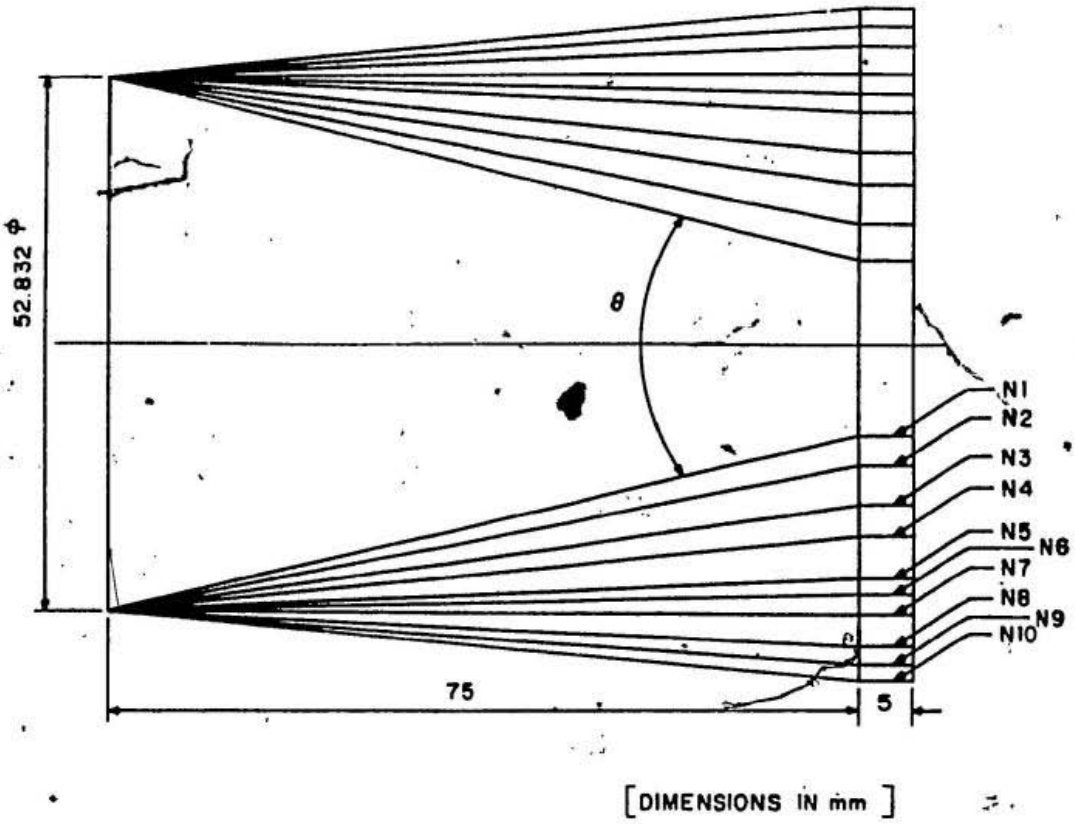

Fig. 9 Nozzle Profiles Used in the Investigation

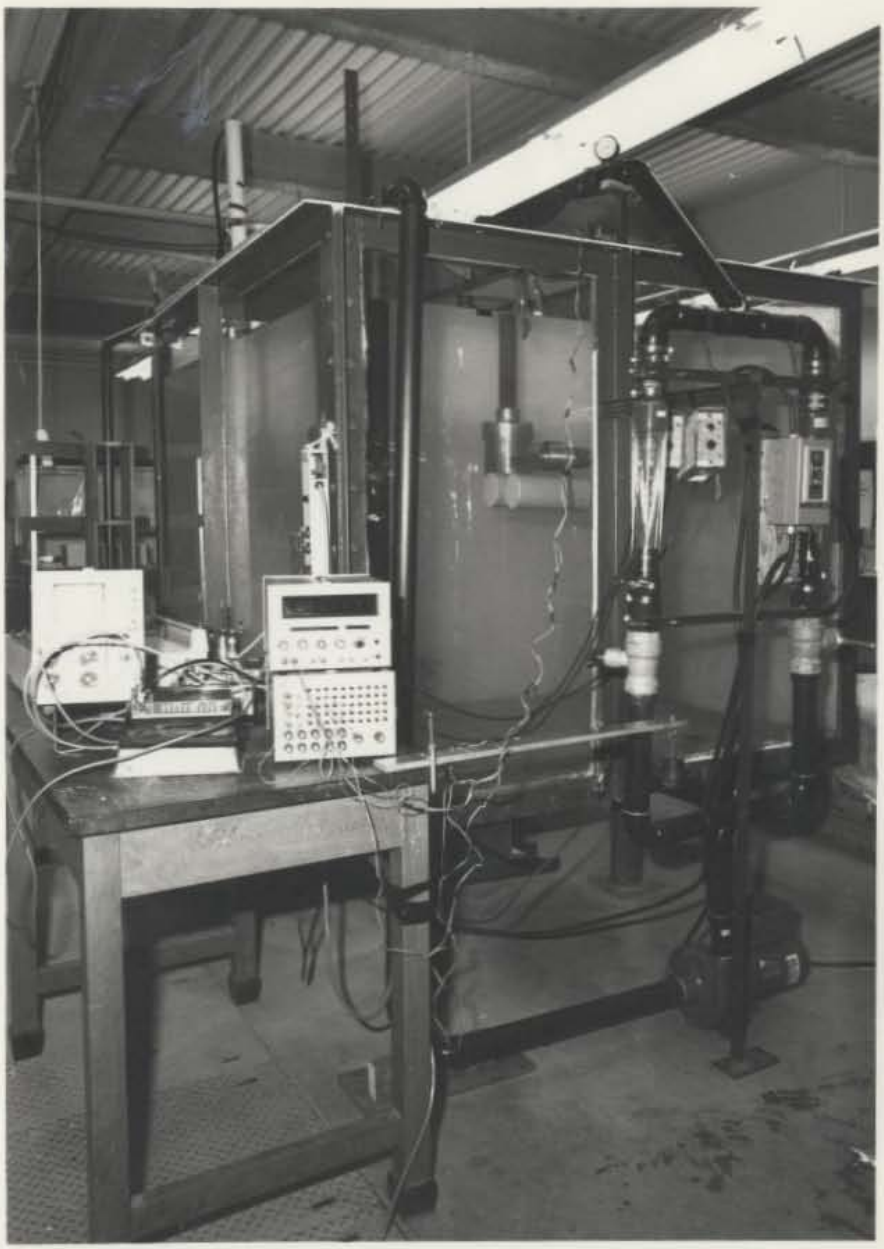

Fig. 10 Photograph of the Set-Up With Instrumentation

4.2.6 NOZZLES:

Nozzles are fabricated from 75 mm diameter transparent plexi-glass rod. Ten different conical nozzle configurations including converging, straight, and diverging sections (Fig.9) were made and tested. In all cases, the inlet diameter of the nozzle and length of the nozzle were fixed at 52.8 mm and 80 mm, respectively. The first 75 mm is conical and the remaining 5 mm is a straight cylindrical section. This is done to avoid the possible scattering of the jet and maximise the thrust.

4.3 INSTRUMENTATION:

4.3.1 THRUST:

Temperature compensated strain gages are primarily used for the measurement of thrust. Two different thrust plates 85cm x 5cm x 0.6cm and 85cm x 5cm x 1.2cm, each housing four strain gages are used (Fig.11). The former plate is used for thrusts less than 40 newtons, while the latter for thrusts greater than 40 newtons. The full-bridge circuit with the strain indicator is employed for the thrust measurement. The strain gages are given a water proof coating. Previous calibration of these gages in terms of load and strain directly give the unknown thrust, knowing the induced strain. The friction at the rotating joint is added to this observed thrust to give the overall net thrust of the nozzle.

4.3.2 FLOW RATE:

The flow rates are measured using the rotameters in parallel. These are calibrated in terms of volume flow (cubic meters per second). The flow rates are varied by gate valves; one positioned below each rotameter so as to have independent operation.

4.3.3 LINEAR VELOCITY:

The angular velocity is first found by noting the time taken for a definite number of rotations by using a stop watch correct to one-hundredth of a second. Knowing the radius (length) of the lever arm, the linear velocity is calculated using the relation:

$$\text{Linear velocity} = \text{Angular Velocity} \times \text{radius of lever arm}$$

4.3.4 TOTAL HEAD:

The Total head at the inlet of the nozzle is measured using a pitot tube assembly and piezo-electric pressure transducer (Fig.12). The electrical signal (output) of the transducer is amplified by an amplifier and then observed in a multimeter and oscilloscope (as volts). The previous calibration of the pressure transducer in terms of pressure and voltage directly give the unknown pressure (or the total head), knowing the voltage produced by the transducer.

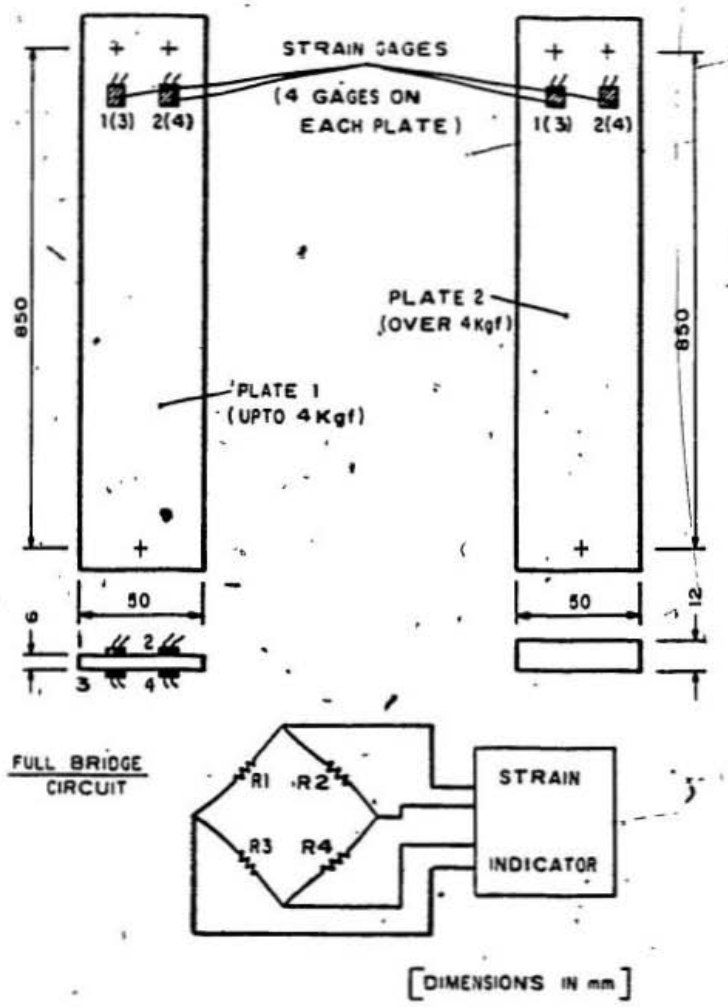

Fig. 11 Thrust Plates and Full-Bridge Circuit

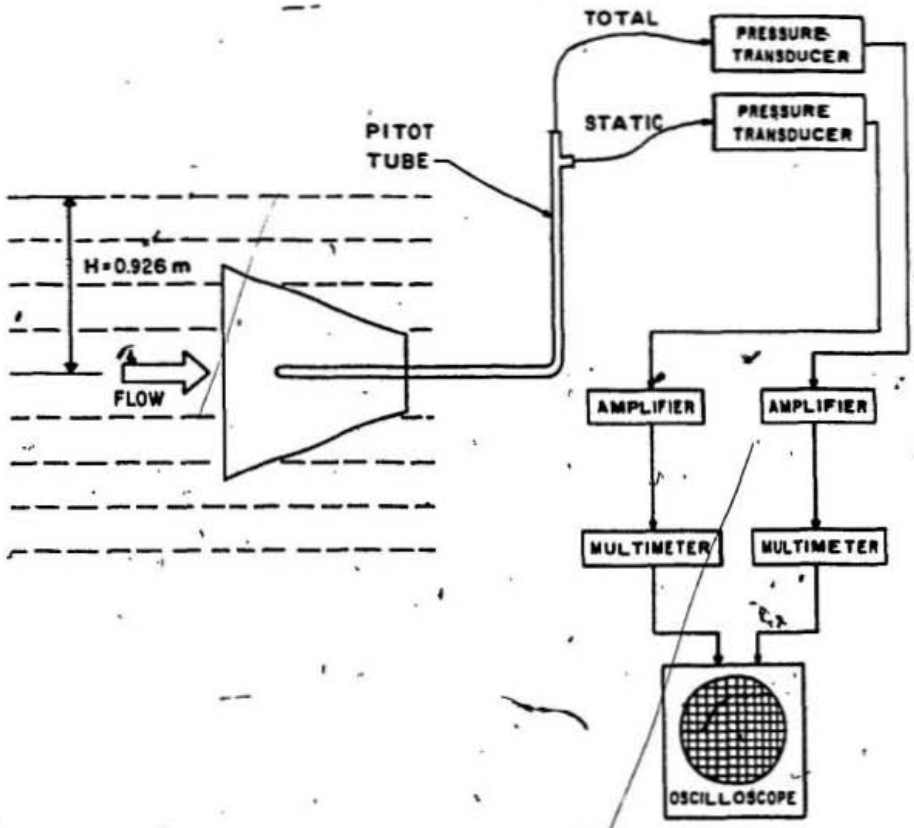

Fig. 12 Measurement of Pressure

4.4 TEST PROCEDURE:

The tank is filled with water to a particular level which is maintained throughout the experimental study. However, the nozzle and the drag plate were fixed before filling up the tank. The thrust plate is placed against the front face of the drag plate for thrust measurements for different flow rates. With the same arrangement, the total head is measured at inlet and exit of the nozzle using a pitot tube. For velocity measurements, the thrust plate is removed and the assembly is allowed to rotate simulating the motion of the vehicle under water. The wall effects are then compensated.

4.4.1 DATA RECORDING:

All the instruments are turned on 30 minutes before each test to allow a warm-up period. The caps of the piezo-electric pressure transducers are removed, cleaned with cotton swabs, dipped in tuner degreaser and recapped each time they are mounted through a brass holder. Great care is taken in mounting the microdot connectors to the pressure transducers and amplifiers as the slightest amount or dirt or humidity near the connection, or a twist in the connector, produced a drifting output voltage. The output of the charge amplifier is fed to the multimeter, an oscilloscope, and a plotter. The strain gages are connected to the strain indicator. The piezo-electric pressure transducers and the strain gages are calibrated so that the voltage measurements directly give the thrust or the total head.

With the thrust plate against the drag plate, for different flow rates as measured by a rotameter, the strain indicator readings are noted down. Also with the pitot tube assembly, the total head at the inlet and exit of the nozzle is measured using a piezo-electric pressure transducer.

The angular velocity is measured by a stop watch correct to one-hundredth of a second. In order to check the repeatability of the results, each parameter is measured at least ten times under similar conditions until reasonably consistent values (within 10%) are obtained.

4.4.2 NOTICEABLE PROBLEMS/RECOMMENDATIONS:

In general, there was a very good consistency in the thrust and total head measurements within the range of 10% deviation. The average of the readings is taken to be the final value. Also the temperature of the water used during the experimental investigation was around 15 degrees celsius.

Certain problems/recommendations noticed include:

(i) Frequent removal and mounting of the thrust plates and pitot-tube assembly made it a must to stick on to the small experimental tank.

(ii) Also the water-tight rotating joint needs to be removed and greased at the start of the experiment so that the friction is almost the same as when calibrated.

(iii) The use of an AC motor could be avoided if a DC motor was available; this results in steady rpm throughout the course of the experiment irrespective of the load fluctuations.

(iv) The output of the piezo-electric pressure transducers sometimes shoots up

and much care is to be taken to get repeatability and consistent values. So also with the strain gages, where fluctuations are quite unavoidable.

(v) The thrust of the nozzle is to be applied gradually so that the strain readings are not erroneous.

4.5 'WATER-TIGHT JOINT' FRICTION CALCULATION:

The friction of the water-tight rotating joint is found experimentally. The drag plates are removed from the end of the lever arm assembly and the assembly is left stationary. The flow through the nozzle is gradually increased until the lever arm assembly just starts to move at a steady minimum speed. From the flow rate, knowing the area of the jet (same as the exit area of the nozzle), the thrust is calculated using the relation:

$$T = \rho A_j V_j^2$$

where,

T = Thrust produced by the nozzle

ρ = Density of the fluid (water)

A_j = Area of the jet

V_j = Velocity of the jet

This thrust should be equal to the friction at the joint. It is observed that for flow rate of $9.11 \times 10^{-4}\ m^3/s$, for the jet area of $2.01 \times 10^{-4}\ m^2$, the assembly moves at a steady speed. From these values, the friction is found to be 4.128 Newtons.

4.6 WALL-EFFECT COMPENSATION:

The wall effects arise due to the presence of the walls close to the jet as the assembly rotates in the tank. Hence wall effects have to be compensated to avoid the effects of the closeness of the walls and the back eddies (whirl) formed by the jet. There was also noticeable 'stirring- effect' of apparatus to the finite mass of water inside the tank (at higher speeds of the model in the tank). The effect of this stirring is to cause some unsteadiness in the motion of the model. The unevenness of this is reduced by taking the velocity over a large number of rotations of the model. However, these were compensated when the assembly was towed in the wave tank. Thus, theory based on steady operation is justified.

The compensation is done (Fig.13) in the following way: The arm assembly is put in the wave tank and towed at different velocities. The drag is measured using a force transducer. Friction of the rotating water-tight joint is added to the drag to give the total drag (the actual thrust or drag in the experimental tank). The deviation of this total drag and the thrust produced, gives the compensation for the wall effects and it is found to be within 30% for the range of speeds encountered in this experimental investigation.

Fig. 13 Photograph of the Wall-Effect Compensation

CHAPTER 5

EXPERIMENTAL RESULTS AND DISCUSSION

5.1 GENERAL:

This chapter is organised into three major sections. The first part is a discussion of the performance parameters in the experimental tank, for various nozzles. In the second part, the energy losses are presented and compared with the theoretical results. In the last part, the wall-effect compensated results are put-forth. The experimental work is limited to finding an optimum nozzle for a range of flow rates and velocities encountered in real practice for ROV's. The general water-jet propulsion system for surface vessels have been studied in depth by various authors [1],[7],[8],[9],[10],[28].

5.2 EXPERIMENTAL TANK RESULTS:

Program 3 and 6 (in appendix A) gives the calculation of the propulsion efficiency and thrust from the measured data. The results are plotted for comparison. It can be seen that as the nozzle exit diameter is increased from 16 mm to 64 mm (for the same inlet diameter of 52.832 mm), the propulsion efficiency increased upto an exit diameter of 44mm and later upon further increase in exit diameter, the efficiency dropped down (Figs. 14 to 19).

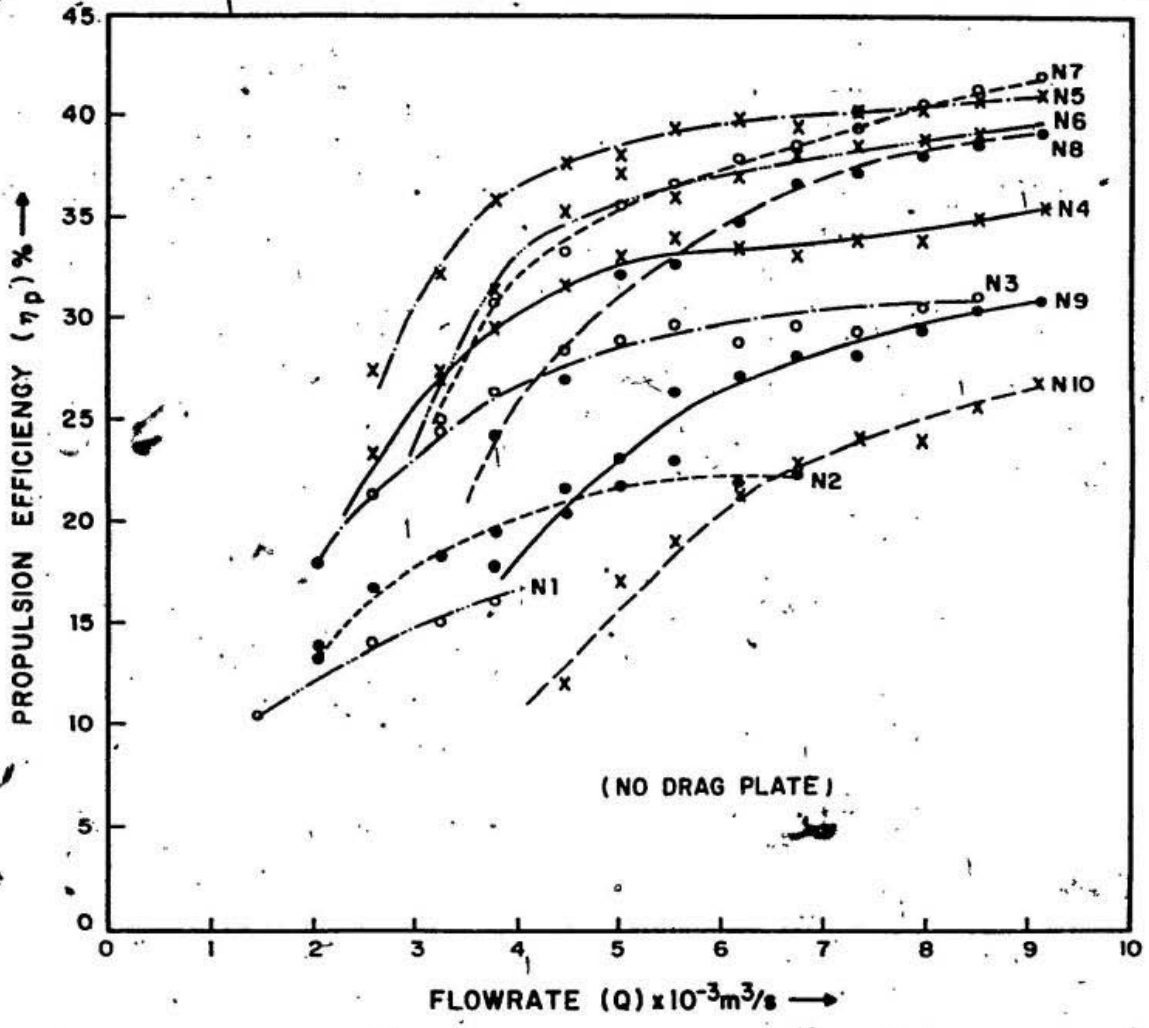

Fig. 14 Propulsion Efficiency Vs Flow Rate for No-Drag Plate

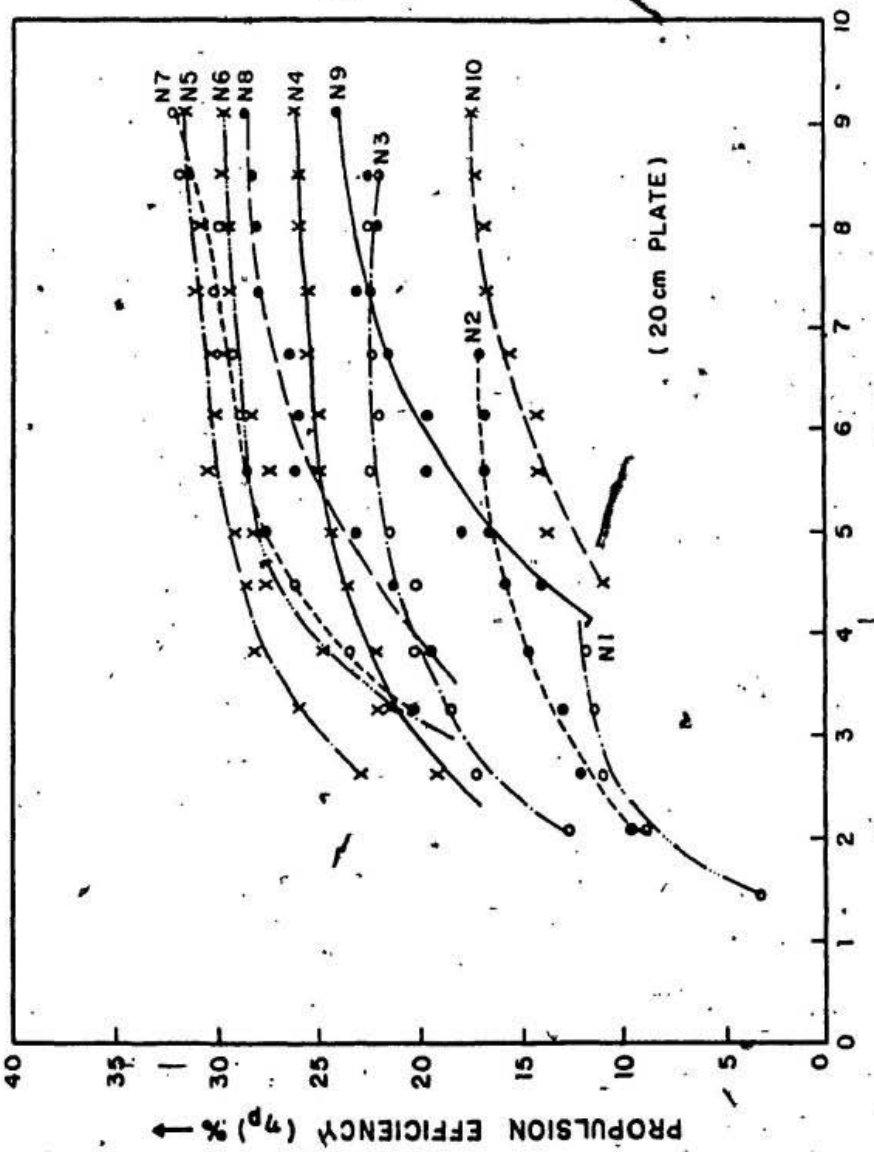

Fig. 15 Propulsion Efficiency Vs Flow Rate for 20-cm Drag Plate

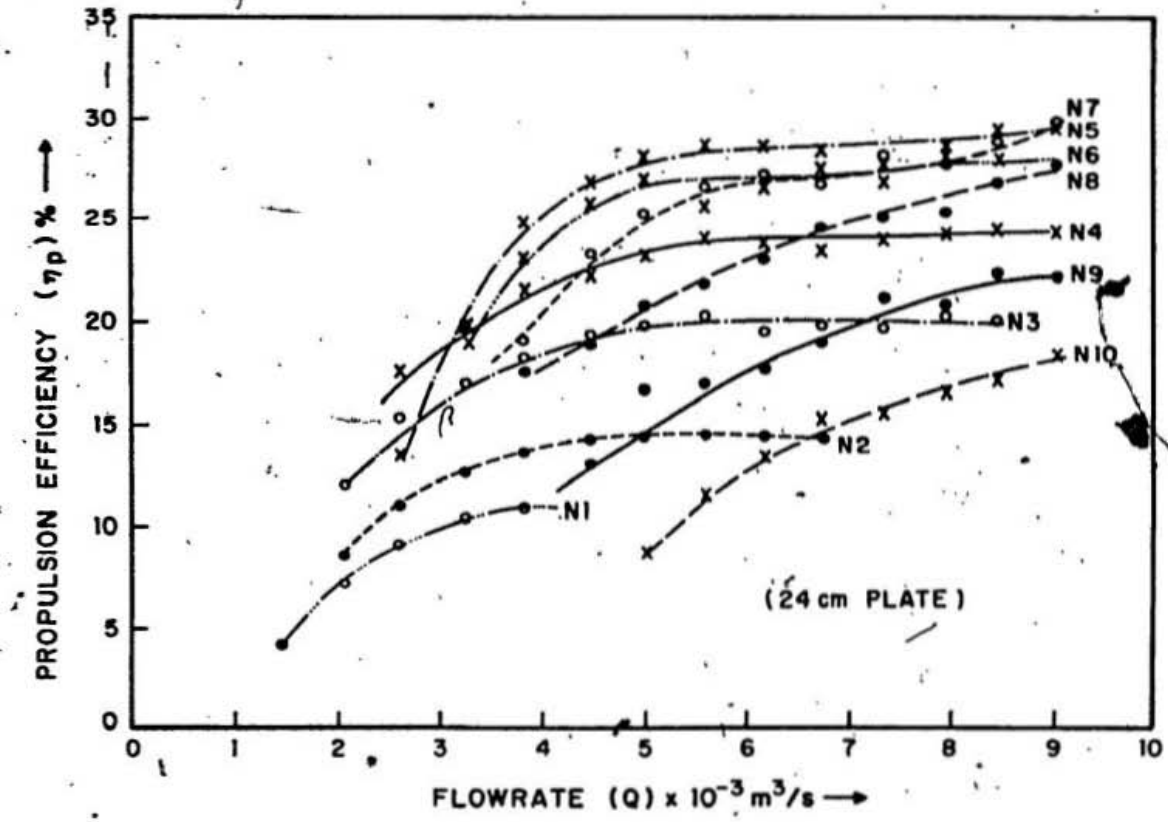

Fig. 16 Propulsion Efficiency Vs Flow Rate for 24-cm Drag Plate

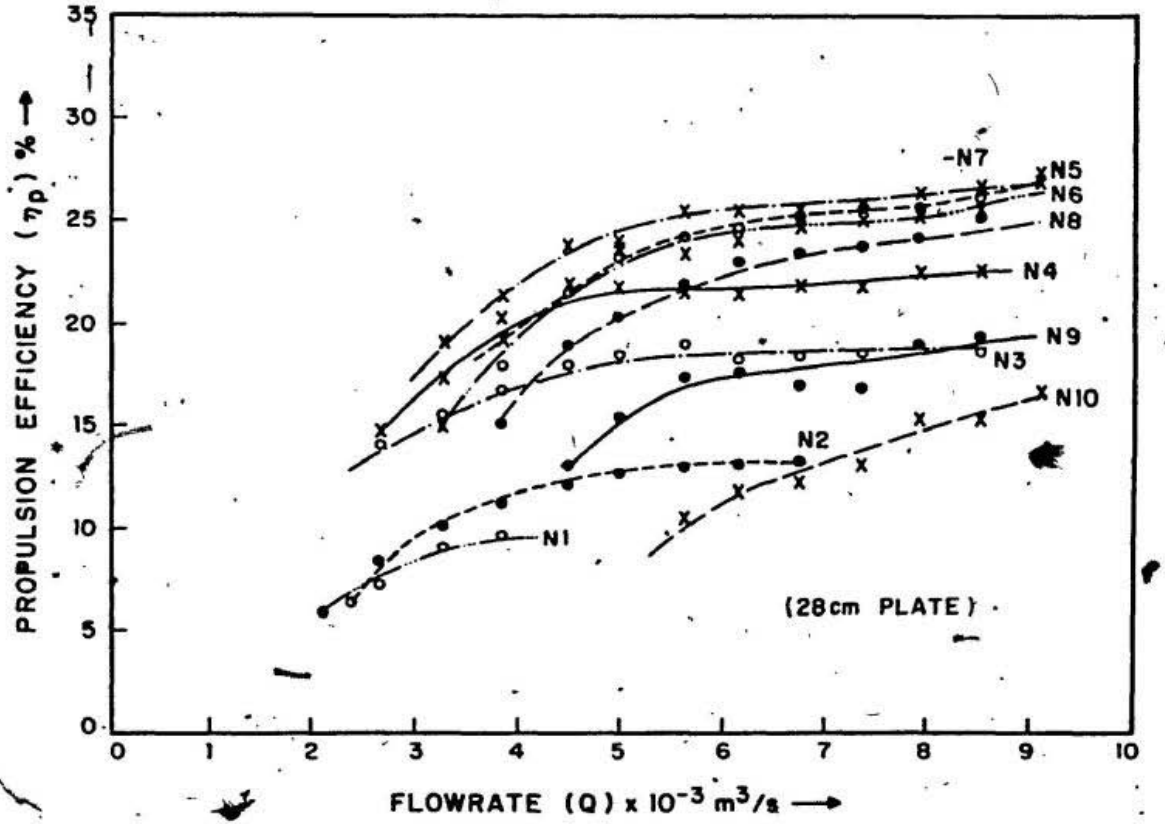

Fig. 17 Propulsion Efficiency Vs Flow Rate for 28-cm Drag plate

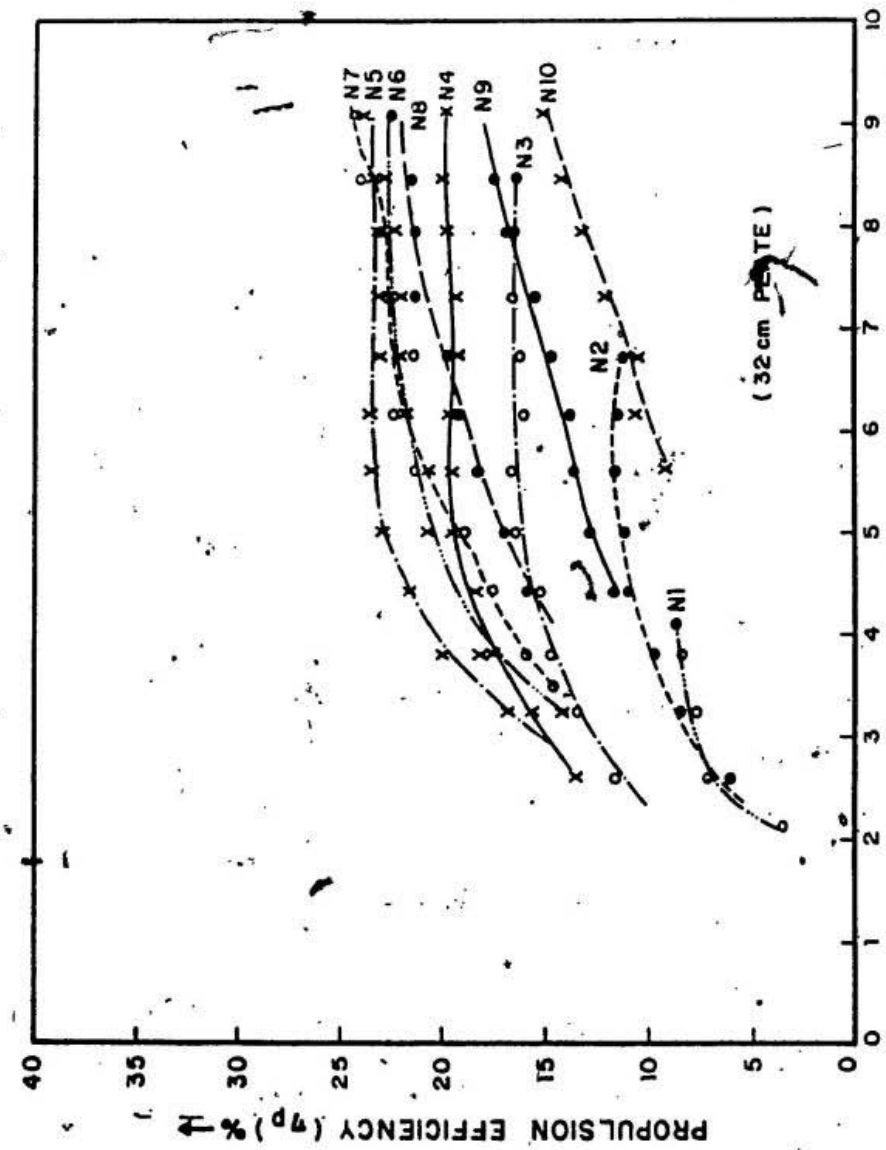

Fig. 18 Propulsion Efficiency Vs Flow Rate for 32-cm Drag plate

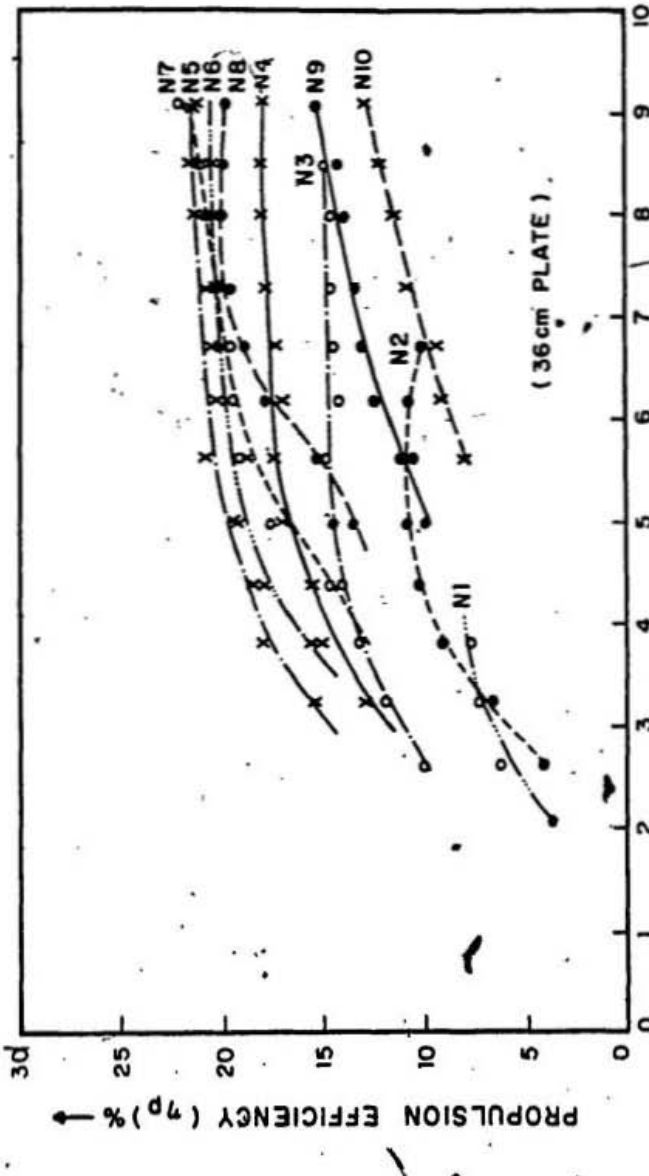

Fig. 19 Propulsion Efficiency Vs Flow Rate for 36-cm Drag plate

The highest propulsion efficiency of 42% was reached for the 'no-drag plate' condition. Comparison of the efficiency curves for different nozzles with different drag plates reveal the same type of characteristic, showing that the nature of the performance is almost a constant.

The main point to be discussed herein is the variation of efficiency with variation of exit diameters. Though the velocity of jet decreases as the exit diameter is increased, there is a peak value for efficiency. This can be visualised considering the fact that the efficiency is maximum when the velocity of the vehicle is close to the velocity of the jet. But when the exit diameter is increased more, the vehicle velocity drops more rapidly than the jet velocity, thereby making their difference more and consequently, leading to the reduction in efficiency.

The fact that efficiency is maximum when the velocity of vehicle is close to the jet velocity is applicable to high speed applications where the inlet head recovery cannot be neglected. However, equation (5) has been derived for slow speed applications as in ROV's, neglecting the inlet head recovery. That is the reason why the experimental values of efficiency are lesser than 50% as dictated by equation (5). Also, the points where the propulsion efficiency is maximum, the vehicle velocity is found closer to the jet velocity than at other points which is quite a good comparison.

Improving the efficiency necessarily involves the lowering of the pump head and increasing the flow rate. Lowering the pump head needs the incorporation of an axial flow pump for slow moving applications. Increase in flow rate does not mean an increase in nozzle size. More than one nozzle can be incorporated at suitable locations in the vehicle for easy maneuverability.

5.3 ENERGY LOSS[illegible] THE NOZZLE:

It is found that the energy losses decrease (Figs. 20 and 21) and the loss coefficient increase (Fig. 22) when the exit diameter is increased. This is due to the fact that even though the losses increase with the flow rate and decrease with higher numbered nozzles, the velocity head at the exit for the higher numbered nozzles is less, thereby making the loss coefficient to increase with higher numbered nozzles. maximum deviation is about 25% for N1 and minimum is 3% for N10 for the maximum flow rates encountered for each of these cases.

The reason for the greater difference in error between the experimental and the theoretical energy loss curves from N10 to N1 is due to the fact that the turbulence is higher for lower numbered nozzles as the exit diameter is smaller for a given flow. This variation of the degree of turbulence might have caused this difference.

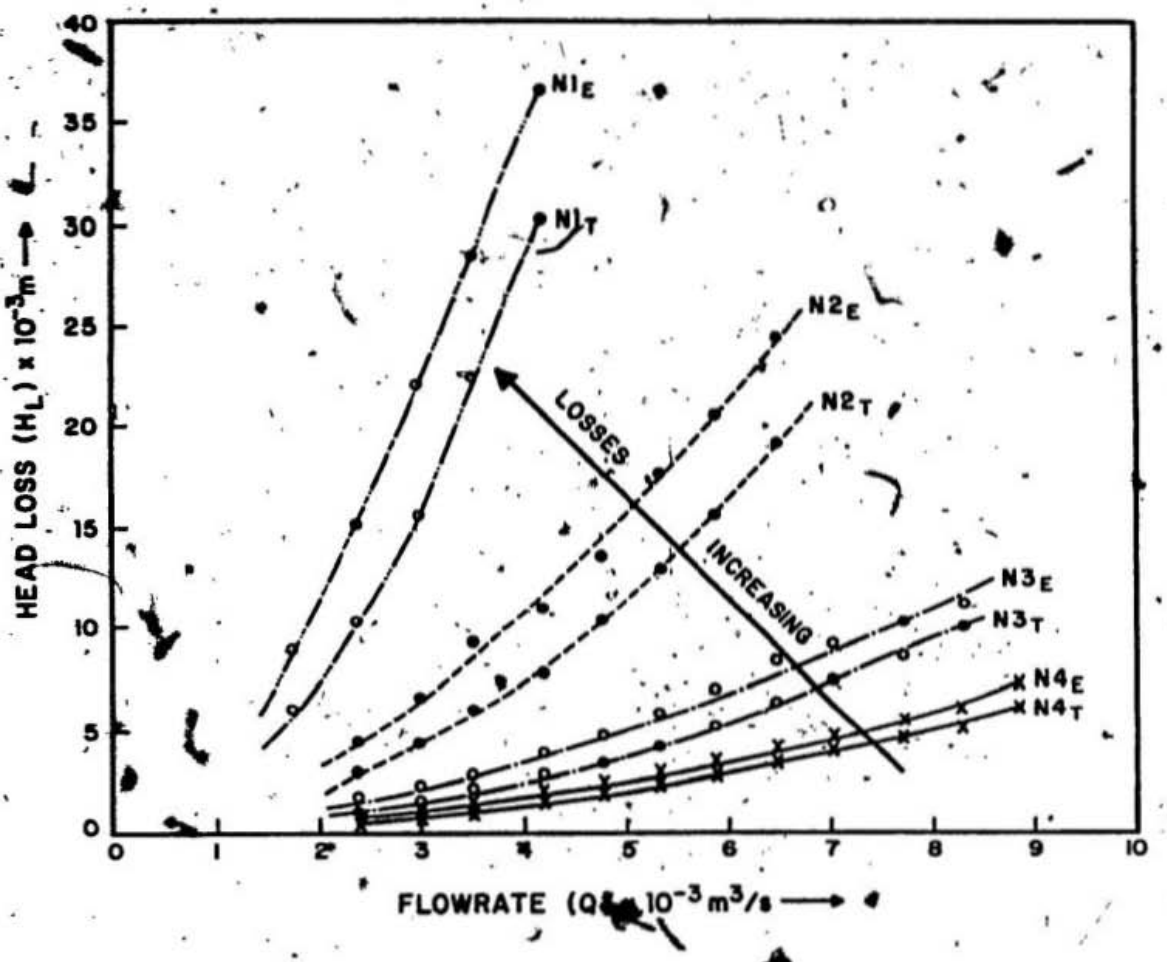

Fig. 20 Head Loss Vs Flow Rate for N1, N2, N3, N4

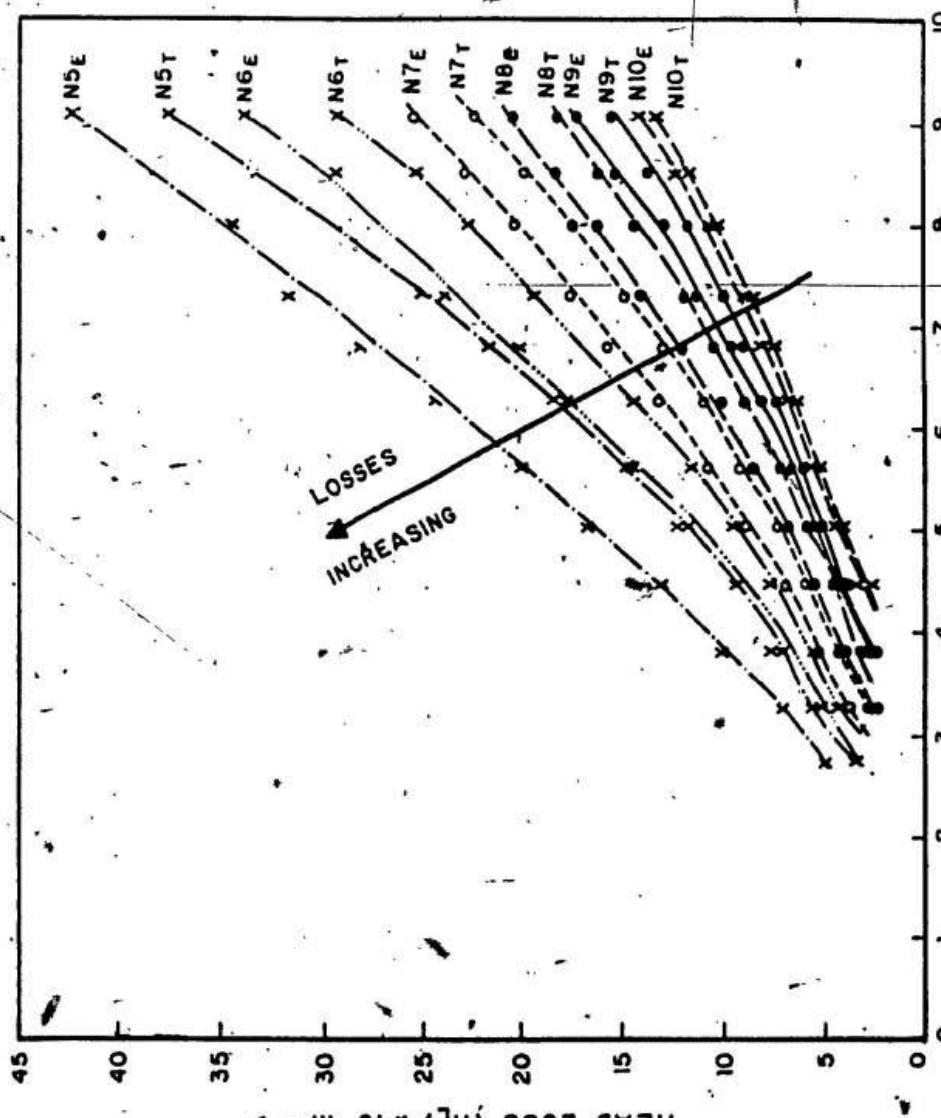

Fig. 21 Head Loss Vs Flow Rate for N5, N6, N7, N8, N9, N10

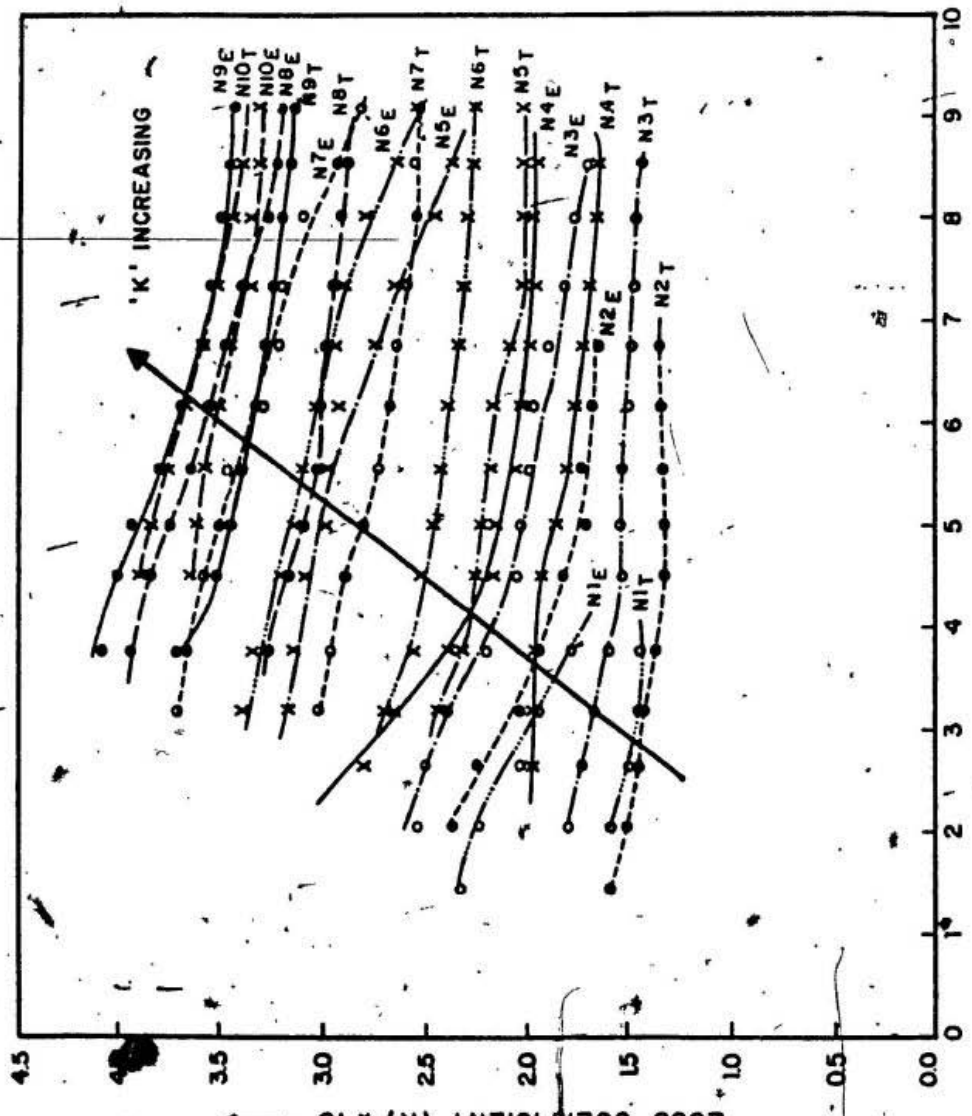

Fig. 22 Loss Coefficient Vs Flow Rate for All Nozzles

5.4 WALL-EFFECT COMPENSATED RESULTS:

The results after wall effects have been compensated are shown in the figures 23 to 59. It can be seen that as the vehicle velocity becomes higher, the wall effects tend to be more. The propulsion efficiency for 'no-drag plate' condition was almost the same, whereas for the other drag plate conditions, the wall effect compensation resulted in the increase of the propulsion efficiency by about 10 to 25%, which is quite considerable.

5.5 DISCUSSIONS:

Figures 23 to 28 give an idea of the vehicle velocities for different flow rates. The vehicle velocity is observed to be maximum for 'no-drag plate' condition for N2. Also, N2 has the highest vehicle velocity for all drag plates.

From Fig.29, the maximum efficiency of 43% is obtained for the maximum flow rate of $9.1 \times 10^{-3}\ m^3/s$ for N5 without a drag plate. Also N5 has overall good performance characteristics for range of flow rates from 2.5×10^{-3} to $9.1 \times 10^{-3}\ m^3/s$. N1, N2, N3, N4,....N10 have maximum efficiencies of 16%, 22%, 29%, 35%, 43%, 40%, 41%, 38%, 31%, 26% respectively. From Fig.30, the maximum efficiency of 39% is obtained for the maximum flow rate of $9.1 \times 10^{-3}\ m^3/s$ for N5 with 20 cm diameter drag plate. N5 has overall good performance characteristic from 3.5×10^{-3} to $9.1 \times 10^{-3}\ m^3/s$. N1, N2, N3, N4,....N10 have maximum efficiencies of 15%, 21%, 28%, 33%, 39%, 37%, 38%, 36%, 29%, and 25% respectively.

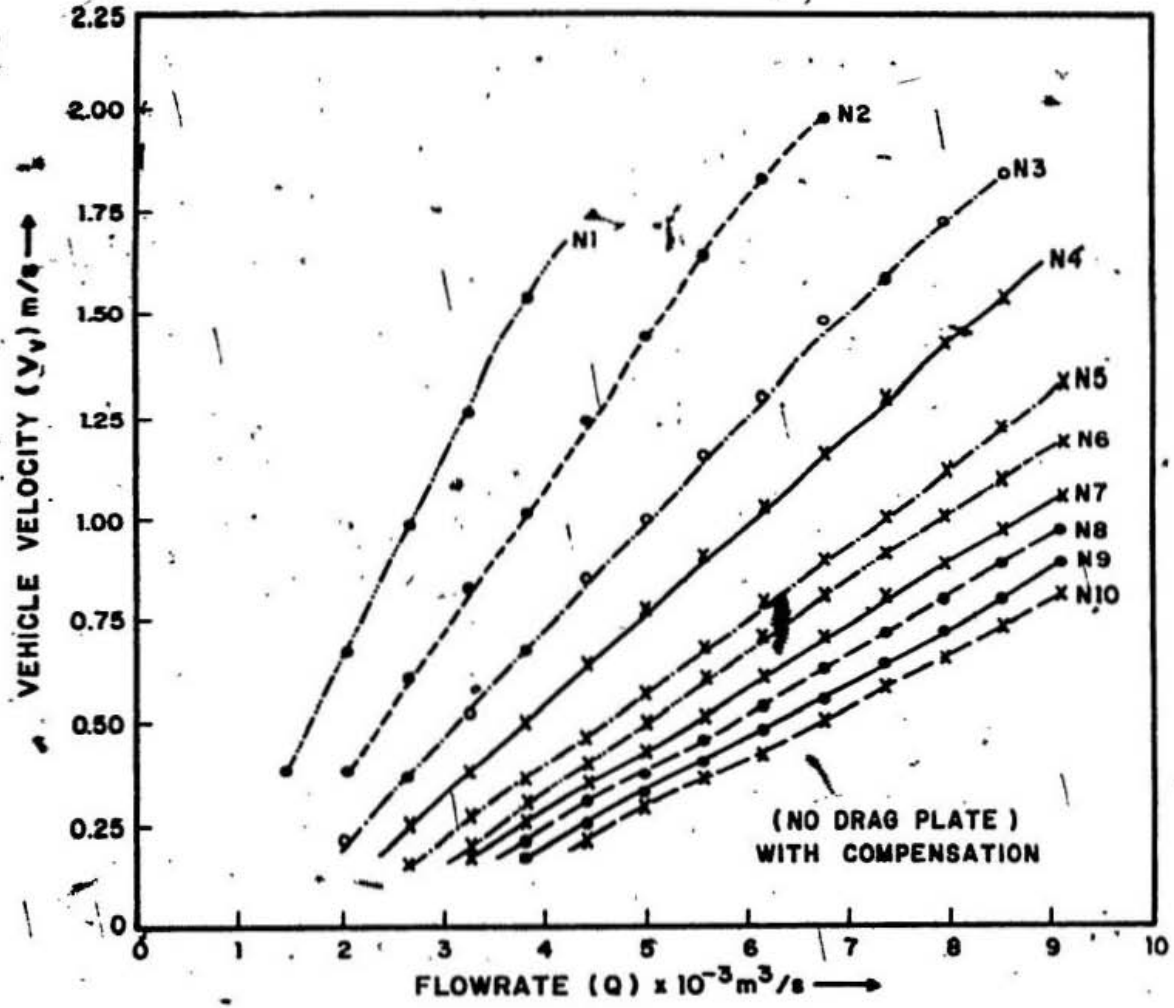

Fig. 23 Vehicle Velocity Vs Flow Rate for No-Drag Plate (Compensated)

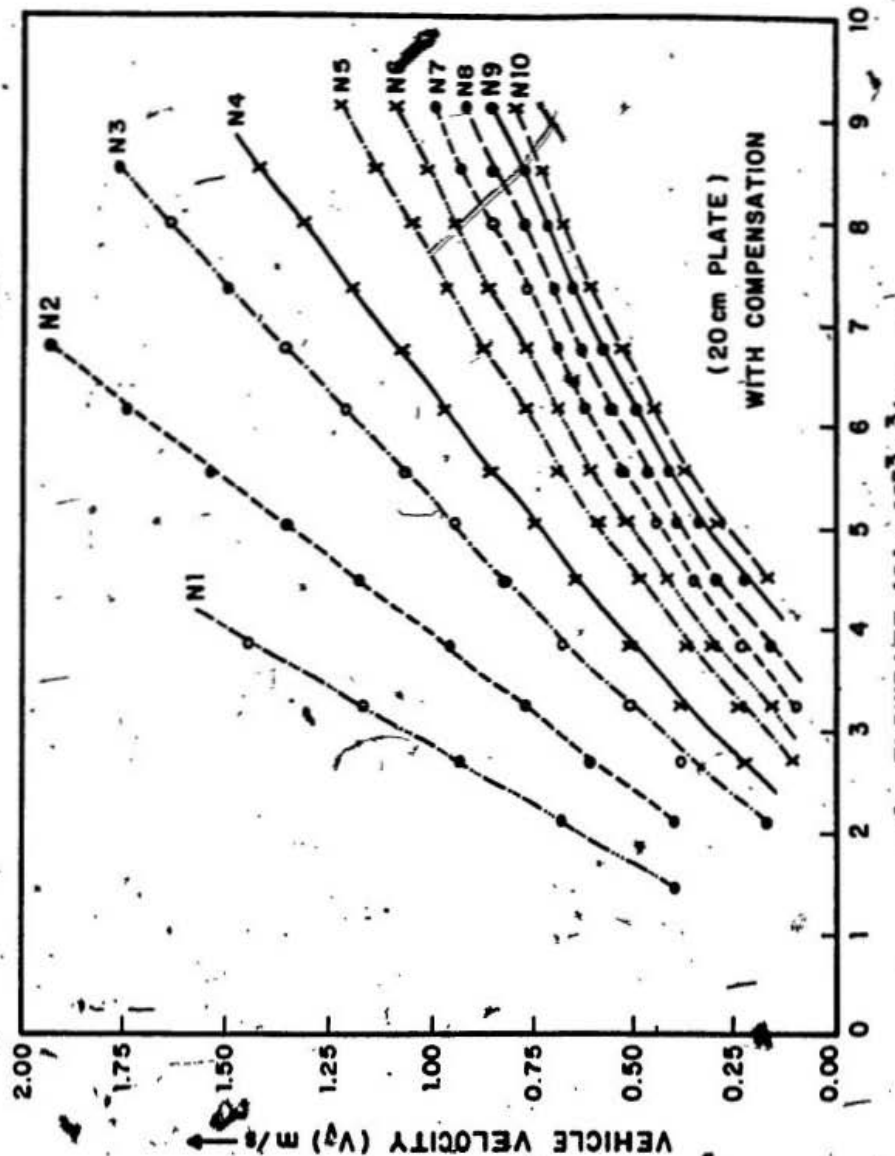

Fig. 24- Vehicle Velocity Vs Flow Rate for 20-cm Plate (Compensated)

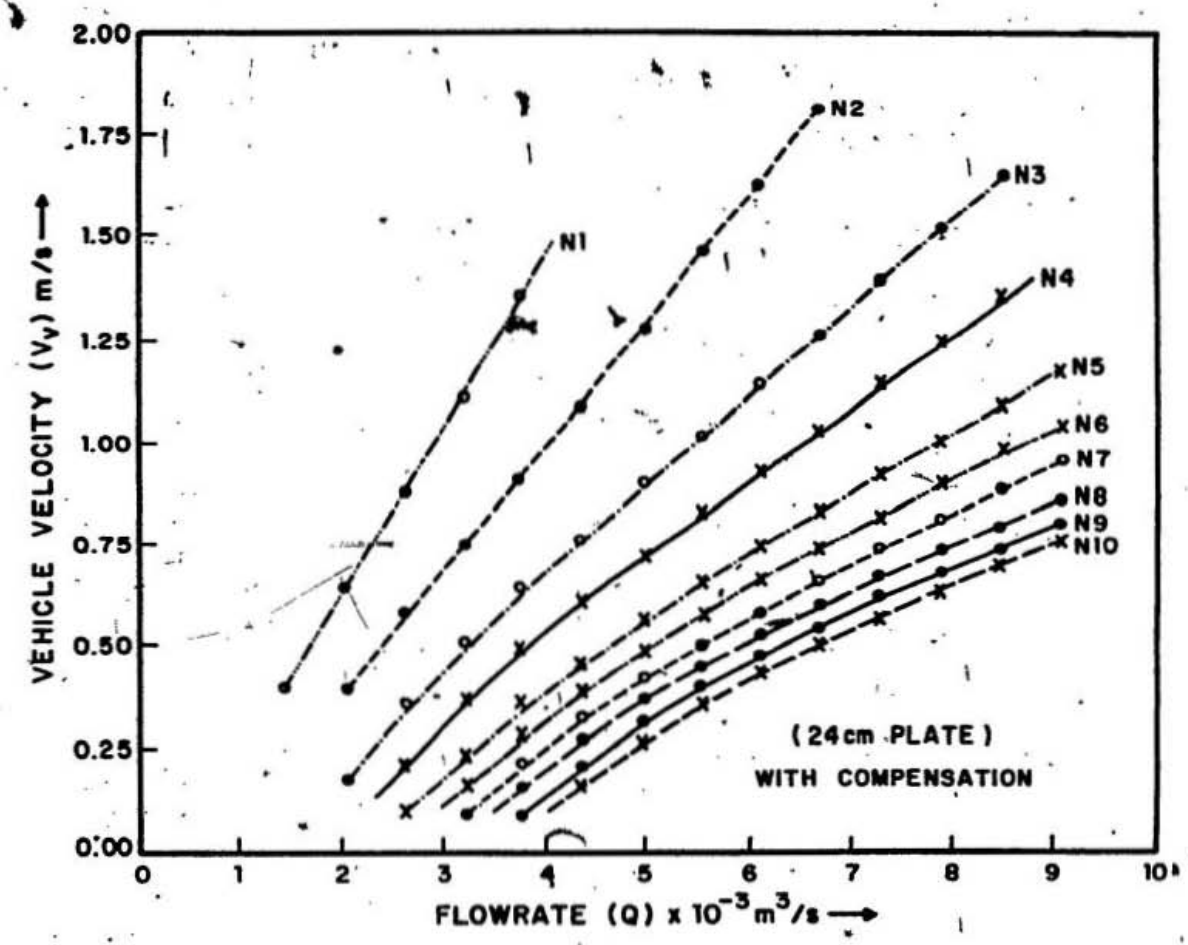

Fig. 25 Vehicle Velocity Vs Flow Rate for 24-cm Plate (Compensated)

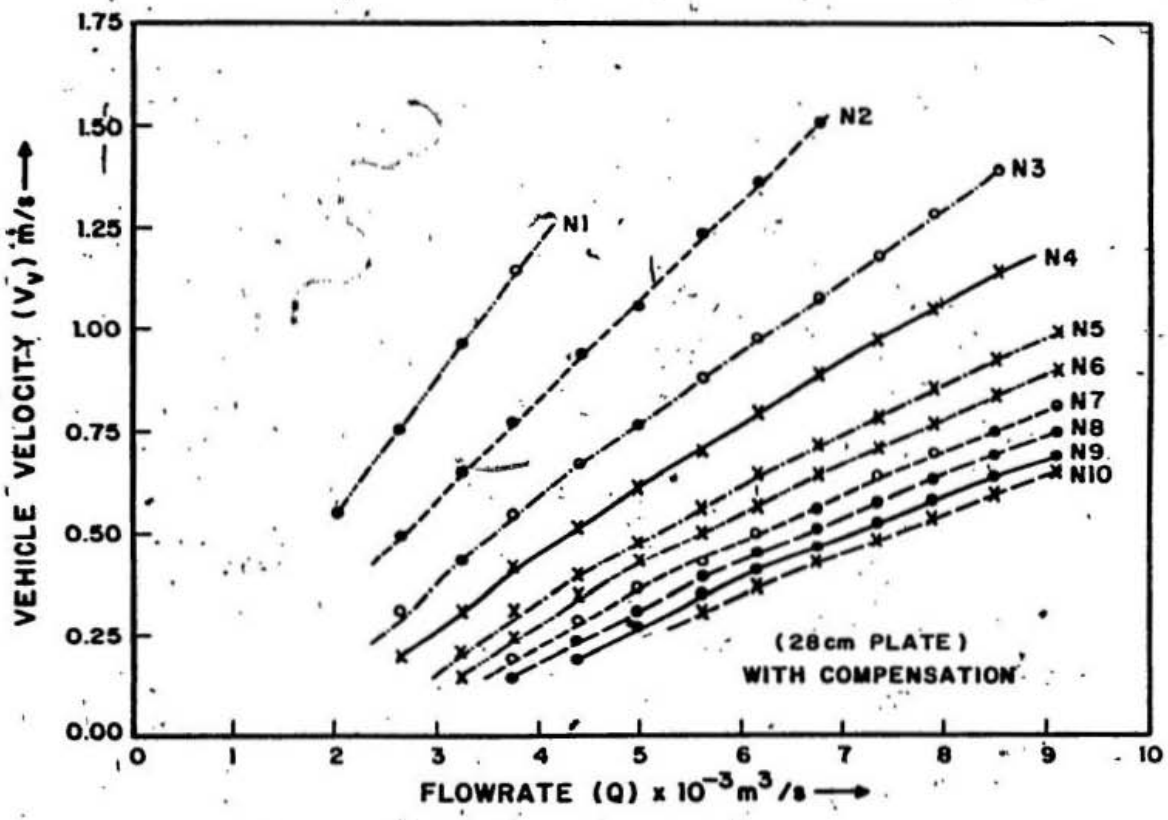

Fig. 26 Vehicle Velocity Vs Flow Rate for 28-cm Plate (Compensated)

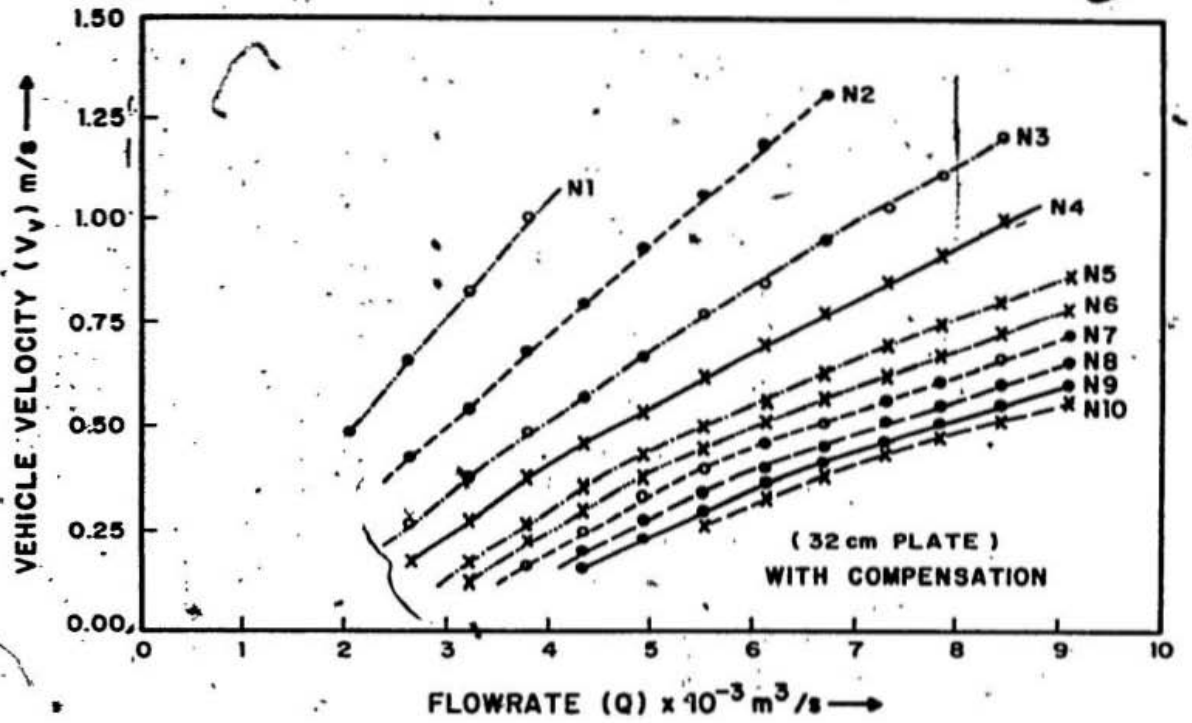

Fig. 27 Vehicle Velocity Vs Flow Rate for 32-cm Plate (Compensated)

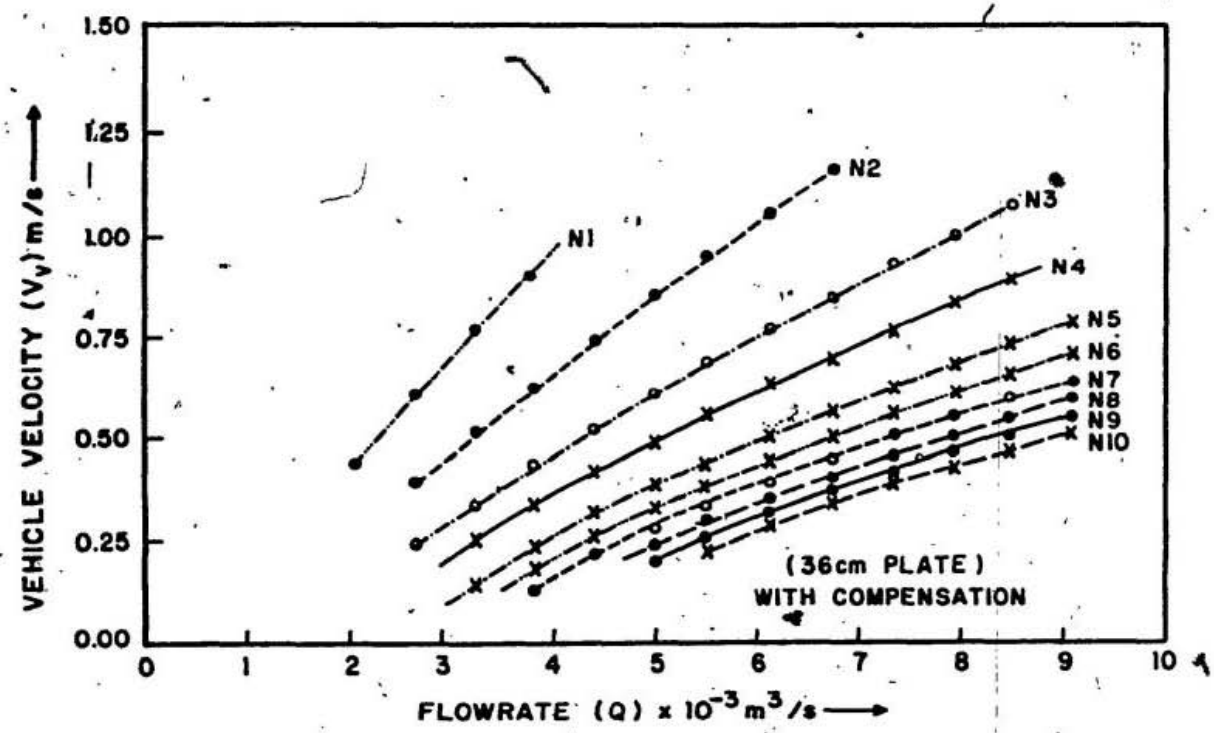

Fig. 28 Vehicle Velocity Vs Flow Rate for 36-cm Plate (Compensated)

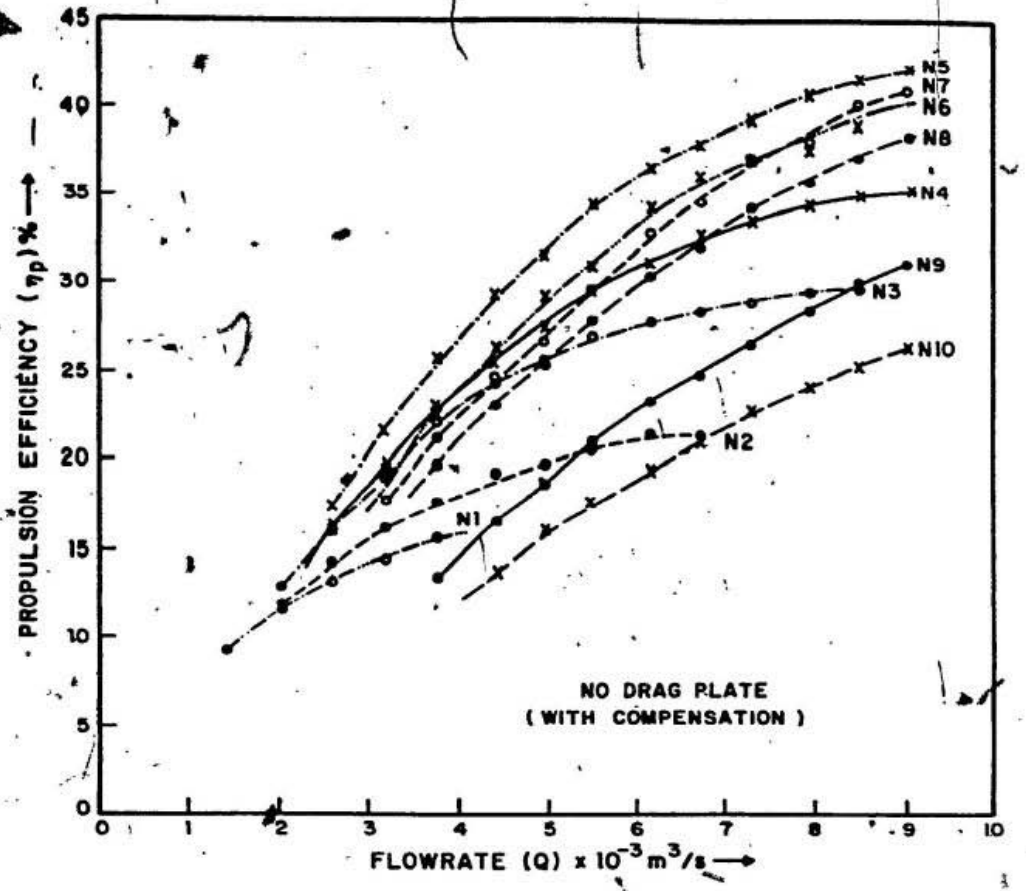

Fig. 29 Propulsion Efficiency Vs Flow Rate for NDP (Compensated)

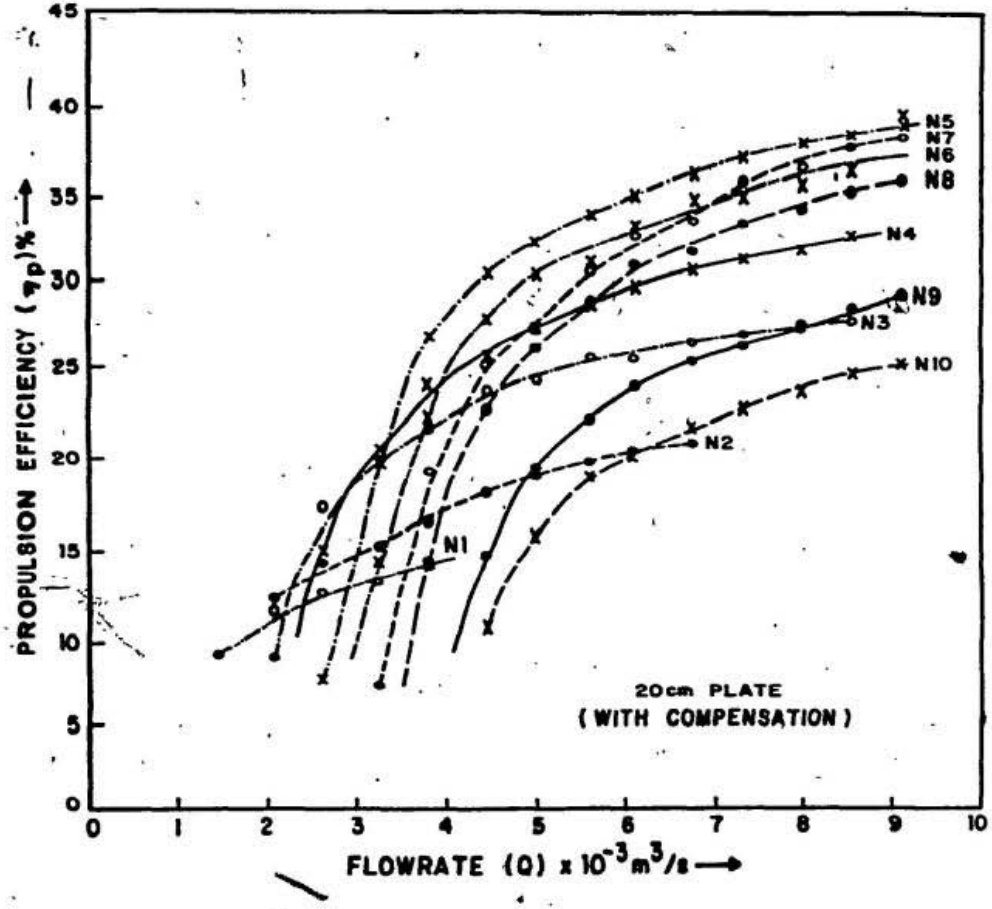

Fig. 30 Propulsion Efficiency Vs Flow Rate for 20-cm Plate (Compensated)

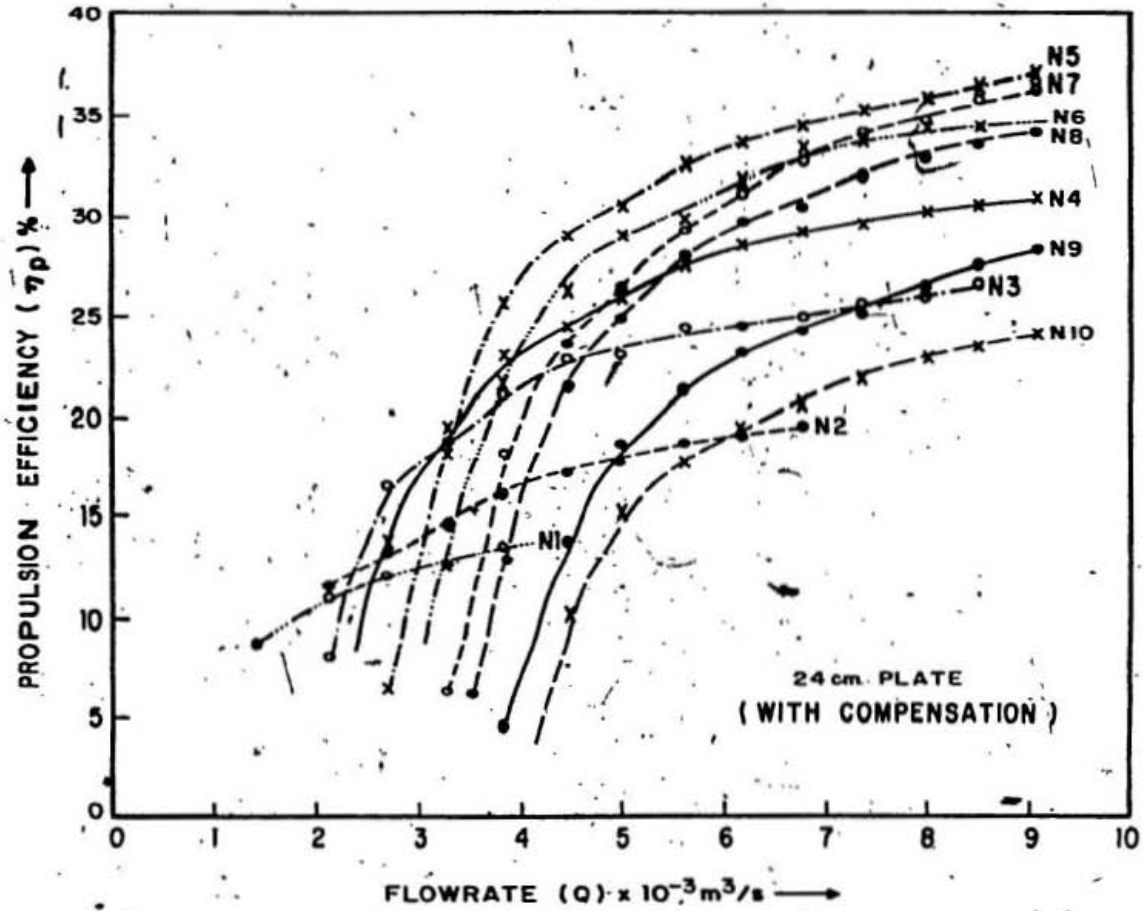

Fig. 31 Propulsion Efficiency Vs Flow Rate for 24-cm Plate (Compensated)

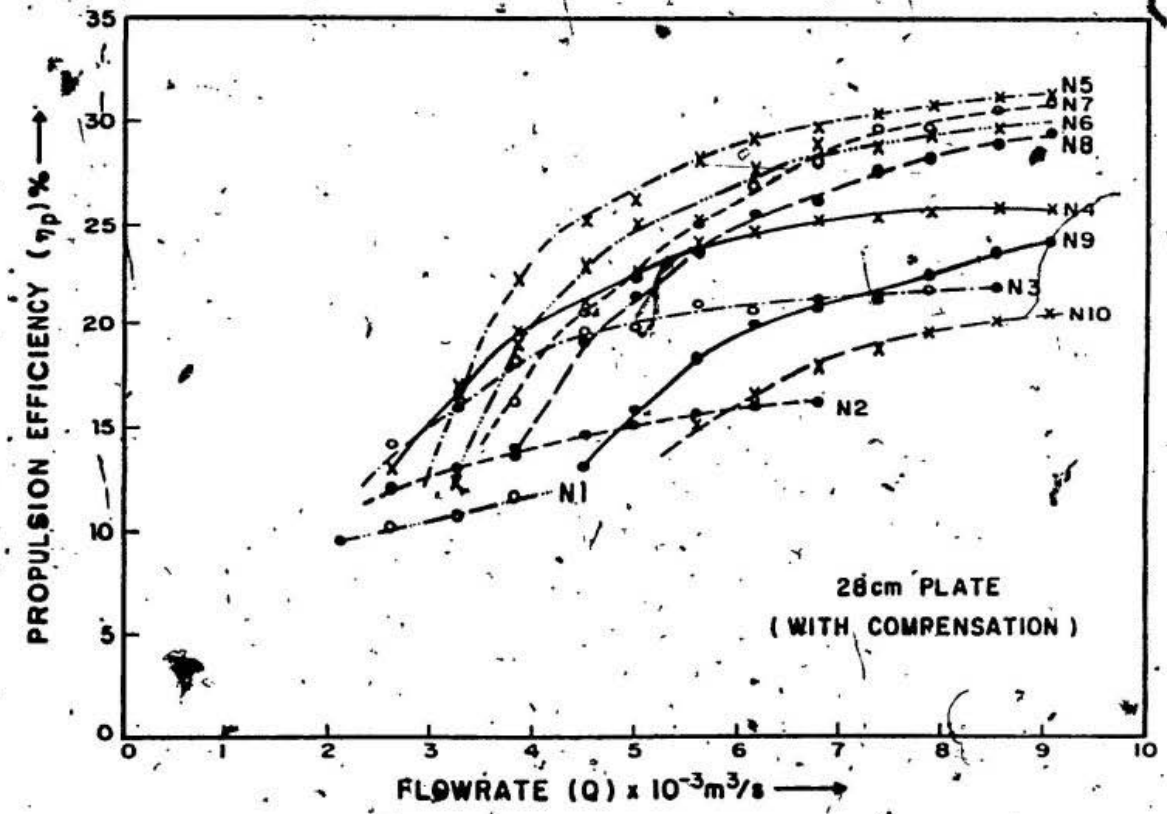

Fig. 32 Propulsion Efficiency Vs Flow Rate for 28-cm Plate (Compensated)

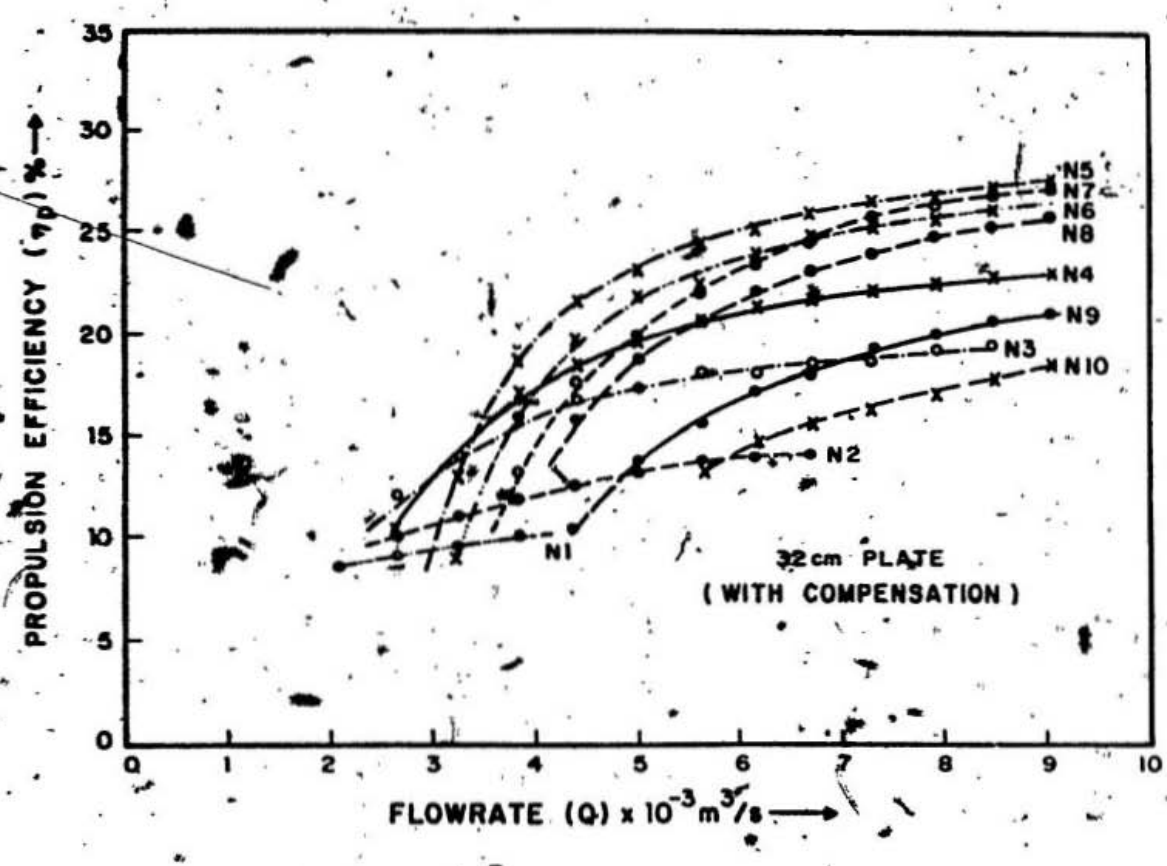

Fig. 33 Propulsion Efficiency Vs Flow Rate for 32-cm Plate (Compensated)

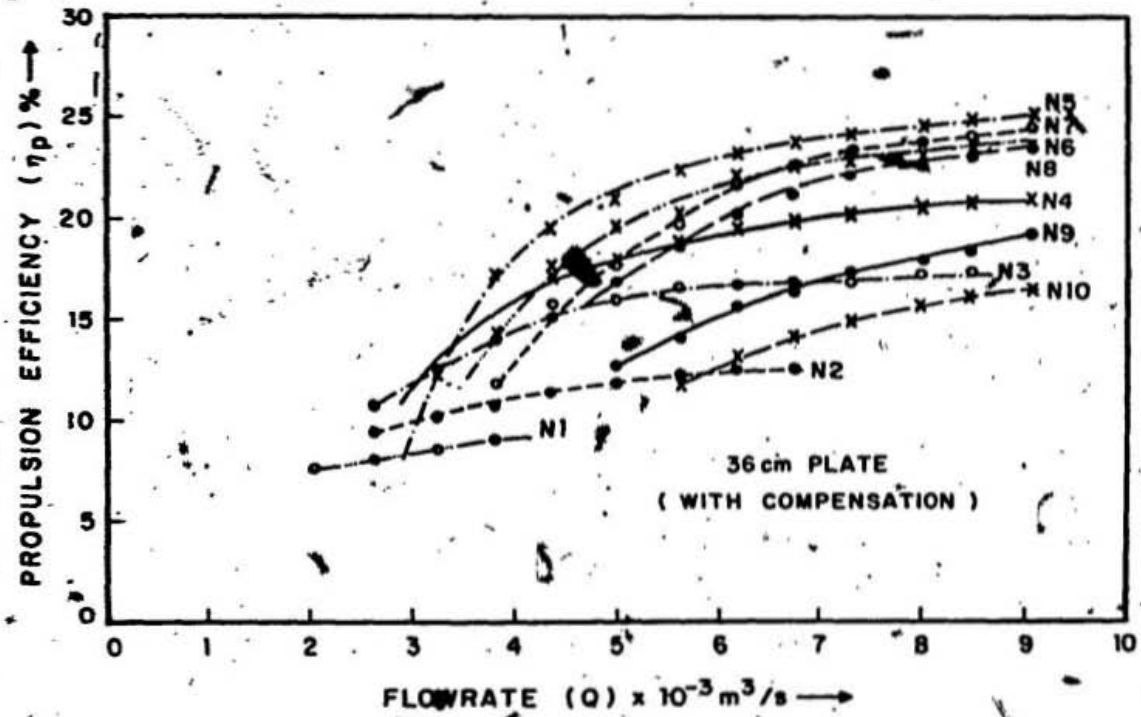

Fig. 34 Propulsion Efficjency Vs Flow Rate for 36-cm Plate (Compensated)

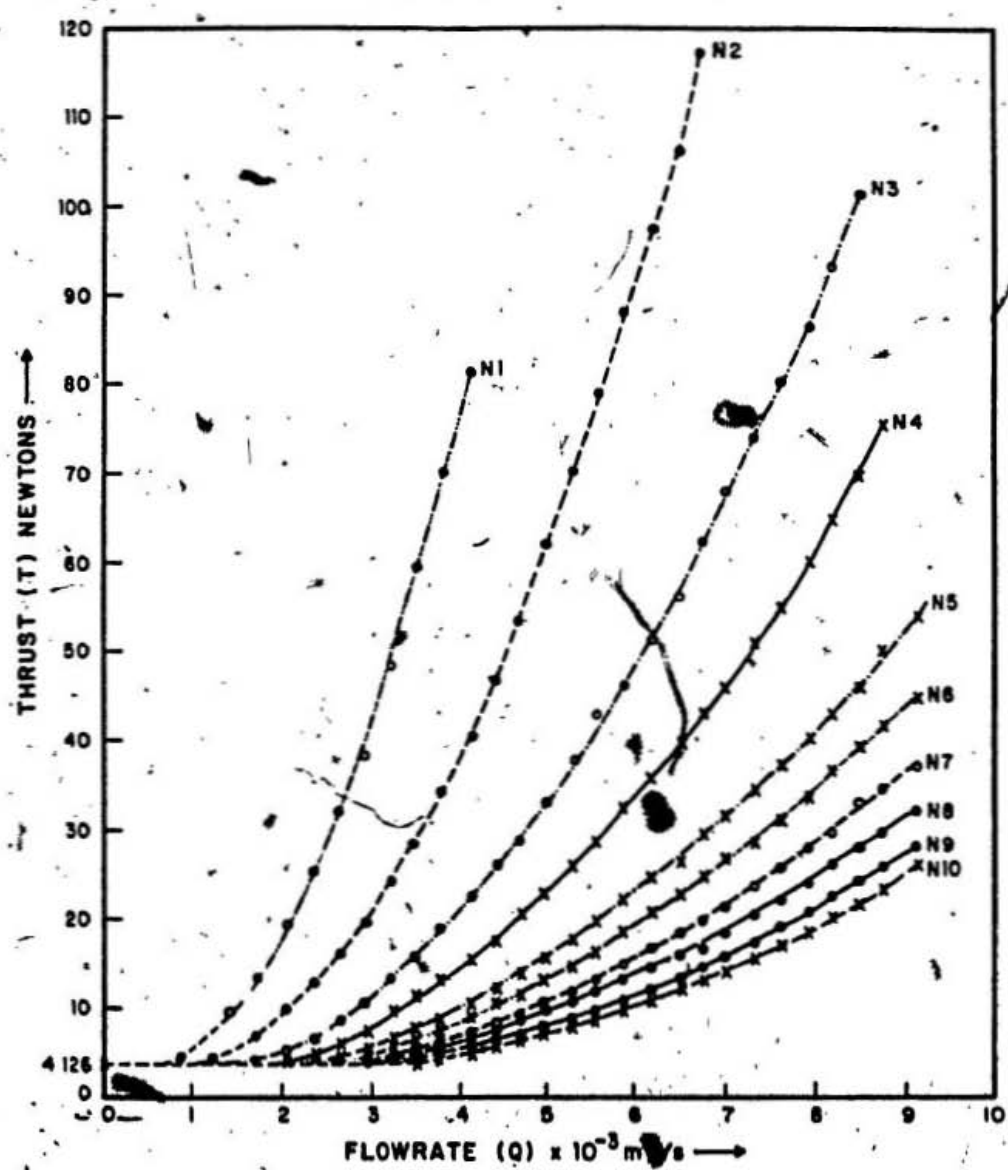

Fig. 35 Thrust Vs Flow Rate for All Nozzles

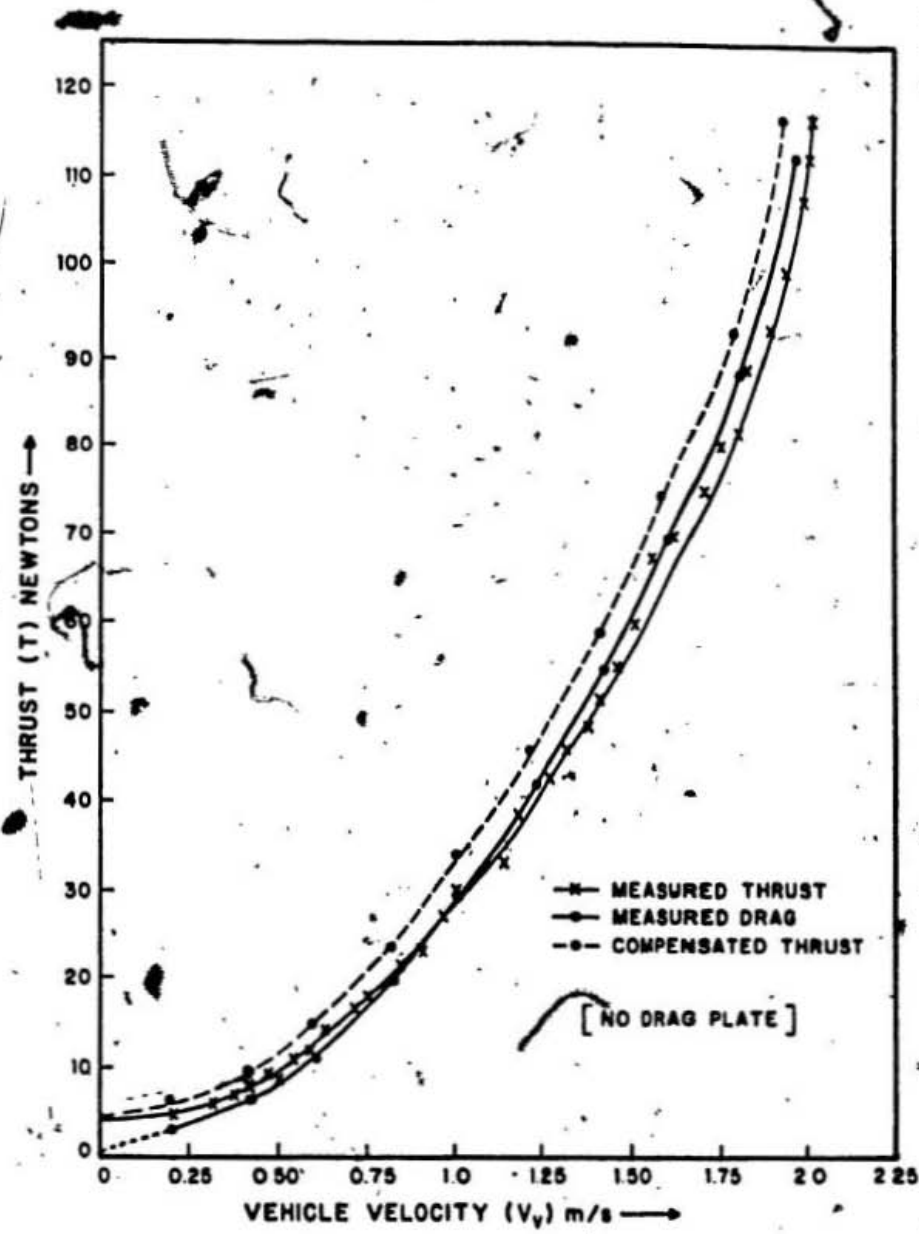

Fig. 36 Thrust Vs Vehicle Velocity for NDP

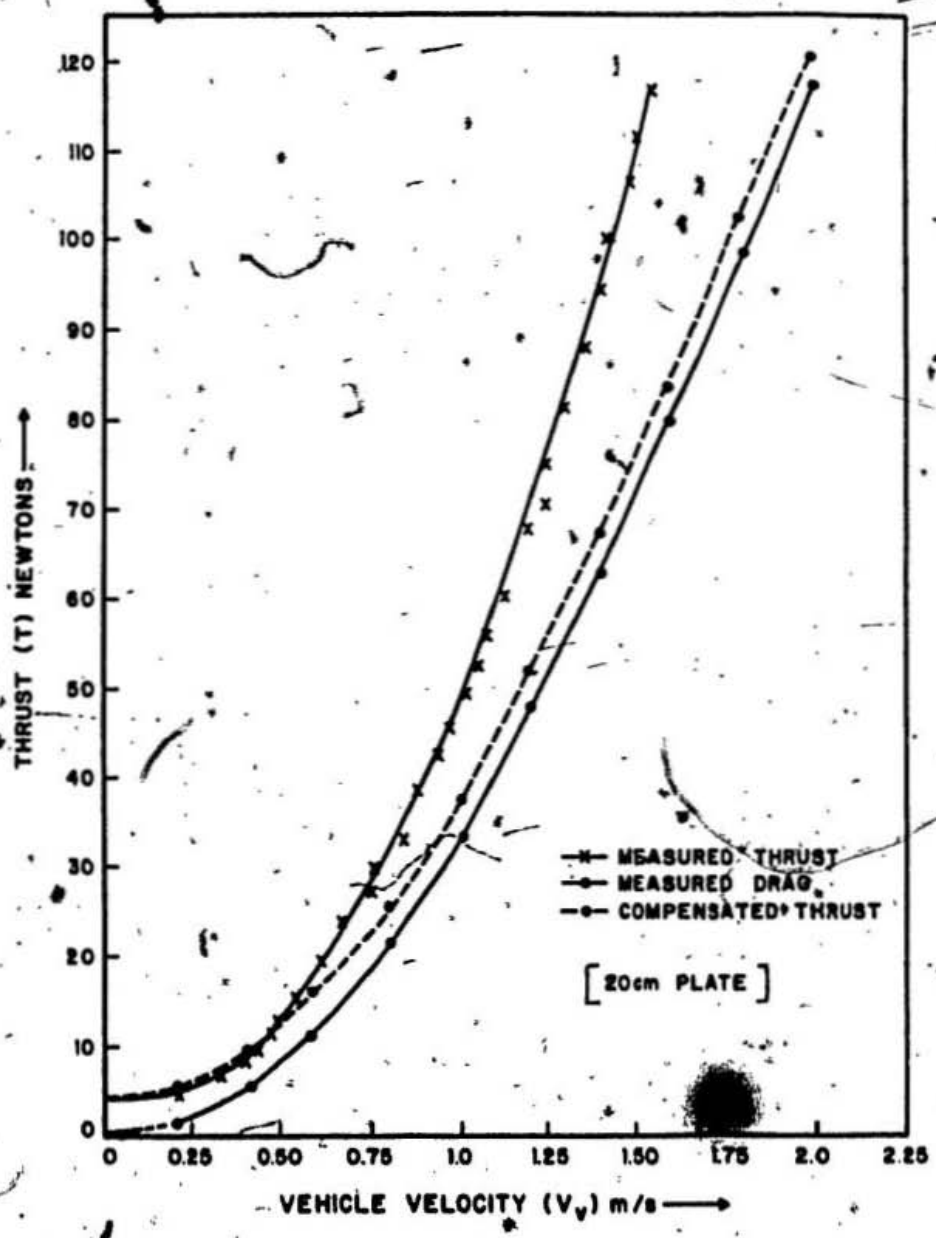

Fig. 37 Thrust Vs Vehicle Velocity for 20-cm Plate

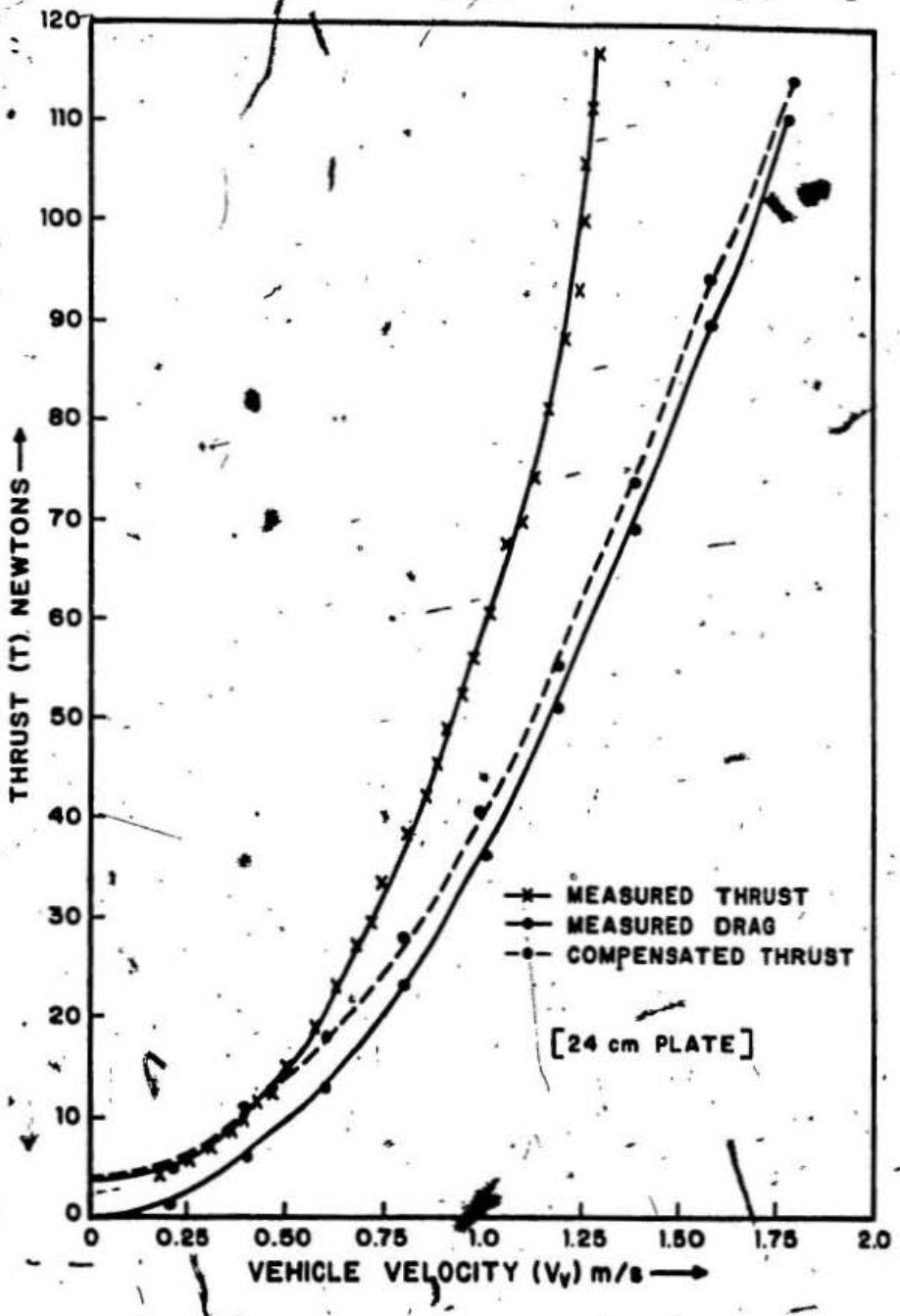

Fig. 38 Thrust Vs Vehicle Velocity for 24-cm Plate

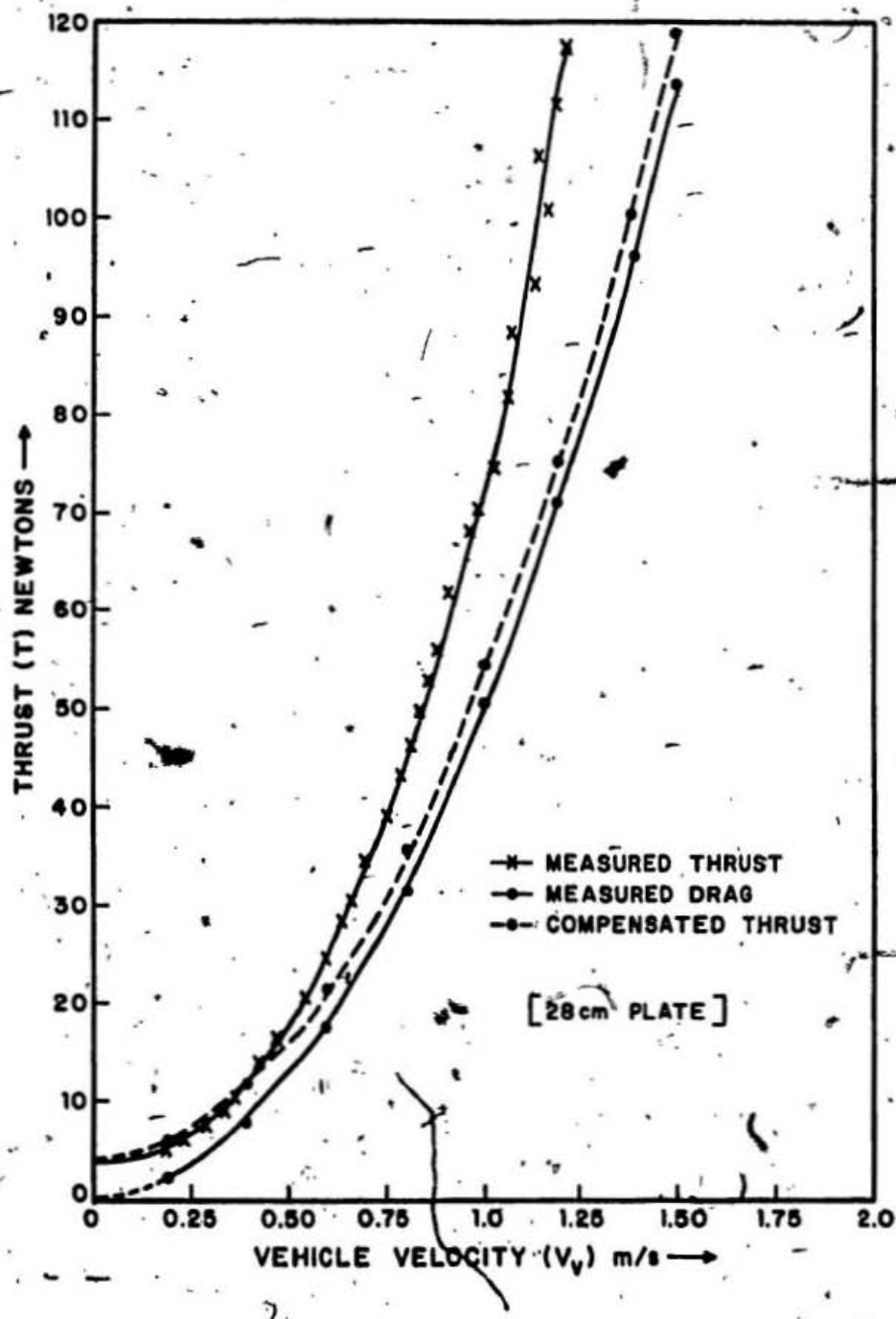

Fig. 39. Thrust Vs Vehicle Velocity for 28-cm Plate

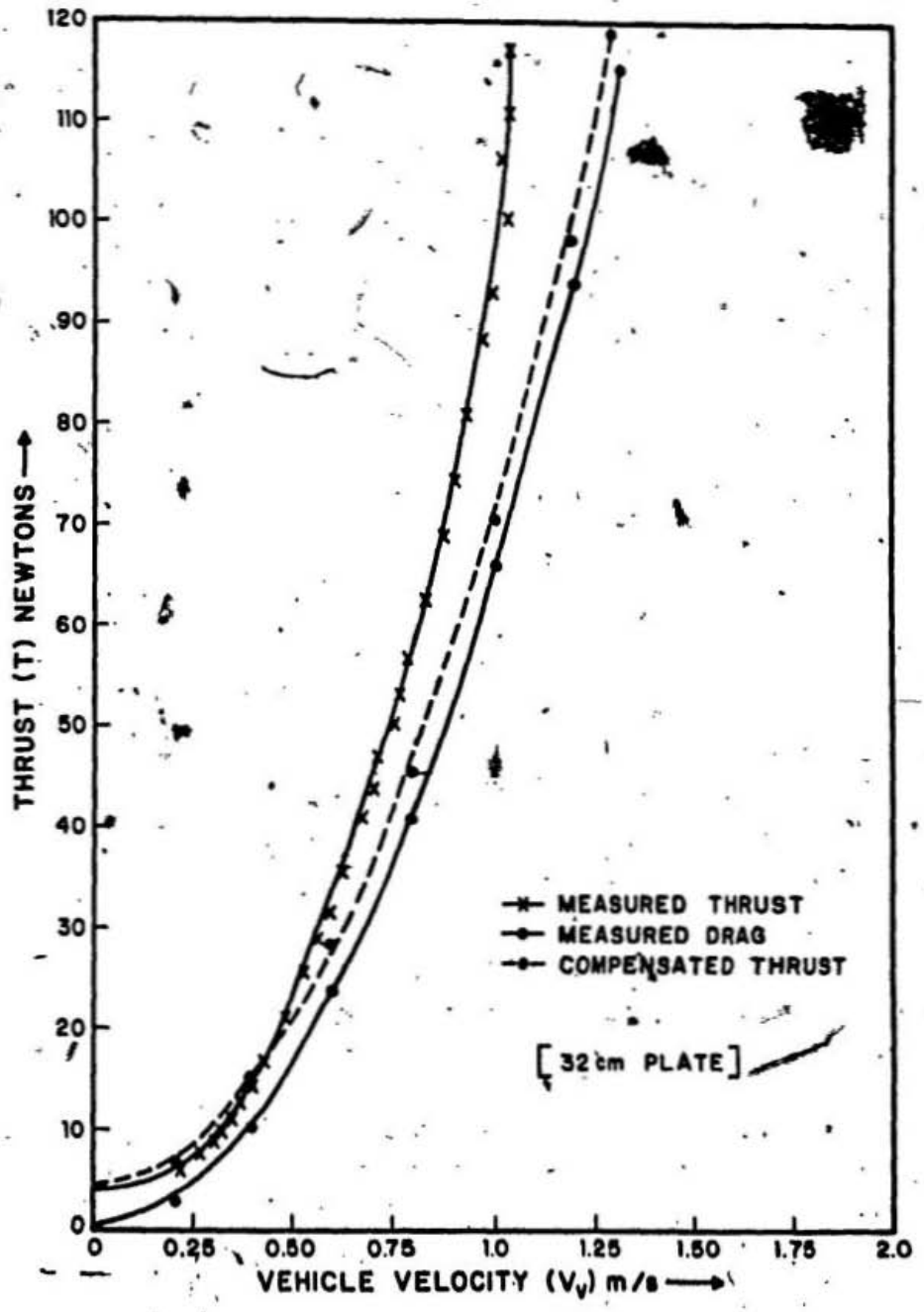

Fig. 40 Thrust Vs Vehicle Velocity for 32-cm Plate

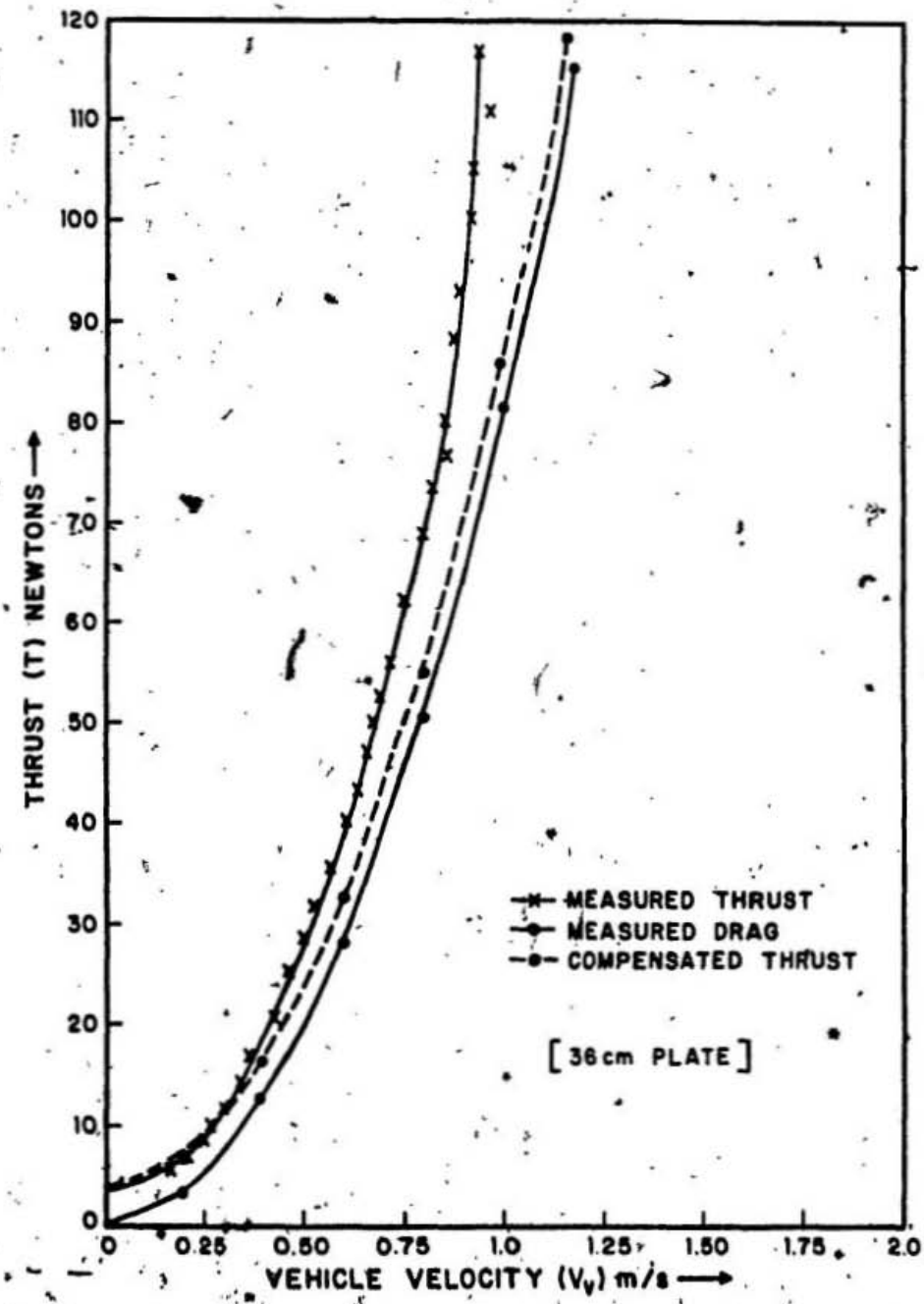

Fig. 41 Thrust Vs Vehicle Velocity for 36-cm Plate

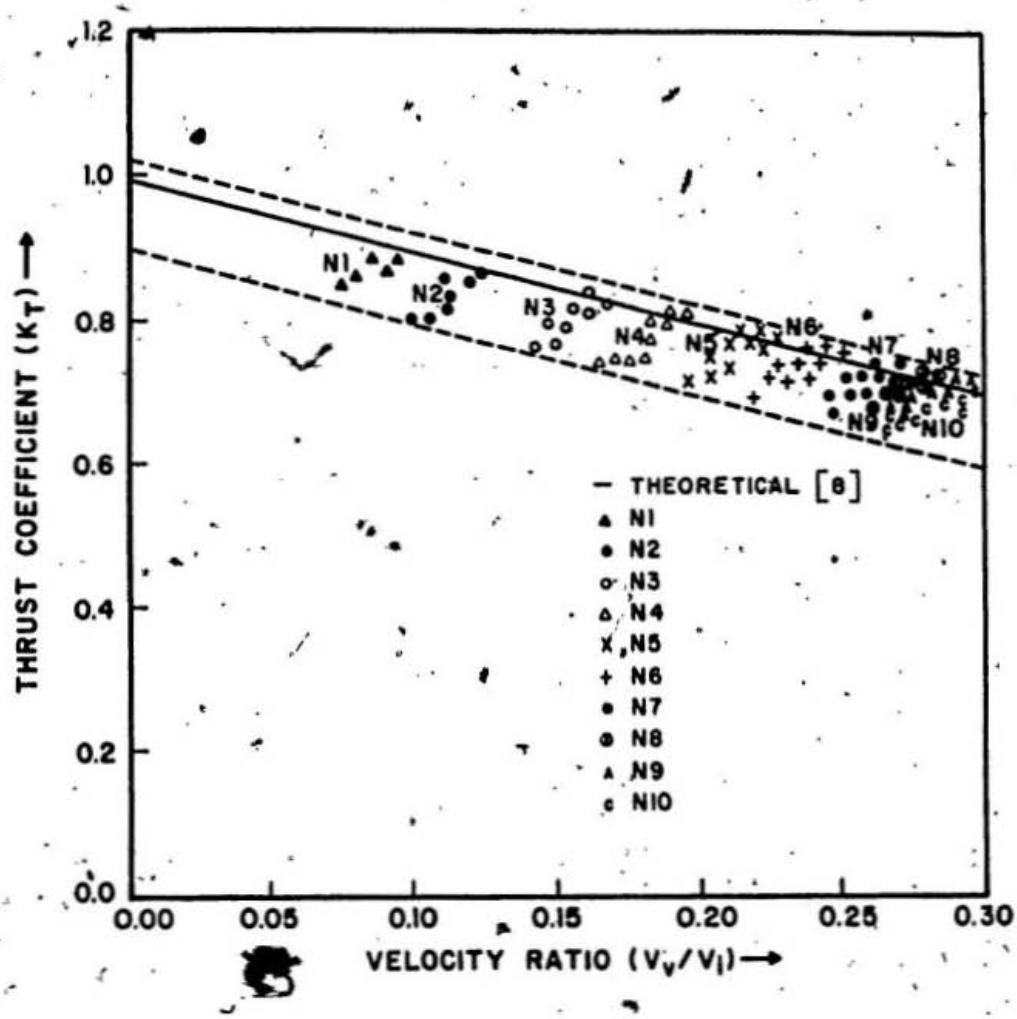

Fig. 42 Thrust Coefficient Vs Velocity Ratio

Fig. 43 Efficiency Vs Velocity Ratio for NDP (Compensated)

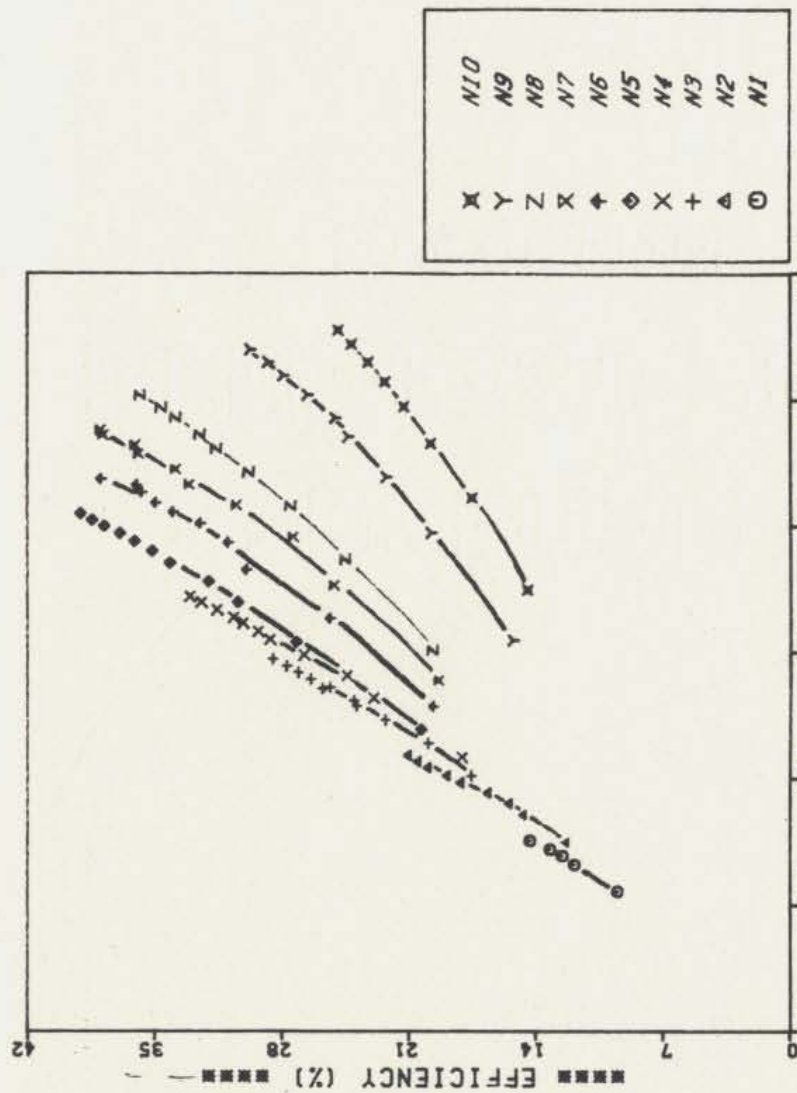

Fig. 44 Efficiency Vs Velocity Ratio for 20-cm Plate (Compensated)

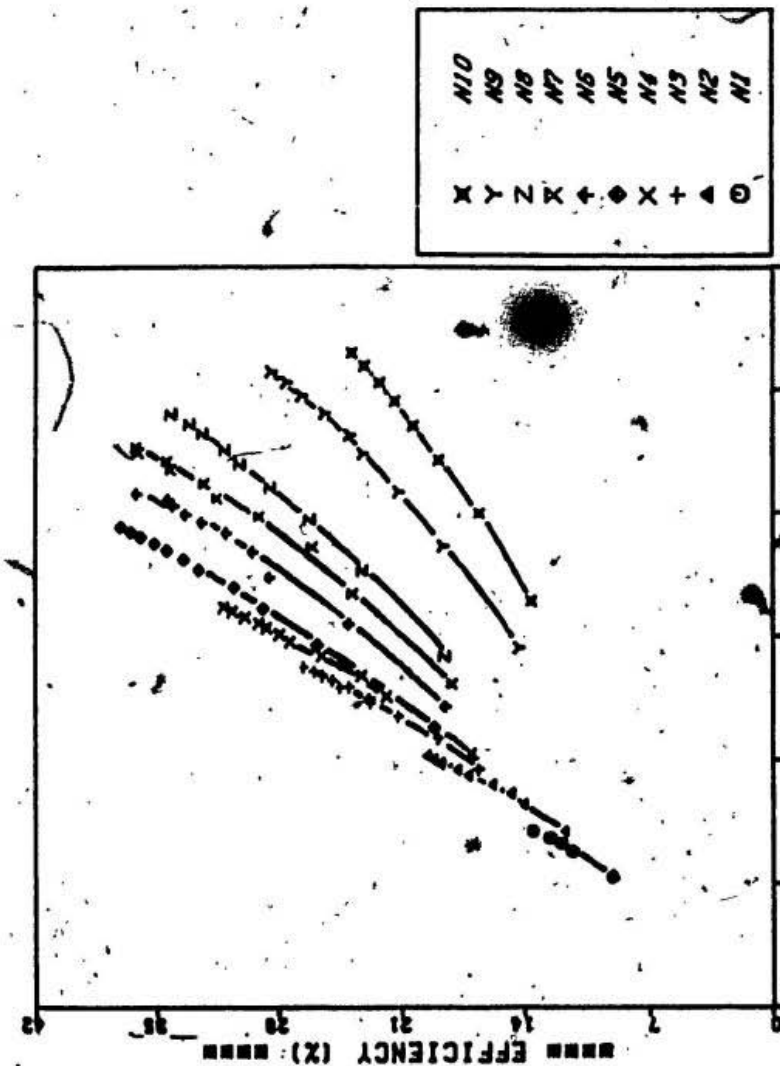

Fig. 45 Efficiency Vs Velocity Ratio for 24-cm Plate (Compensated)

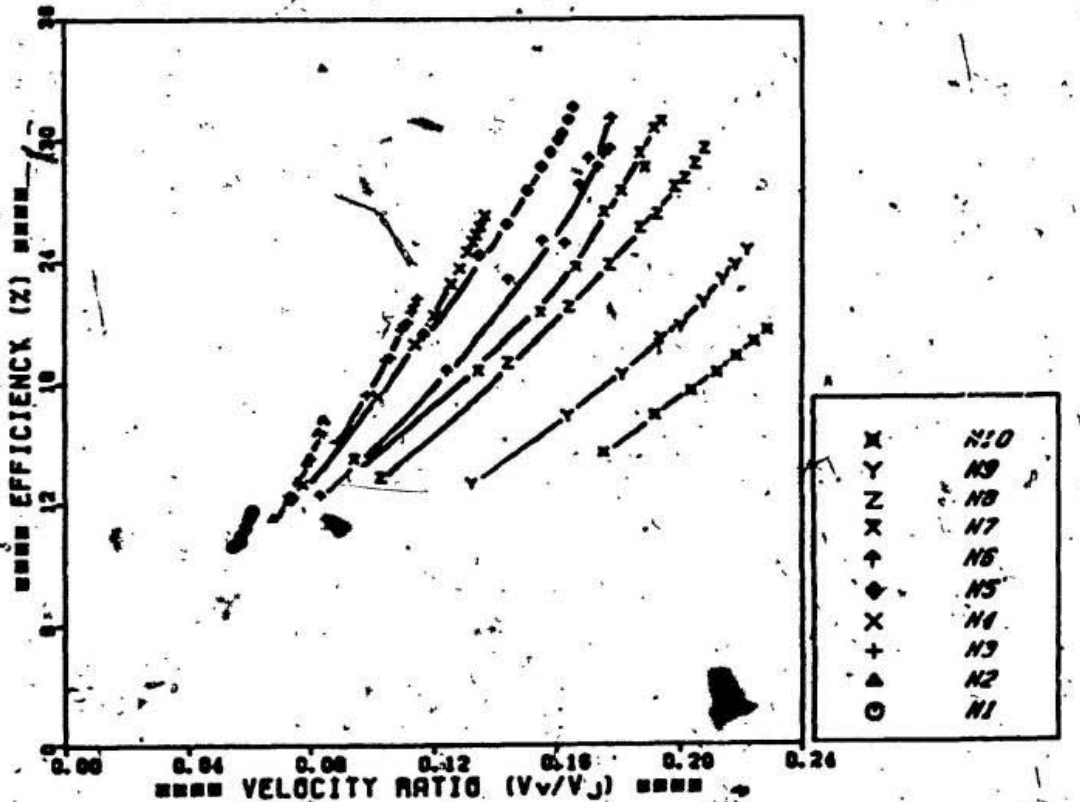

Fig. 46 Efficiency Vs Velocity Ratio for 28-cm Plate (Compensated)

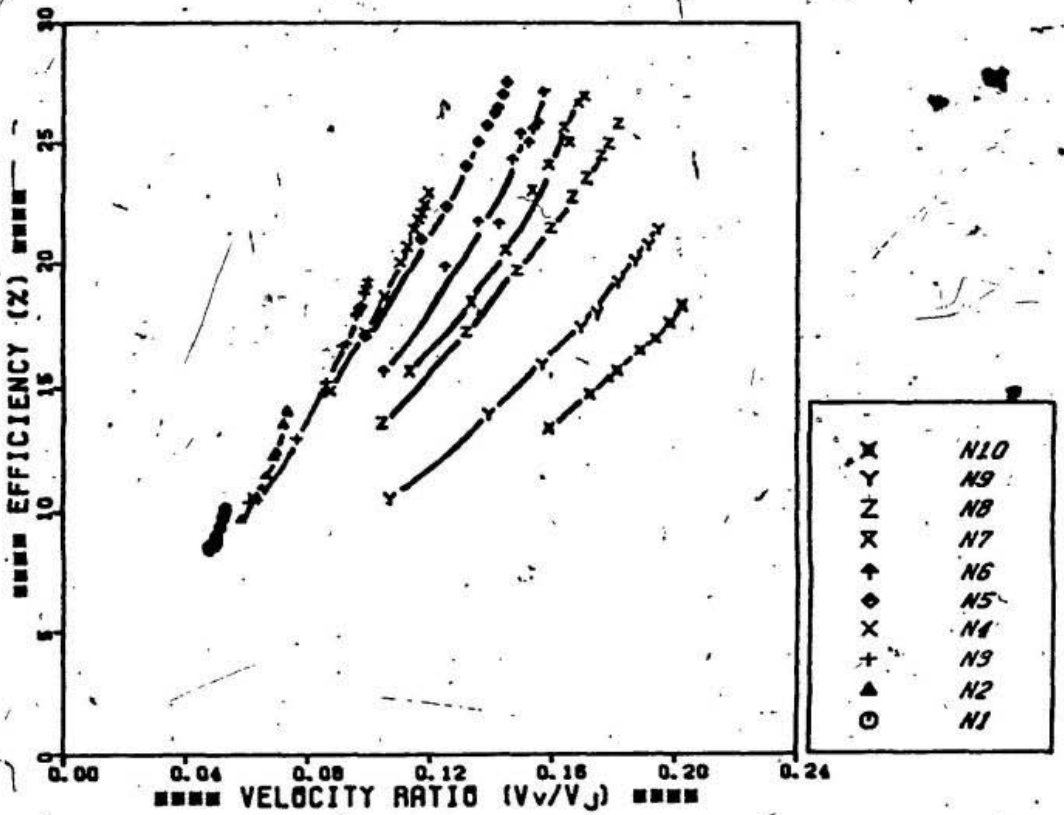

Fig. 47 Efficiency Vs Velocity Ratio for 32-cm Plate (Compensated)

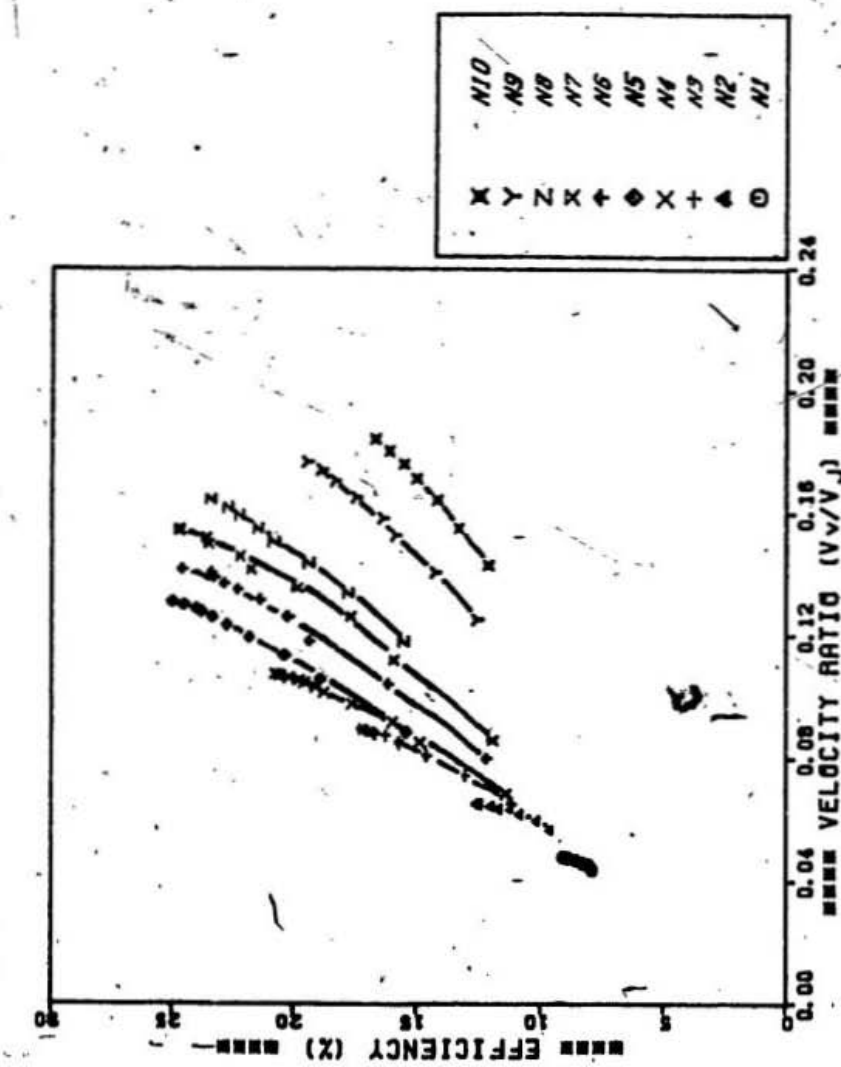

Fig. 48 Efficiency Vs Velocity Ratio for 36-cm Plate (Compensated)

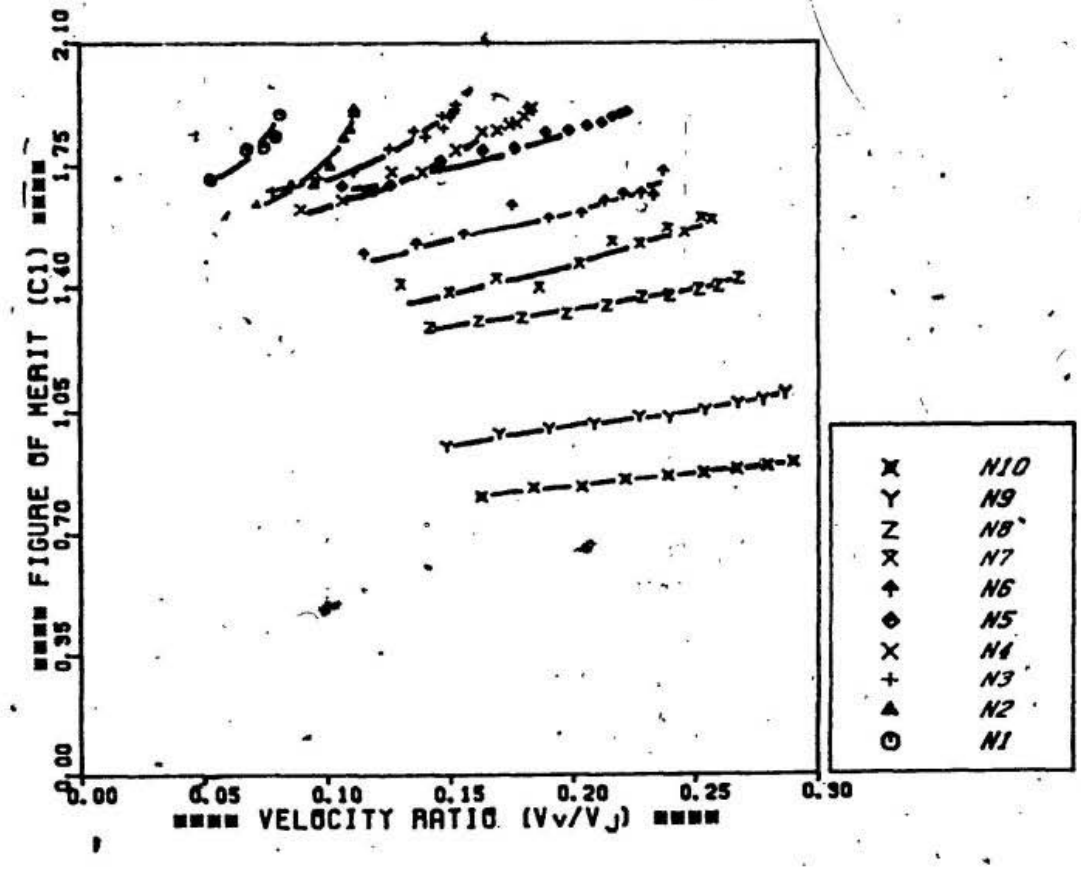

Fig. 49 Figure of Merit Vs Velocity Ratio for NDP (Compensated)

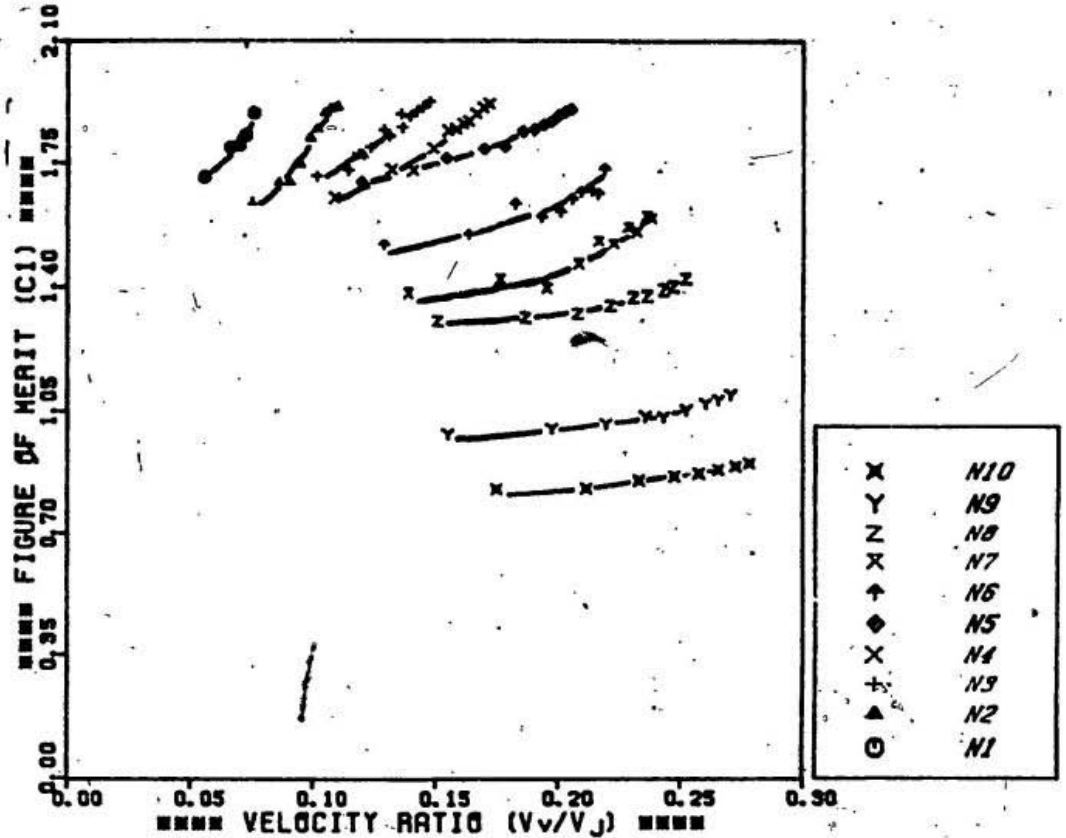

Fig. 50 Figure of Merit Vs Velocity Ratio for 20-cm Plate (Compensated)

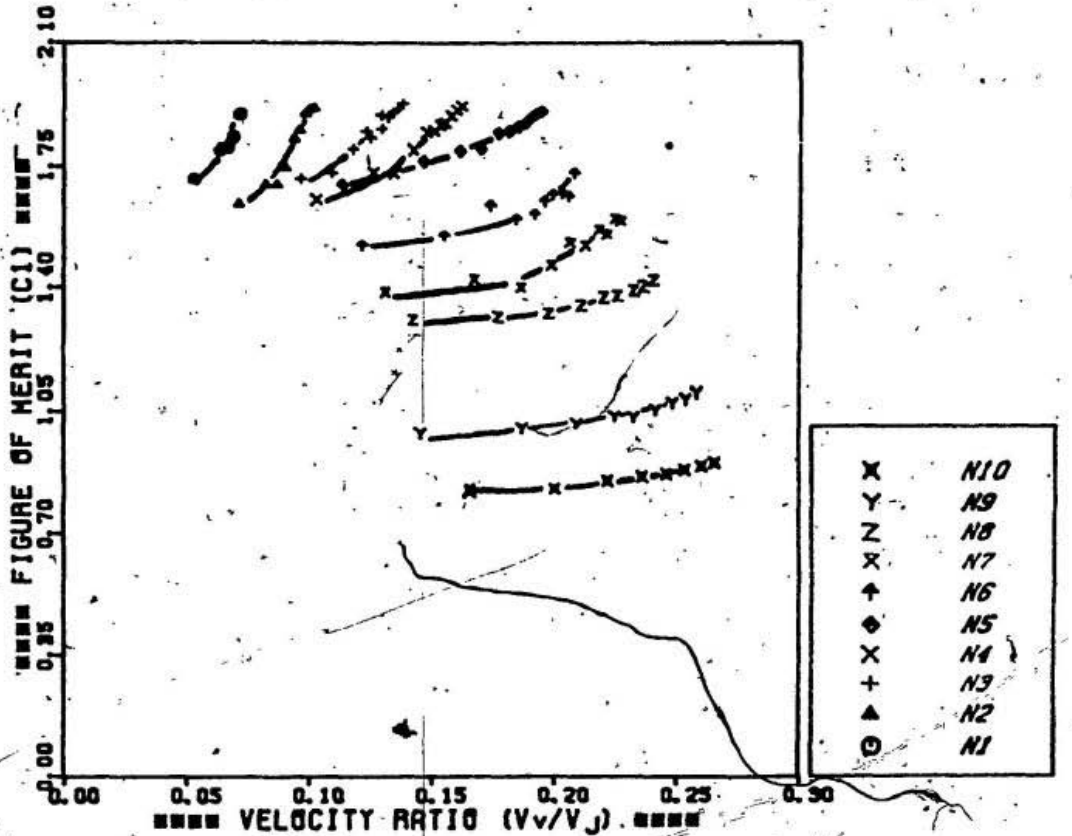

Fig. 51 Figure of Merit Vs Velocity Ratio for 24-cm Plate (Compensated)

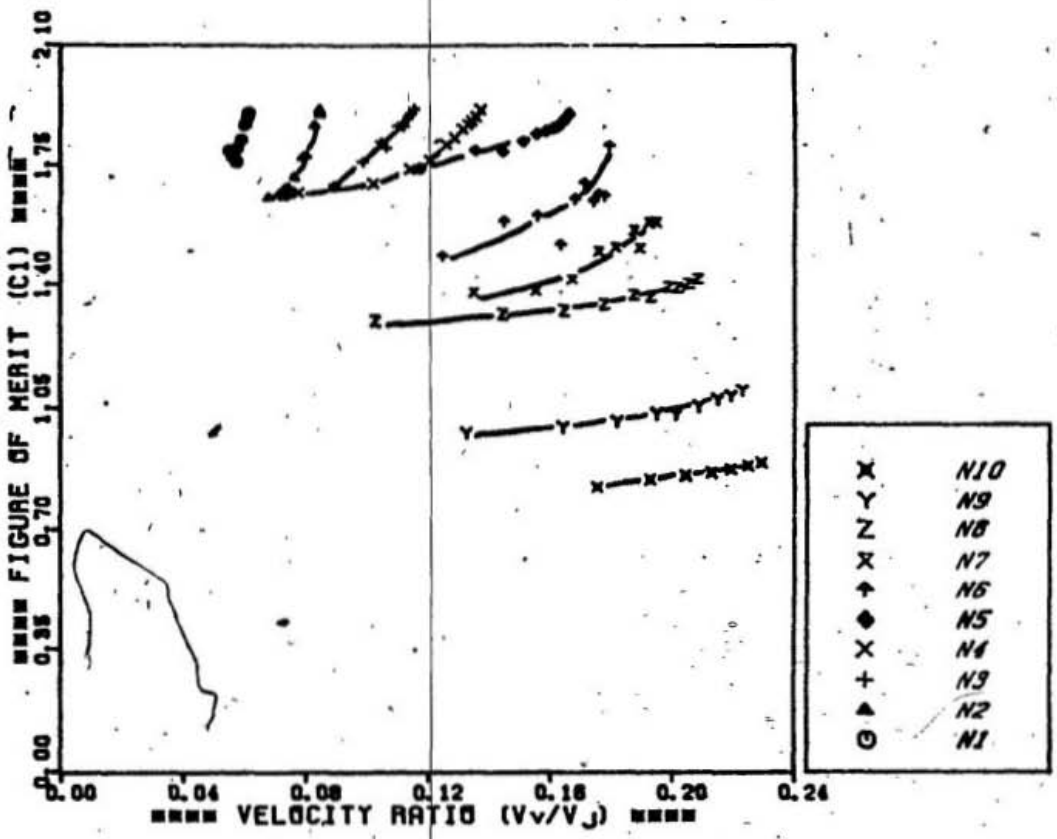

Fig. 52 Figure of Merit Vs Velocity Ratio for 28-cm Plate (Compensated)

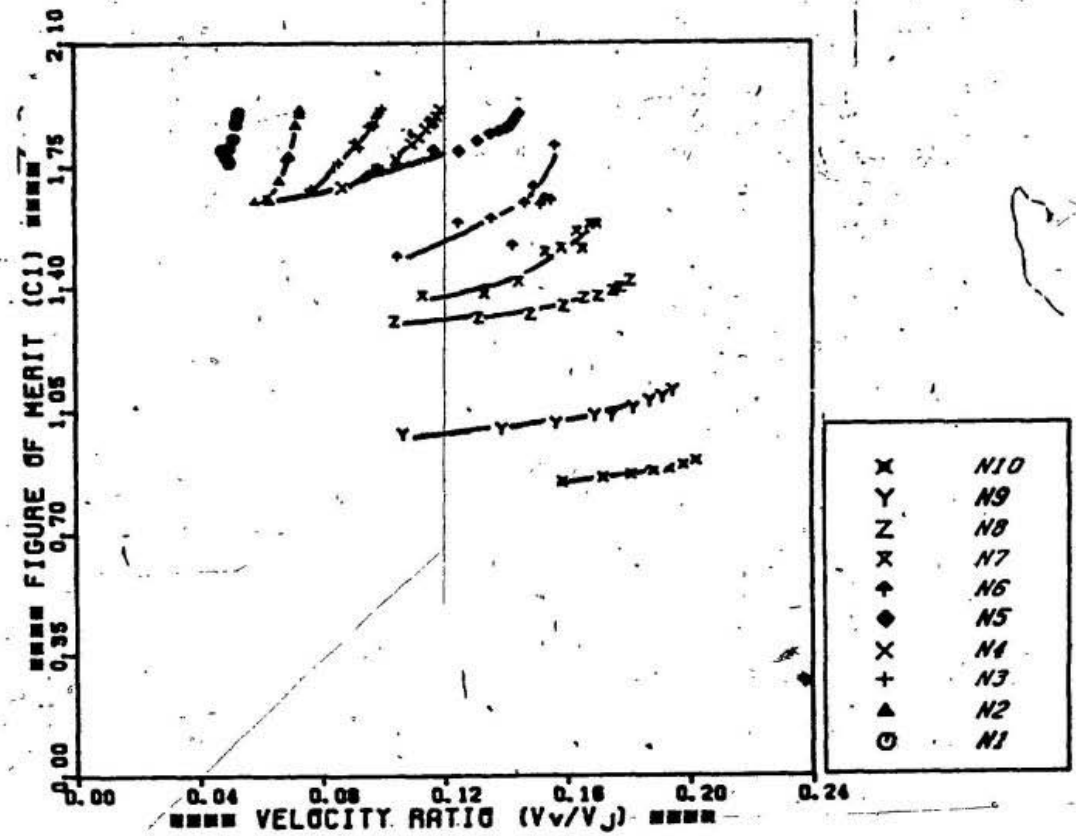

Fig. 53 Figure of Merit Vs Velocity Ratio for 32-cm Plate (Compensated)

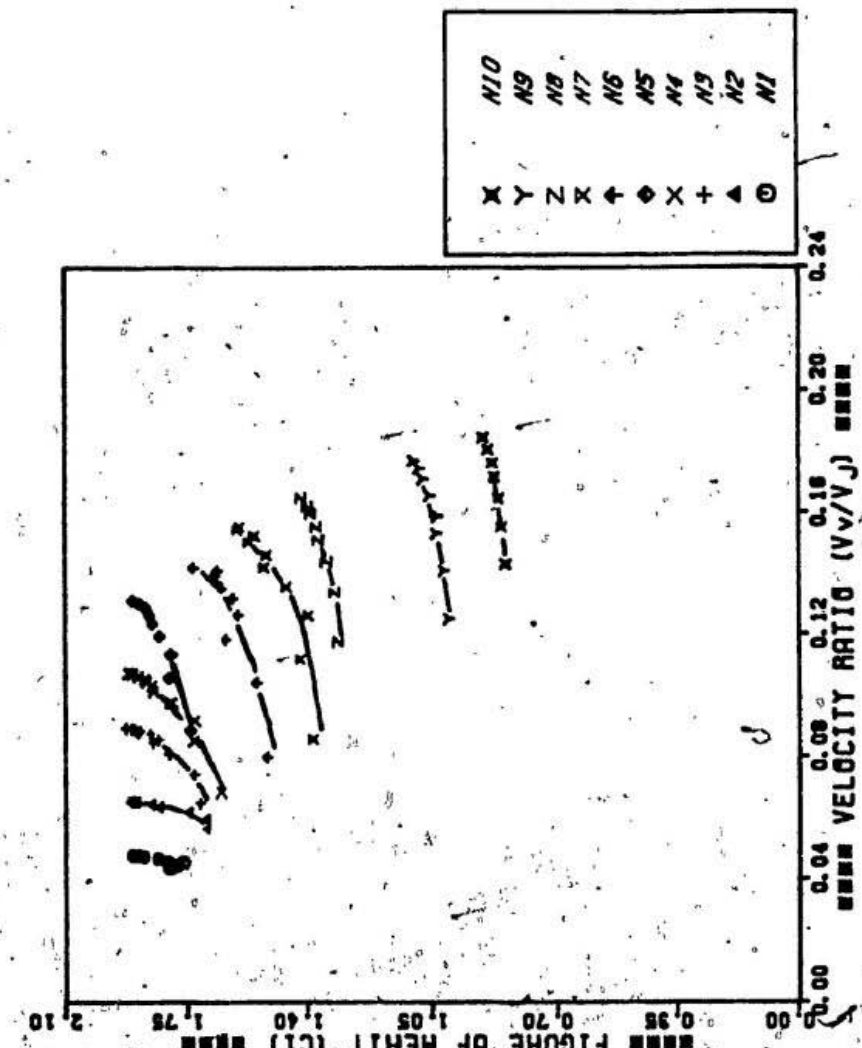

Fig. 54 Figure of Merit Vs Velocity Ratio for 38 cm Plate (Compensated)

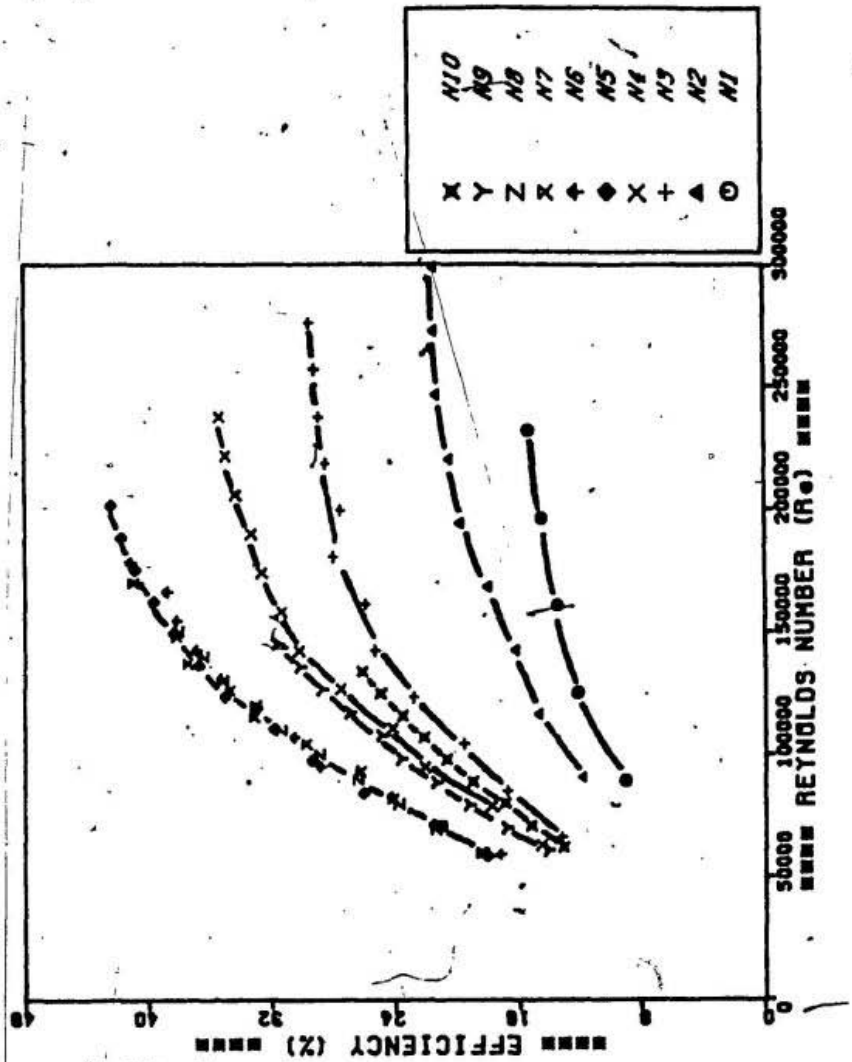

Fig. 55 Efficiency Vs Reynolds Number for NDP (Compensated)

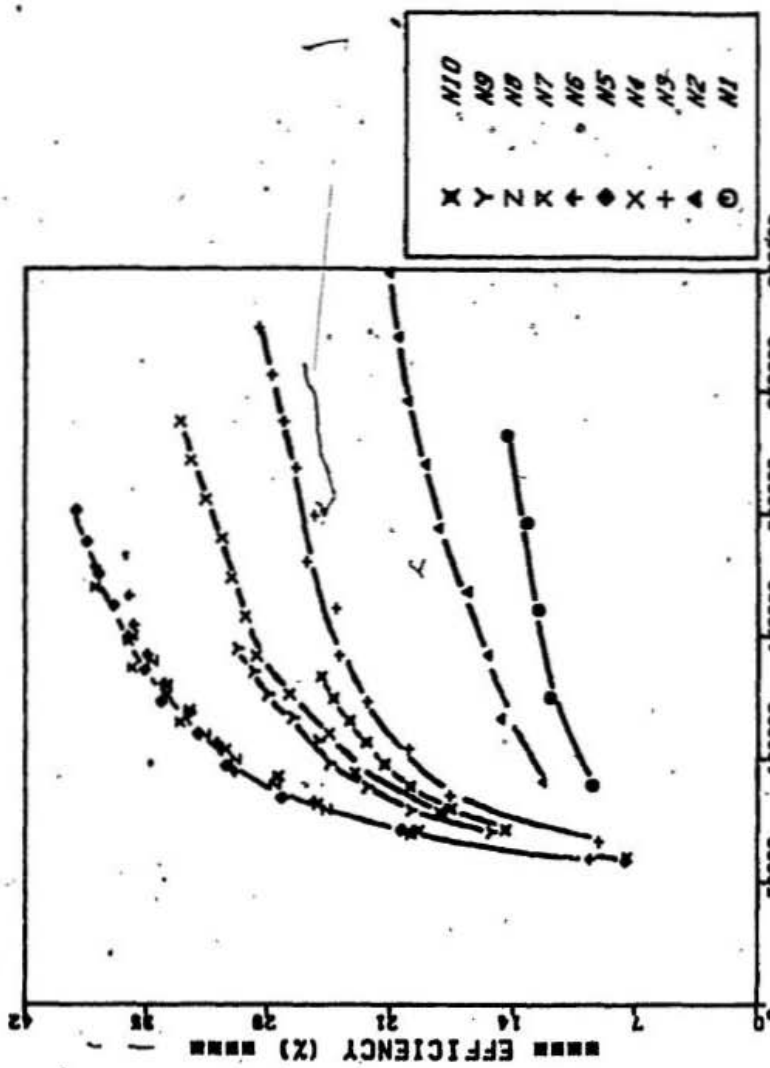

Fig. 56 Efficiency Vs Reynolds Number for 20-cm Plate (Compensated)

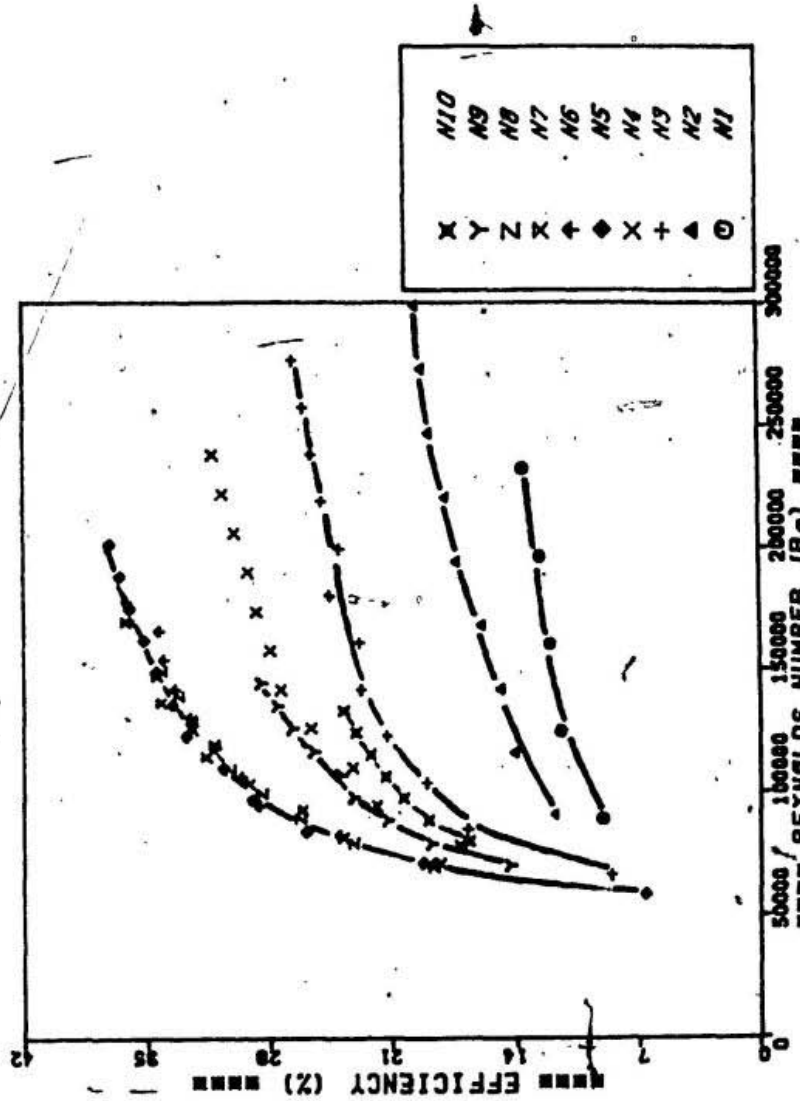

Fig. 57 Efficiency Vs Reynolds Number for 24-cm Plate (Compensated)

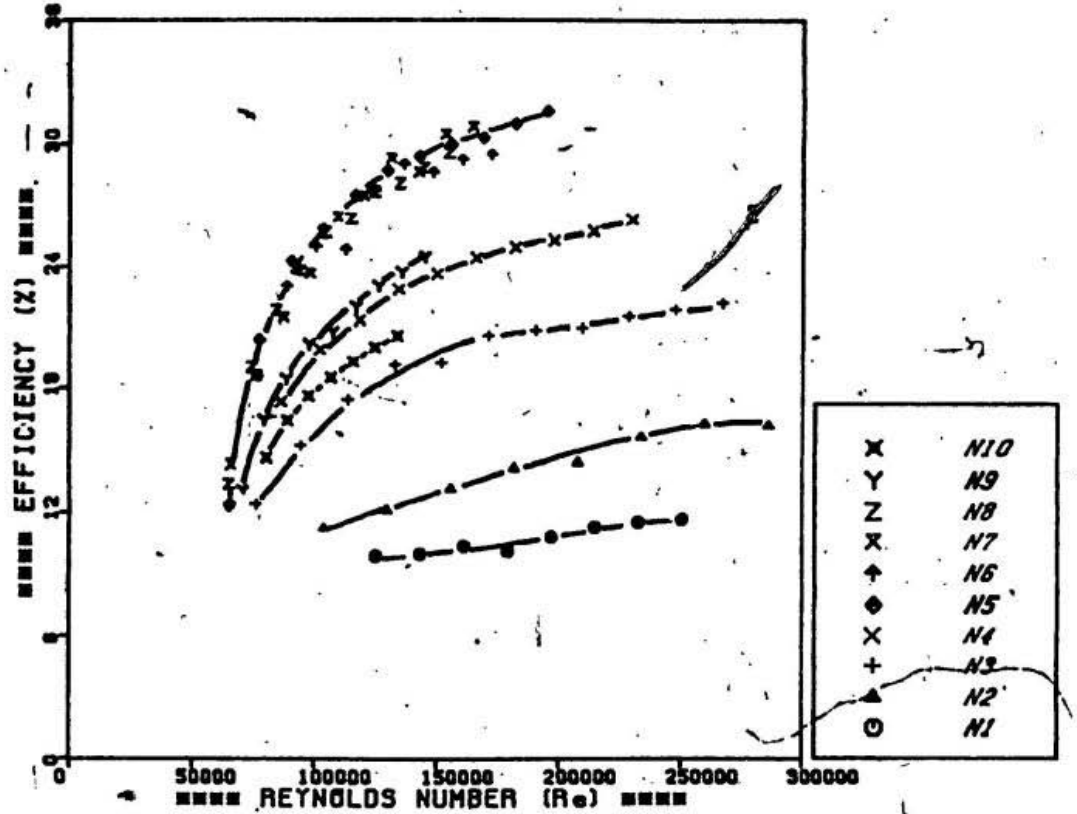

Fig. 58 Efficiency Vs Reynolds Number for 28-cm Plate (Compensated)

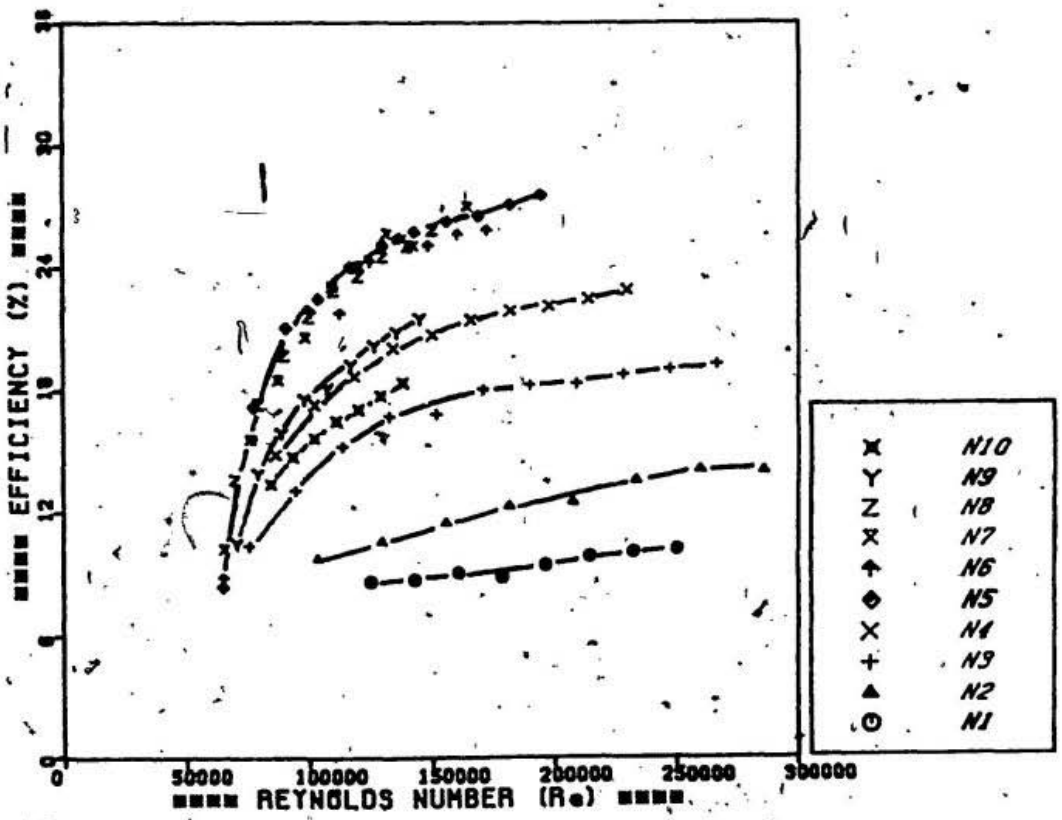

Fig. 59 Efficiency Vs Reynolds Number for 32-cm Plate (Compensated)

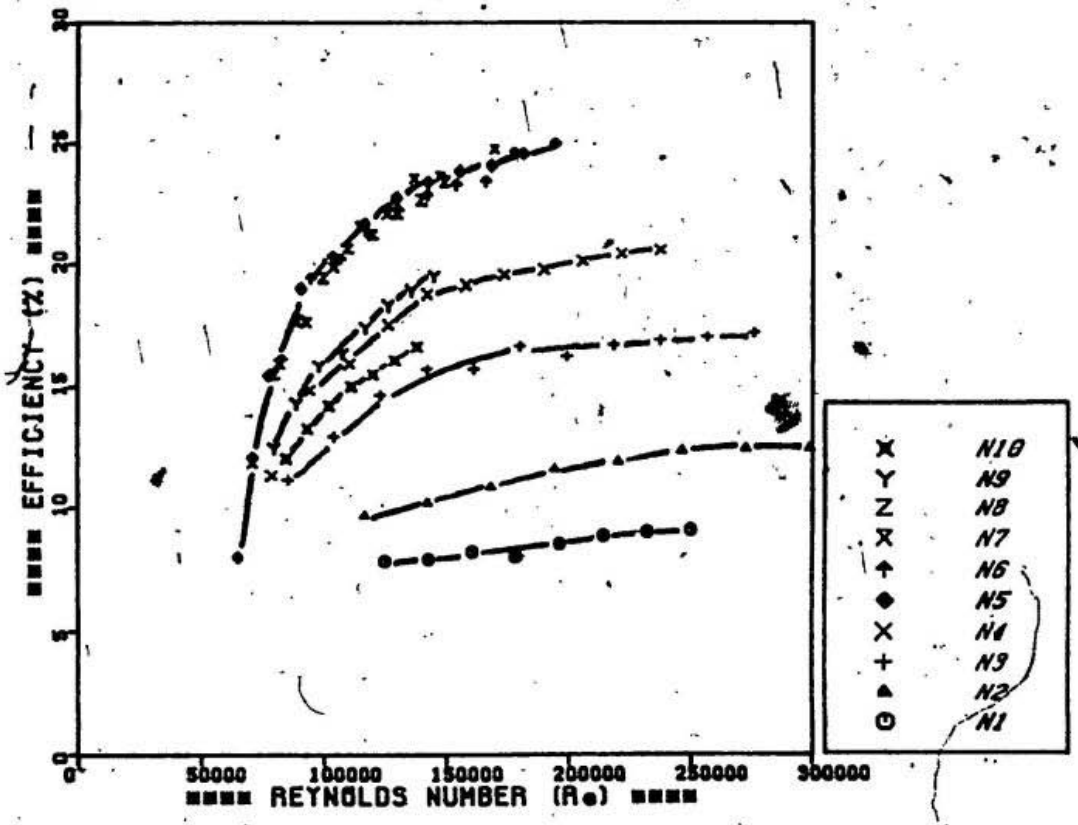

Fig. 60 Efficiency Vs Reynolds Number for 36-cm Plate (Compensated)

From Fig. 31, the maximum efficiency of 37% is obtained for maximum flow rate of $9.1 \times 10^{-3}\ m^3/s$ for N5 with 24 cm drag plate. N5 has overall good performance characteristics for range of flow rates from 3.5×10^{-3} to $9.1 \times 10^{-3}\ m^3/s$. N1, N2, N3, N4,....N10 have maximum efficiencies of 14%, 19%, 26%, 31%, 37%, 35%, 36%, 34%, 28%, 24% respectively. From Fig.32, the maximum efficiency of 32% is obtained for maximum flow rate of $9.1 \times 10^{-3}\ m^3/s$ for N5 with 28 cm diameter drag plate. N5 has overall good performance characteristics for the range from 3.2×10^{-3} to $9.1 \times 10^{-3}\ m^3/s$. N1, N2, N3, N4,....N10 have maximum efficiencies of 12%, 17%, 22%, 26%, 32%, 30%, 31%, 29%, 26%, 21% respectively.

From Fig. 33, the maximum efficiency of 28% is obtained for maximum flow rate of $9.1 \times 10^{-3}\ m^3/s$ for N5 with 32 cm diameter drag plate. N5 has overall good performance characteristic for the range from 3.2×10^{-3} to $9.1 \times 10^{-3}\ m^3/s$. N1, N2, N3, N4,....N10 have maximum efficiencies of 10%, 14%, 19%, 23%, 28%, 26%, 27%, 25%, 21%, 18% respectively. From Fig.34, the maximum efficiency of 25% is obtained for maximum flow rate of $9.1 \times 10^{-3}\ m^3/s$ for N5 with 36 cm diameter drag plate. N5 has overall good performance characteristics in the range from 3.3×10^{-3} to $9.1 \times 10^{-3}\ m^3/s$. N1, N2, N3, N4,....N10 have maximum efficiencies of 9%, 13%, 17%, 21%, 25%, 23%, 24%, 23%, 19%, 16% respectively.

From Fig. 35, N2 gives the maximum thrust of 117 newtons compared to other nozzles for the flow rate of $6.7 \times 10^{-3}\ m^3/s$. In addition, N1, N3, N4, N5 has the maximum thrust of 81, 101, 75, 54 newtons for flow rate of 4.1×10^{-3}, 8.5

x 10^{-3}, 8.7 x 10^{-3}, 9.1 x 10^{-3} m^3/s respectively. This is due to the fact that the flow gets choked for N1, N2, N3, N4, N5 at these flow rates. Thrust is reduced from N6 to N10 as the exit diameter of the nozzle is increased and the maximum flow rate is held constant. A friction of 4.128 Newtons must be compensated for at the rotating watertight joint before the thrust is measured.

Figs. 36 to 41, show the wall effect compensation for no drag plate, 20 cm, 24 cm, 28 cm, 32 cm, 36 cm diameter drag plates. For no drag plate the wall effects are less. Wall effects increase as the vehicle velocity increases and the maximum encountered is around 25% for the maximum speed of 1.6 m/s with 20 cm drag plate. The maximum wall effects decrease as the size of the drag plate is increased from 25% (max) to 10% (min).

Fig. 42 gives the thrust coefficient versus velocity ratio. It is seen that the values fall within the theoretical range (dotted lines). Figs. 43 to 48 show how the propulsion efficiency varies with the velocity ratio. Figs. 49 to 54 give an idea of how the figure of merit varies with the velocity ratio. Figs. 55 to 60 give the results put in non-dimensionalised parameters i.e. Propulsion efficiency versus Reynolds number.

These graphs indicate that as the flow rate is increased, the thrust and hence the vehicle velocity is increased. Comparison of the efficiency curves for different nozzles with different drag plates reveal the same type of characteristic.

The point to be noted is the variation of efficiency with the change in exit diameters. Though the velocity of jet decreases as the exit diameter is increased, there is a peak value for efficiency. The efficiency is at a maximum when the

velocity of the vehicle is close to the velocity of the jet. As the exit diameter is increased further, the vehicle velocity drops more rapidly than the jet velocity, thereby increasing the difference and consequently leading to a reduction in efficiency.

Improving the efficiency involves the lowering of the pump head and increasing the flow rate, which needs the incorporation of an axial flow pump.

The losses in the nozzle were found to decrease as the exit diameter of the nozzle was increased (table 1). However, the loss coefficients were decreasing as the exit diameter was increased (table-2 and 3). There is no correlation between the losses occuring in the nozzle to the propulsion efficiency obtained. The propulsion efficiency depends on the parameters like head developed by pump, the flow rate, the jet and vehicle velocities, and thrust produced. The loss coefficient of the whole system will play a role in determining the propulsion efficiency since losses in the nozzle are only about 5 to 10% of the entire losses.

Nozzle type	Flow Rate $Q \times 10^{-3}\ m^3/s$	Exptl. Loss $H_{L\,E}(m)$	Theoretical Loss $H_{L\,T}(m)$
N1	4.3	0.354	0.303
N2	6.8	0.260	0.213
N3	8.5	0.125	0.110
N4	8.8	0.075	0.063
N5	9.1	0.043	0.036
N6	9.1	0.034	0.029
N7	9.1	0.026	0.026
N8	9.1	0.021	0.018
N9	9.1	0.018	0.016
N10	9.1	0.014	0.013

Table 1 Experimental and Theoretical Energy Loss (Maximum)

Nozzle type	Flow Rate $Q \times 10^{-3}\ m^3/s$	Exptl. Loss Coefft. $K_E \times 10^{-2}$	Theoretical Loss Coefft. $K_T \times 10^{-2}$
N1	1.46	2.36	1.61
N2	2.08	2.38	1.62
N3	2.08	2.63	1.78
N4	2.31	2.81	2.01
N5	2.92	3.22	2.51
N6	3.21	3.41	2.75
N7	3.21	3.70	3.04
N8	3.80	3.91	3.35
N9	3.80	4.09	3.72
N10	4.50	3.75	3.91

Table 2 Exptl. and Theoretical Loss Coefficients (Maximum)

Nozzle type	Flow Rate $Q \times 10^{-3}$. m^3/s	Exptl. Loss Coefft. $K_E \times 10^{-2}$	Theoretical Loss Coefft. $K_T \times 10^{-2}$
N1	4.1	1.66	1.49
N2	6.8	1.72	1.35
N3	8.5	1.75	1.46
N4	8.8	1.95	1.63
N5	9.1	2.32	2.01
N6	9.1	2.54	2.25
N7	9.1	2.90	2.61
N8	9.1	3.22	2.81
N9	9.1	3.47	3.34
N10	9.1	3.50	3.56

Table 3 Exptl. and Theoretical Loss Coefficients (Minimum)

CHAPTER 6

FEASIBLE ROV DESIGN WITH TILTING TYPE NOZZLES

6.1 GENERAL:

This chapter deals with the feasible design of a jet propelled ROV with tilting type nozzle. The vehicle is designed neutrally buoyant [13], [18],[27] and checked for stability. The experimental results from the 32 cms diameter drag plate can be utilised for this ROV design. Detailed drawings of the vehicle are presented. Also, a control flow diagram is given. The hydraulic system presently in use is described and compared with the design.

6.1.1 ORIGINALITY OF THE ROV DESIGN:

The proposed ROV design came out of an innovative idea of using a jet propulsion system for small, slow-moving ROV applications. The design presented is 100% original and upto date, this type of propulsion with tilting type nozzles have not been tried for ROV applications. The tilting type nozzles improve the maneuverability of the vehicle. The whole system becomes simpler and compact. The fact that less number of components need to be pressure compensated, adds to the advantage over the previous designs.

6.2 FEASIBLE ROV DESIGN:

6.2.1 DESIGN REQUIREMENTS:

It is essential that the following requirements are satisfied:

(i) the centre of gravity (G) and the centre of buoyancy (B) are on the same vertical line. This is necessary to avoid any overturning couple.

(ii) the centre of gravity (G) should be well below the centre of buoyancy (B). This is necessary to ensure stability of the vehicle in all propulsion modes.

6.2.2 ROV COMPONENTS:

The description of the components used in the ROV design is presented. The materials chosen are to be light in weight, low in cost and suitable for ocean environment.

(i) Motors: There are two motors used in this design. One is the main propulsion motor (three phase 440 Volts AC), with variable frequency for adjustable speeds, The power required to drive the designed vehicle is 5 h.p.(maximum). Second is a stepper motor (with double end shaft), for tilting the nozzles. This has a capability of 1.8 degree rotation per step. Both these motors are fluid filled pressure compensated electric motors.

(ii) Pump: An axial flow pump with high discharge to produce the required thrust is used. The discharge can be varied with the speed of the propulsion motor. A filter mesh at the inlet of the pump is essential to screen off the debris.

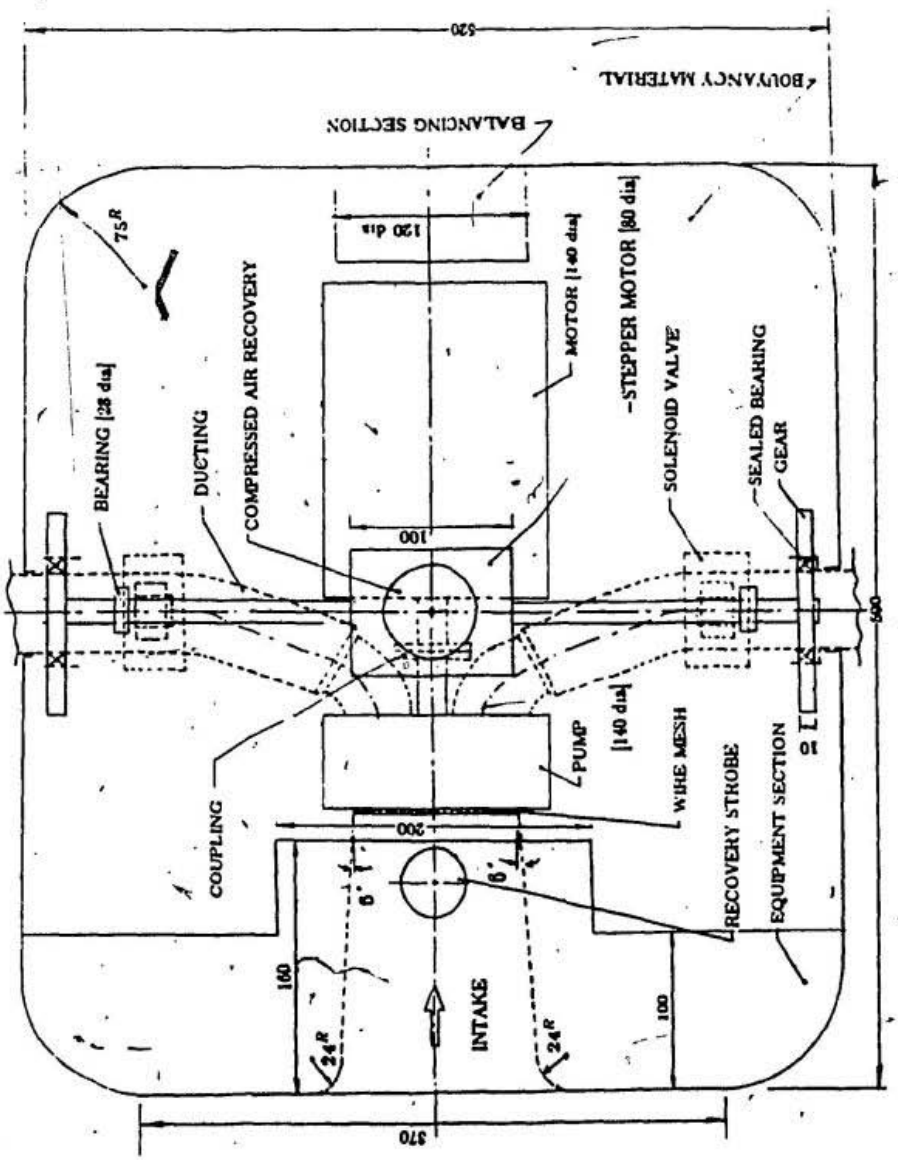

Fig. 61 Plan-View of the ROV Designed

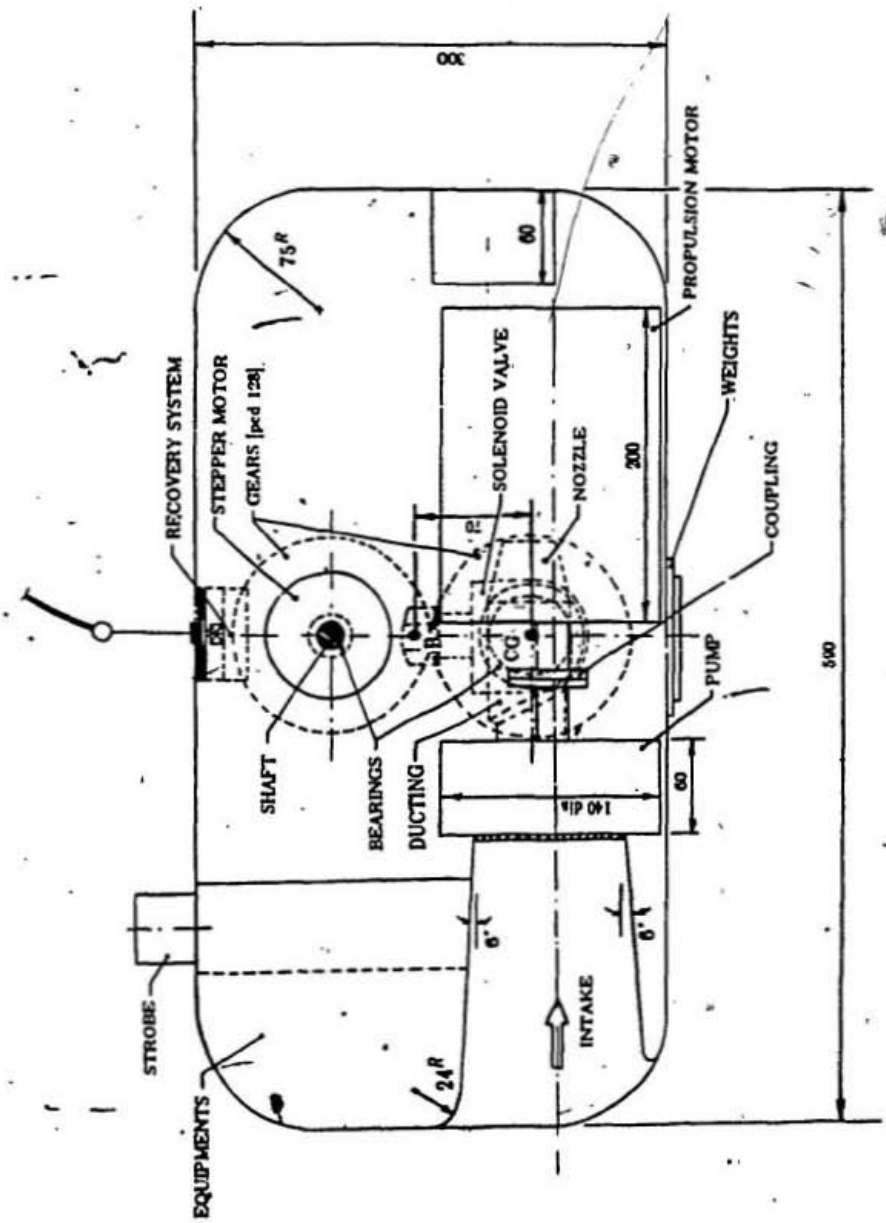

Fig. 62 Elevation-View of the ROV Designed

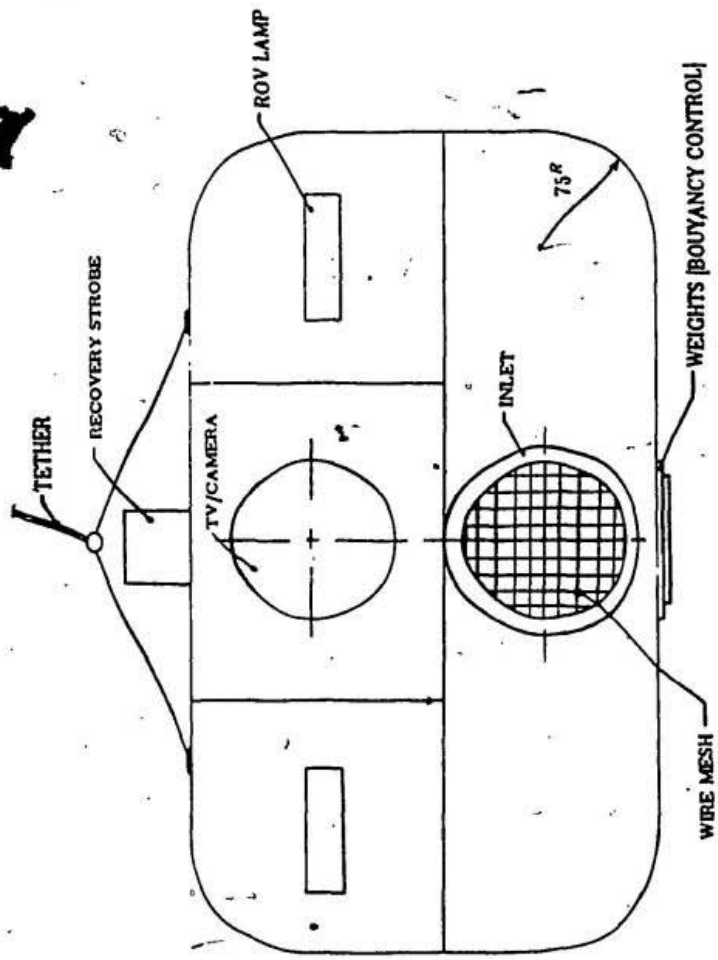

Fig. 63 Front-View of the ROV Designed

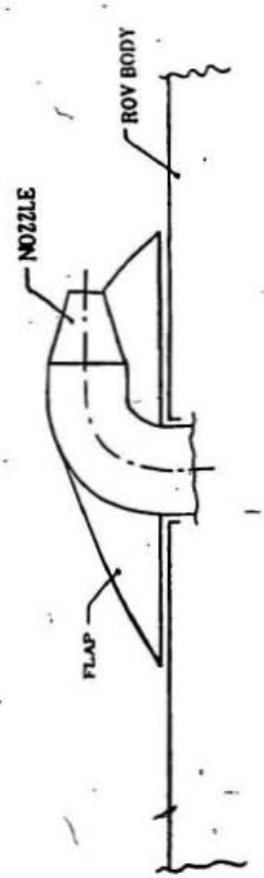

Fig. 64 Nozzle Arrangement

(iii) Solenoid valves: Two pressure compensated solenoid valves are used: one for each nozzle to permit differential flow. These valves could be of two types as either open/close or gradual open and gradual close. Here, gradual open and gradual close type is preferred.

(iv) Hull/Structure: The ROV has an enclosed type of hull which reduces the drag compared to the open frame construction. Fibre-reinforced Plastic is used because of its strength and resistance to corrosion. For buoyancy, liquid foam (a kind of syntactic foam) is used because of its ability to to reach great depths (20,000 feet) and can be used in any volume or shape.

(v) Sensors: The primary sensor for most ROV's is the TV camera. For illumination, a light source is essential. For search of debris and recovery applications, a sonar system is needed. Vehicle status monitors include a wide variety of sensors, but three of the more important ones are the compass, depthometer, and the altimeter. NDT equipment is needed if the ROV is to perform some non-destructive testing. Also, a strobe flash is essential for easy location of the ROV while recovery.

6.3 ROV DESCRIPTION:

The ROV has a "rectangular-box" like appearance with dimensions of 590 x 520 x 300 mm^3 having smooth corner sections and weighing about 40 Kg. The intake is located at the front end in the centre and is cylindrical having an outside diameter of 125 mm with slight tapering of 6 ° inward. The intake end is connected to a high flow rate axial flow pump. There is a wire mesh at the inlet

to the pump to avoid the intake of debris. The discharge is varied by the speed of the drive motor (diameter 140 mm), by varying the frequency from board. The drive motor is connected to the pump by a large coupling with provision to absorb shocks. The impeller diameter is about 140 mm. There are two outlet discharge sections of 45 mm diameter from the pump and which in turn is connected to a 50 mm diameter ducting. The ducting is separated at the ends and sealed bearings are employed; one at each end to facilitate the rotation of the nozzles along with the 90° elbow ducting. Nozzles are connected at the end of the elbow joint.

A stepper motor of 80 mm diameter and 100 mm in length is placed such that its centre of gravity lies 128 mm above and on the same vertical line as the centre of gravity of the ROV. The stepper motor has a double end shaft and two fibre reinforced plastic spur gears (of PCD 128 mm) are attached; one at each end of the shaft. There are two bearings between the gears and the stepper motor. These spur gears mesh with the gears of the same PCD and same number of teeth mounted on the ducting. Two spheroidal valves, one for each ducting, are placed in front of the gears. These are of the gradual open/close type to facilitate easy maneuvering of the vehicle.

A balancing weight section of 120 mm diameter and 60 mm in length is positioned at the rear end of the ROV with its centreline at a height of 110 mm from the base. Also weights are placed at the bottom of the ROV in line with the ROV's centre of gravity. These ensure proper balancing and neutral buoyancy for the ROV. Since the ROV is neutrally buoyant, a flexible air bag (operated in case

of power failure) is placed at the top centre end of the ROV for recovery of the vehicle. The front end of the ROV (about 100 to 160 mm) is for equipment such as TV/Camera, NDT, SONAR, etc., All the electrical components such as the main propulsion motor, the stepper motor and solenoid valves need to be pressure compensated by enclosing them in a oil container and exposing one end to the ambient pressure by means of bellows.

6.4 NOZZLE CONFIGURATIONS:

The configurations that could be used for ROV applications fall into two categories:

(i) Stationary type

(ii) Swivel type

(i) Stationary type: In this case the nozzles are held stationary with respect to the ROV body. Hence for each direction of motion of the ROV, there is a nozzle in that direction. That is to say for six motions (Fig. 65), there should be six nozzles with suitable solenoid valves. This increases the weight and the drag of the ROV. Rotations are possible by differential flow through a pair of nozzles.

(ii) Swivel type: In this case, the nozzles are swivelled with respect to the ROV body. Hence, only one pair of nozzles is required. Also, this type ensures motions in all possible directions by swivelling the nozzle to the required direction. For rotations, as in the case of stationary type, differential flow through the nozzles would be required.

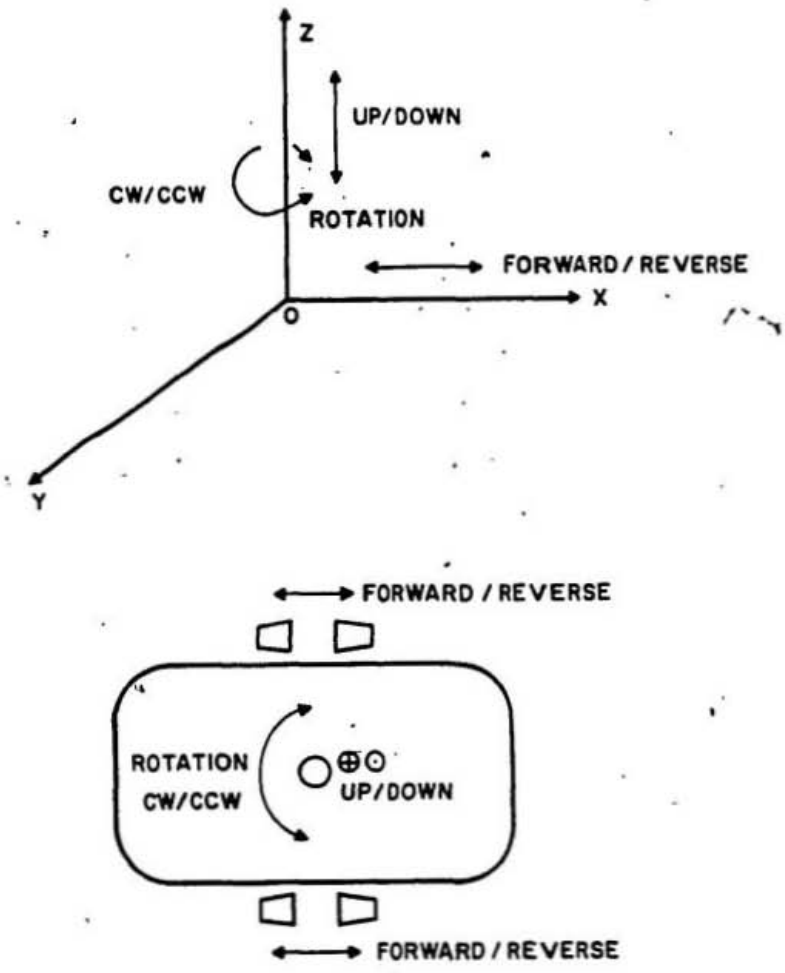

Fig. 65 ROV Movements and Nozzle Positions

Component	Weight(Kg)
Propulsion Motor	15
Pump	3
Stepper Motor	5
Solenoid Valve(2)	2
TV/Camera, NDT equipments	5
Rectifier AC/DC	2
Bearing(4)	0.25
Gear(4)	0.25
Flange Coupling	0.20
Nozzle Arrangement(2)	0.50
Other Accessories	5

The total weight of the ROV is 40 Kg. The centre of gravity (G) is located on the same vertical line 70 mm below the centre of Buoyancy (B).

In comparisons of both the types, with reference to ROV applications, the swivel type is preferable due to:

(i) Lower system weight.

(ii) Movements in all possible directions is attainable.

(iii) Improved maneuvering qualities.

(iv) Less drag.

(v) System is simpler.

However, the system with a swivel type needs a stepper motor for rotating the nozzle pair precisely to the required direction. This makes pressure compensation of the stepper motor essential.

6.5 EXPERIMENTAL SIMULATION:

The designed vehicle in forward translation, simulates the experimental drag obtained by using the drag plates. This is done by considering the vehicle to be elliptical box-shaped and equating the vehicle drag and the model disc drag, knowing the coefficient of drag for both these cases. The actual drag considering the cross section alone for both the ROV and the model will be different (the disc has a higher drag); However, since the drag coefficients are taken quite precisely, we can equate these two drag and find the size of the disc which has the same drag as the designed ROV.

$$\textit{Drag of the vehicle} = \frac{1}{2} C_{D\,V}\, \rho\, A_V\, V_V^2$$

$C_{D\,V} \approx 0.525$ (considering the section to be elliptical - box shaped; reference 27)

$$Drag\ of\ the\ model\ disc = \frac{1}{2} C_{D\,M}\ \rho\ A_M\ V_V^2$$

V_V is same for both simulation and design cases.

$C_{D\,M} \approx 1.03$ (considering circular disc drag plate for reynolds number greater than 2×10^4; reference 27)

Using the drag formula for the model disc, the drag of the circular disc plate can be found.

Under simulated conditions, drag of both cases should be the same.

Thus,

$$\frac{1}{2} C_{D\,V}\ \rho\ A_V\ V_V^2 = \frac{1}{2} C_{D\,M}\ \rho\ A_M\ V_V^2$$

Hence,

$$A_M = \frac{C_{D\,V}}{C_{D\,M}}\ A_V$$

Since $A_M = \frac{\pi}{4} D_M^2$ and $A_V = 30 \times 52\ cm^2$,

$D_M \approx 32\ cm$ *diameter* disc plate for forward translations

$D_M \approx 44\ cm$ *diameter* disc plate for vertical translations

Though there might be some means of estimating wake induced drag, a direct estimation for the experimental set-up under investigation is difficult. However, since the velocity is measured over a large number of revolutions, the effect of wake will have been implicitly considered in the measured velocity. After a few

revolutions, the experimental observations demonstrated a steady state behaviour. The unsteadiness due to the walls have however been compensated by towing the model in the wave tank and the compensated velocities are used in the calculation of the propulsion efficiency.

6.6 EXPERIMENTAL RESULTS IN ROV DESIGN:

The experimental results obtained in this investigation gives an insight into the jet propulsion system for small, slow-moving ROV applications. Firstly, the magnitude of the propulsion efficiency (around 40%), that is obtained by using jet propulsion for slow speed applications. Secondly, the energy losses that are occuring in the nozzles for these range of flow rates required to propel the ROV. Finally, the experiments help to choose the best nozzle for a particular application taking into account the flow rate and the drag of the ROV. Interchanging of the nozzles could be done with ease to obtain the best performance of the ROV.

6.7 HYDRAULIC SYSTEM:

The system that is currently in use is the hydraulic system. This is basically an electro-hydraulic system having inherent advantages as reliability, ease of maintenance, and versatility in adaptation of underwater work tools. Normally, a pressure compensated electric motor is used to drive a continuously running positive displacement hydraulic pump at a certain speed. System pressure is set at a

definite level over ambient sea water pressure by high pressure relief valve. A pressure reducing valve provides a less pressure supply for various low power requirement actuators (Fig.66).

A fully pressure compensated hydraulic system could be utilized. This includes a reservoir, with a compensating bladder, within which all valving is contained. This compensated system is also tied into the thruster shaft housings to eliminate high pressure seal and pressure housing requirements. With this, the hydraulic system is capable of application to far greater depths without modification.

Fig.67, shows an electrical and control system used in the hydraulic system. The power converter consists of a tapped three phase transformer set in order to accommodate a variety of line voltage and umbilical cable lengths, a ground detector, appropriate circuit protectors and a motor starter. A fully pressure compensated submersible electric motor drives the hydraulic pump. This motor is operated continuously with a constant load and as a result, voltage regulation problems are nearly non-existent. Other electrical equipments are operated from transformers and regulated voltage supplies (AC/ DC).

But however, due to more number of components to be pressure compensated in the case of a hydraulic system, the design putforth in this thesis is preferred. Fig.68 gives the block diagram of a computer control of an ROV. It is discretised into two areas, namely the computer on board and the ROV. The complete history of the vehicle at each position is well monitored with vehicle feed back, and a good control of the vehicle is achieved. Fig.69 gives the block

diagram of the various parameters controlled by the computer and guidance system of the ROV.

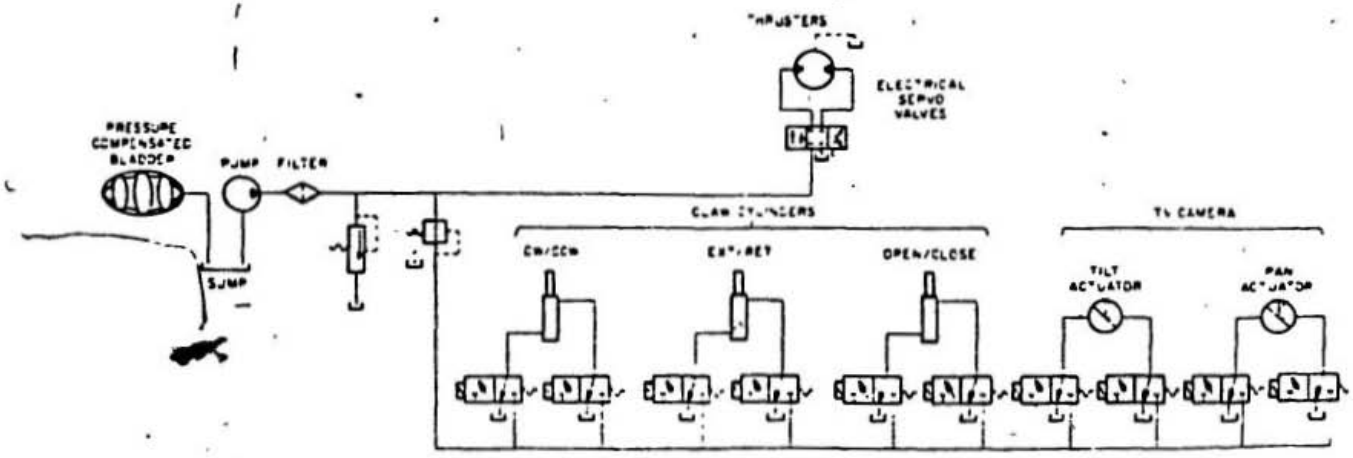

Fig. 66 Hydraulic Circuit for ROV [20]

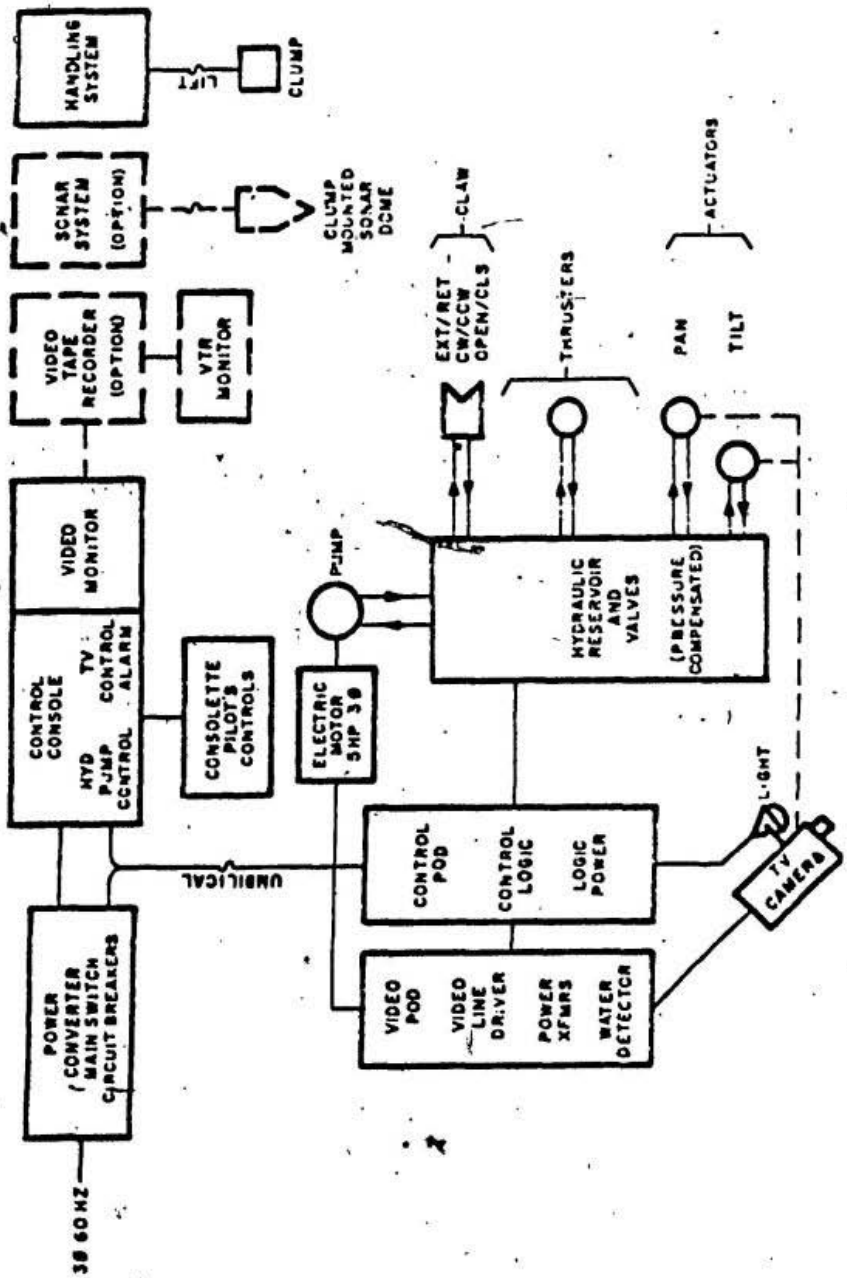

Fig. 67 Block Diagram of Hydraulic Control System for ROV [20]

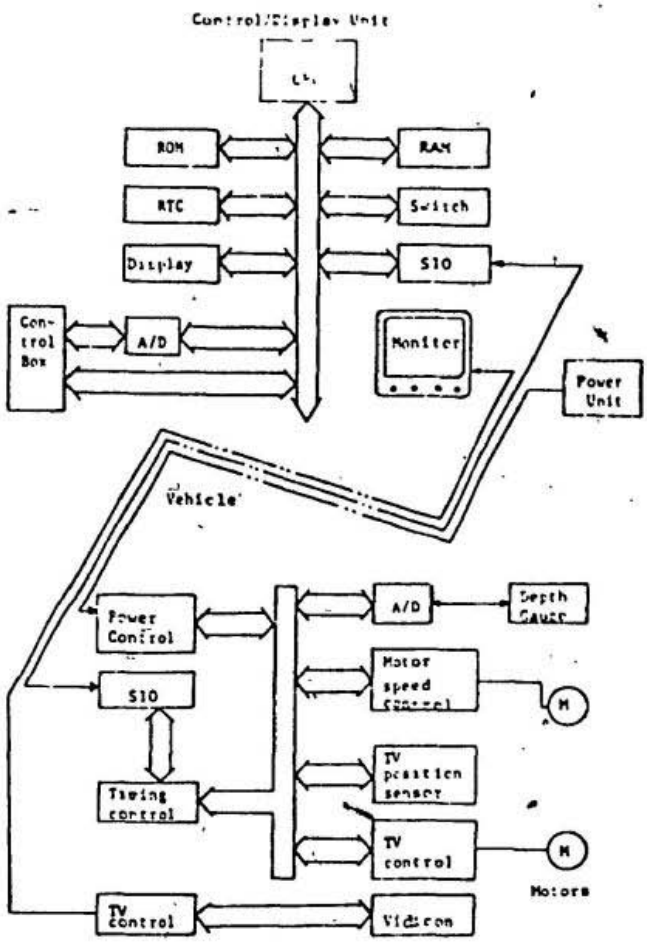

Fig. 68 Block Diagram of Control System for ROV [22]

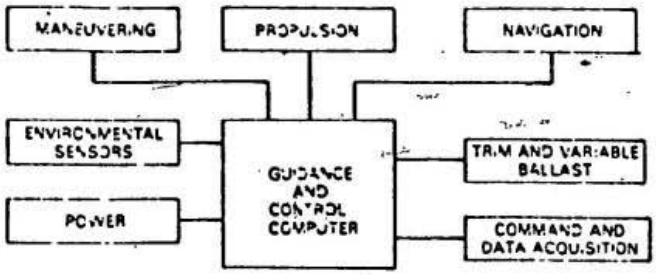

Fig. 69 Block Diagram Showing Parameters Controlled [14]

CHAPTER 7

SUMMARY AND CONCLUSIONS

7.1 DISCUSSION:

The results of the research reported in this thesis is an outcome of previous lack of experimental results to evaluate the feasibility of using a jet propulsion system for small, slow-moving ROV's (velocities not exceeding 4 knots), utilising ambient fluid for its movements. The experimental investigation is aimed at studying the effect of different conical nozzles on the propulsion performance and arriving at the optimum nozzle configuration.

Ten different nozzles of various conical profiles were used for five different circular shaped disk type drag plates simulating the drag of an ROV moving under water. The energy loss in the nozzles was determined by experimental and analytical methods. A feasible design of a jet propelled ROV with tilting type nozzles is presented. Compensation for wall effects were done by towing the model in an open water wave tank.

It was found that the nozzle having an exit diameter of 44 mm has a better performance characteristic compared to other nozzles.

Losses for nozzle having exit diameter of 64 mm were found to be minimum.

7.2 SUGGESTIONS FOR FUTURE WORK:

The design put forward in this thesis is, of late, a very new concept. It is recommended to fabricate and test the ROV designed, from a hydrodynamic point of view to exploit its commercial worthiness. Also, the control systems aspects of the ROV should be looked into as regards to programming, the proper directional control of the ROV.

Hence to conclude, jet propulsion for ROV's is feasible in view of better maneuverability and control of the vehicle.

BIBLIOGRAPHY AND LIST OF REFERENCES

(1) Arcand L. and Comolli C.R.," Waterjet Propulsion for High-speed Ships ", AIAA/SNAME Advance Marine Vehicles Meeting, May 1967.

(2) Barr R.A. and Etter R.J.," Selection of Propulsion System for High Speed Advance Marine Vehicles ", Marine Technology, Vol.12, no 1, pp 33, Jan 1975.

(3) Brandaux J.H.," Aspects of Performance Evaluation of Waterjet Propulsion Systems and a Critical Review of the State-of-Art ", AIAA/SNAME Advance Marine Vehicles Meeting, May 1967.

(4) Bruce Fugitt R.," Design and Operation of Two Remotely Manned Undersea Vehicles ", IEEE Oceans 75.

(5) Chrisholm M.A, Kentis D.H., and Reichert G.," Analysis Report of Waterjet Inlet Hydrodynamics ", Lockheed Missiles and Space Company Report LMSC/D313032, Dec 1974, FOUO.

(6) Contractor D.N.," Design Study of Waterjet Propulsion Systems for Shallow Draft Boats ", Hydronautics, Incorporated Technical Report 516-1, April 1965.

(7) Contractor D.N.," Experimental Investigation of a Waterjet Propulsion System for Shallow Draft Boats ", Hydronautics, Incorporated Technical Report 516-2, May 1966.

(8) Contractor D.N.," Waterjet Propulsion ", Hydronautics, Incorporated Technical Report, July 1966.

(9) Delao M.M.," Practical Considerations of Waterjet Propulsion ", SAE paper 650630, August 1965.

(10) Eilers R.E., and Shrout L.S.," Waterjet Propulsion Thrust Measurement Using a Reaction Elbow ", Boeing Marine Systems, May 1977.

(11) Gasiunas A., and Lewis W.P.," Hydraulic Jet Propulsion: A Theoretical and Experimental Investigation into the Propulsion of Sea Craft by Waterjets ", Proceedings of the Institution of Engineers, 1963-64.

(12) Hankley D.W.," Full Scale Propulsion Characteristics of Two Marine Waterjets Rated at 500 hp and 1050 hp ", NAVSEC NORDIV Report no 6660-6, Jan 1971.

(13) Johnson H.A.," Design Features and Test Results of an Unmanned Free Swimming Submersible ", Naval Research laboratory, Washington D.C., 1980.

(14) Jim MacFarlane," Remote Controlled Vehicle Development in Canada ", Technical paper of " International Submarine Engineering ",Vancouver, 1982.

(15) Jim R. MacFarlane and D. Petters, " Submersibles in Underwater Mining ", Engineering Digest, February 1986.

(16) Johnson V.E., Jr. et al., " Design and Performance of Diffusers, Fixed-Area Inlets and Variable-Area Inlets in Integrated Inlet-Diffuser Subsystems ", Hydronautics, Incorporated Technical Report 7152-1, August 1972, FOUO.

(17) Martin Delao," Some Experimental Results of a Low Speed Waterjet Propulsion System ", AIAA/USN 2nd. Marine Systems and ASW Conference, August 1966.

(18) McBeth J.B.," Reliability and Safety considerations in the Design of the Submersible Leo I ", IEEE Oceans 76.

(19) Miller H.A., Newman J.P., and Nunn G.," Recon II - An Unmanned Remote Operated Work Vehicle ", IEEE Oceans 76.

(20) Miller E.R.," Waterjet Propulsion System Performance Analysis ", Hydronautics, Incorporated Technical Report, 1976.

(21) Mutsuo Hattori," A Micro-Computer Controlled Tethered Vehicle, JTV-1 ", Japan Marine Science and Technology Center, IEEE 1981.

(22) Poquette G.M., and Etter R.J.," Waterjet Inlet/Duct Development Phase II, XR-1B Correlation Tests ", Hydronautics, Incorporated Technical Report 7244-2, March 1973, FOUO.

(23) Sherman P.M., and Lincoln F.W.," Ram Inlet Systems for Waterjet Propulsors ", AIAA 2nd. Advance Marine Vehicles and Propulsion Meeting, May 1967.

(24) Theobald C.," The Effect of Nozzle Design on the Stability and Performance of Turbulent Waterjets ", Fire Safety Journal, vol 4, pp 1-13, 1981.

(25) Torda T.P., and Kos D.W.," Analysis of Jet Propulsion for Deep Submergence Vessels: Ideal Fluid Analysis and Boundary Layer Control ", SNAME, spring meeting, May 1971.

(26) Traksel J. and Beck," Waterjet Propulsion For Marine Vehicles ", AIAA paper no. 62-245, March 1965.

(27) Vennard J.K., and Street R.L., " Elementary Fluid Mechanics ", 6th. edition, John Wiley and Sons, 1982.

(28) Wernli R.L.," Experience with an Unmanned Vehicle-Based Recovery System ", Marine Technology, vol 20, no 1, pp 71-77, Jan 1983.

(29) Wislicknus G.," Hydrodynamic Design Principles of Pumps and Ducting for Waterjet Propulsion ", NSRDC report 3990, June 1973.

(30) HYDROPRODUCTS, A Tetra Tech Company, Box 2528, San Diego, California.

APPENDIX A

COMPUTER PROGRAMS

PROGRAM 1:

```
C*****************************************************************
C       THIS PROGRAM COMPUTES THE ENERGY LOSS IN THE NOZZLE.
C       THE FRICTION FACTOR TAKEN IS COMPUTED AS PER THE
C       EQUATION IN THE PROGRAM.
C*****************************************************************

        REAL A(200)
        OPEN (UNIT=27,FILE='FLOWO.DAT',TYPE='OLD')
        OPEN (UNIT=28,FILE='LOSS.DAT',TYPE='NEW')
        READ (27,*)M,(A(J),J=1,M)
        R=80.0
        N=1000
        PI=3.141592
        Y1=26.416
        DO 50 J=1,M
        X=0.0
        HF1=0.0
        DO 10 I=1,N
        X=X+R/N
        IF((X.GE.0).AND.(X.LE.75)) GO TO 20
        IF((X.GT.75).AND.(X.LE.80)) GO TO 30
        IF(X.GT.80)GO TO 60
20      Y=-0.2455466*X+26.416
        GO TO 40
30      Y=8.0
40      D=(Y1+Y)*1.0E-3
        RE=4.0*A(J)*1000.0/(PI*D*1.139E-3)
C       PRINT*,'A(',J,')=',A(J)
C       PRINT *,'RE=',RE
        F=0.02803163-0.1464504E-6*RE+0.6957930E-12*RE**2
     *  -0.1108229E-17*RE**3
C       PRINT *,'F=',F
        HF=(F*(R/N)*1.0E-3*16.0*(A(J)**2))/(2.0*9.81*(PI**2)*(D**5))
C       PRINT *,'HF=',HF
        Y1=Y
        H=HF+HF1
        HF1=H
10      CONTINUE
60      PRINT *,H
        WRITE (28,*)H
50      CONTINUE
        STOP
        END
```

PROGRAM 2:

```
C*****************************************************************
C       THIS PROGRAM CALCULATES THE K VALUES FROM THE
C       THEORETICAL LOSS
C*****************************************************************
        REAL A(100),B(100)
        OPEN (UNIT=32,FILE='LOSS1.DAT',TYPE='OLD')
        OPEN (UNIT=33,FILE='FLOWO.DAT',TYPE='OLD')
        OPEN (UNIT=34,FILE='L.DAT',TYPE='NEW')
        A=44.0E-03
        G=9.81
        READ (32,*)N,(A(I),I=1,N)
        READ (33,*)N,(B(I),I=1,N)
        DO 10 I=1,N
        V=B(I)/A
        Y=V**2/(2.0*G)
        Z=A(I)/Y
        PRINT *,A(I),Z
        WRITE (34,*)Z
10      CONTINUE
        STOP
        END
```

PROGRAM 3:

```
C*****************************************************************
C       THIS PROGRAM CALCULATES THE EFFICIENCY
C*****************************************************************

        REAL X(200),Y(200),Z(200),W(200),U(200)
        OPEN (UNIT=21,FILE='THRUST.DAT',TYPE='OLD')
        OPEN (UNIT=22,FILE='THEAD.DAT',TYPE='OLD')
        OPEN (UNIT=23,FILE='VO.DAT',TYPE='OLD')
        OPEN (UNIT=24,FILE='OVER.DAT',TYPE='NEW')
        PI = 3.141592
        READ (21,*)N
        READ (22,*)N
        READ (23,*)M
        DO 10 I=1,M
        READ (23,*)X(I)
10      CONTINUE
        DO 20 J=1,N
        READ (21,*) A,B,C,D,E
        Y(J)=A
        Z(J)=B
        U(J)=D
20      CONTINUE
        DO 30 K=1,N
        READ (22,*) W(K)
30      CONTINUE
        DO 40 I=1,M/N
        DO 50 J=1,N
        IF (X((I-1)*N+J).EQ.0) GO TO 60
        V=2.0*PI*0.7/X((I-1)*N+J)
        P=Z(J)-V
        Q=V/Z(J)
        RN2=100.0*U(J)*V/(9.81*1000*Y(J)*W(J))
        PRINT *,Y(J),V,Z(J),Q,U(J),RN2
        WRITE (24,90) Y(J),V,Z(J),Q,U(J),RN2
        GO TO 70
60      PRINT *,Y(J),VV,Z(J),Q,U(J)
        WRITE (24,90) Y(J),VV,Z(J),Q,U(J)
90      FORMAT (5F14.8)
70      CONTINUE
50      CONTINUE
40      CONTINUE
        STOP
        END
```

PROGRAM 4:

```
C*****************************************************************
C       THIS PROGRAM CALCULATES THE TOTAL PRESSURE FROM THE
C       PRESSURE TRANSDUCER READINGS. THE DIFFERENCE OF TOTAL
C       HEAD AT INLET AND EXIT GIVES THE LOSS EXPERIMENTALLY
C*****************************************************************

      REAL X(200),Y(200),Z(200),U(200),V(200),W(200),D(200)
     1  ,E(200),F(200),G(200),H(200),O(200)
      OPEN (UNIT=21,FILE='MPRI.DAT',TYPE='OLD')
      OPEN (UNIT=25,FILE='MPRE.DAT',TYPE='OLD')
      OPEN (UNIT=22,FILE='VHEADI.DAT',TYPE='OLD')
      OPEN (UNIT=26,FILE='VHEADE.DAT',TYPE='OLD')
      OPEN (UNIT=23,FILE='EXLOSS.DAT',TYPE='NEW')
      READ (21,*)N
      READ (25,*)N
      READ (22,*)N
      DO 10 I=1,N
      READ (21,*)A,B,C
      X(I)=A
      Y(I)=B
      Z(I)=C
10    CONTINUE
      DO 60 I=1,N
      READ (25,*)P,Q,R
      D(I)=P
      E(I)=Q
      F(I)=R
60    CONTINUE
C     READ (29,*)N,(A(I),I=1,N)
      DO 20 J=1,N
      READ (22,*)D,E,F,G
      U(J)=D
      V(J)=F
      W(J)=G
20    CONTINUE
      DO 70 I=1,N
      READ (26,*)S,T,U,V
      G(I)=S
      H(I)=U
      O(I)=V
70    CONTINUE
      DO 30 K=1,N
      P2OI=(X(K)+0.016)/0.049
      P1OI=(Y(K)+0.028)/0.098
      P5I=(Z(K)+0.041)/0.192
      PTPI=(P2O+P1O+P5)/3.0
      PTMI=PTP*10.33/14.72
      P2OE=(D(K)+0.016)/0.049
      P1OE=(E(K)+0.028)/0.098
      P5E=(F(K)+0.041)/0.192
      PTPE=(P2O+P1O+P5)/3.0
      PTME=PTP*10.33/14.72
      ALOSS=PTMI-PTME
      AK=ALOSS/O(K)
      PRINT*,ALOSS,AK
```

```
      WRITE (23,40)ALOSS,AK
40    FORMAT (2F14.8)
30    CONTINUE
      STOP
      END
```

PROGRAM 5:

```
C*****************************************************************
C     THIS PROGRAM COMPUTES THE THEORETICAL THRUST AND THE
C     MEASURED THRUST AND GIVES THE PERCENTAGE ERROR.
C     TT = THEORETICAL THRUST
C     OT = MEASURED THRUST
C     PE = PERCENTAGE ERROR
C*****************************************************************
      REAL A(40),B(40)
      OPEN (UNIT=21, FILE ='FLOWO.DAT',TYPE ='OLD')
      OPEN (UNIT=22, FILE ='STRAIN.DAT',TYPE ='OLD')
      OPEN (UNIT=25, FILE ='THRUST.DAT',TYPE ='NEW')
      RHO = 1000.0
      PI  = 3.141592
      D   = 16.000E-03
      READ (21,*) N,(A(I),I=1,N)
      READ (22,*) N,(B(I),I=1,N)
      WRITE (25,*)N
      DO 10 I=1,N
      VJ=4.0*A(I)/(PI*D**2)
      TT = 4.0*RHO*(A(I)**2)/(PI*D**2)
      IF (A(I)-0.00294073)80,80,90
80    OT = (1.086*B(I)-25.983)*9.81/1000.0
      GO TO 100
90    OT = (4.659*B(I)-238.0)*9.81/1000.0
100   PE = ((TT-OT)*100.0)/TT
      PRINT *,A(I),VJ,TT,OT,PE
      WRITE (25,*)A(I),VJ,TT,OT,PE
70    FORMAT (5F14.8)
10    CONTINUE
      STOP
      END
```

APPENDIX B

SPECIFICATIONS AND CALIBRATIONS

SPECIFICATIONS:

(i) STRAIN GAGES:

Material	Constantan alloy in self-temperature compensated form with tough flexible polymide film backing
Temperature range	-100 ° to +350 ° F
Resistance	120.0 ± 0.3%
Gage factor at 75 ° F	2.04±0.5%
Fatigue life	10^8 cycles at ±1200$\mu\epsilon$ 10^6cycles at ±1500$\mu\epsilon$
Strain limits (for 1.5 mm gage length)	3 %
Transverse sensitivity factor	+1.0%

(ii) PRESSURE TRANSDUCERS:

Kistler Model 606A/606L Quartz Pressure Transducer

Range full scale	3000 psi (21 MPa)
Resolution	0.005 psi (0.03 KPa)
Maximum pressure	5000 psi (34 MPa)
Sensitivity (nominal)	5.5 pcb/psi (0.8 pcb/KPa)
Resonant frequency (nominal)	130 KHz
Rise time	3.0 microseconds
Linearity (zero based best straight line)	±1%
Capacitance (nominal)	50 picofarads
Insulation resistance	10^{13} ohms
Acceleration sensitivity	<0.005 psi/g (0.03 KPa/g)
Temperature effect on sensitivity	<0.03% per ° F
Temperature range	-350 ° to +450 ° F
Shock, 1 ms pulse width	1000 g
Case material	SS
Weight	0.5 oz (14 gm)

CALIBRATION:

The following devices were calibrated before being used:

(i) the rotameter, to ensure the percentage of flow in terms of cubic metres —per second. A parallel system of rotameters were calibrated by noting the time taken for pumping out a definite volume of water.

(ii) the strain gages on the thrust plate, so that the thrust produced is directly related to the voltage. Strain gages were calibrated by applying a known load and noting the strain produced by a strain indicator.

(iii) the pressure transducer, to read the pressure developed directly in terms of the voltage. Pressure transducers were calibrated using a piston activated oil pressure chamber.

In all the cases, good care was taken and repeatibility observed.

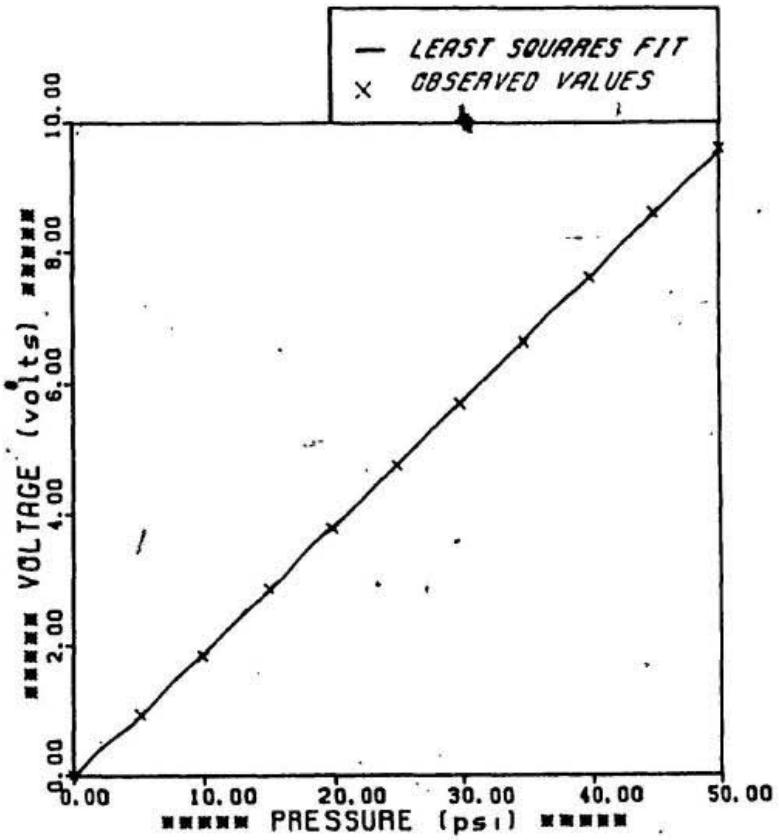

Calibration of Pressure Transducer [5020/5.17 : Range=5]

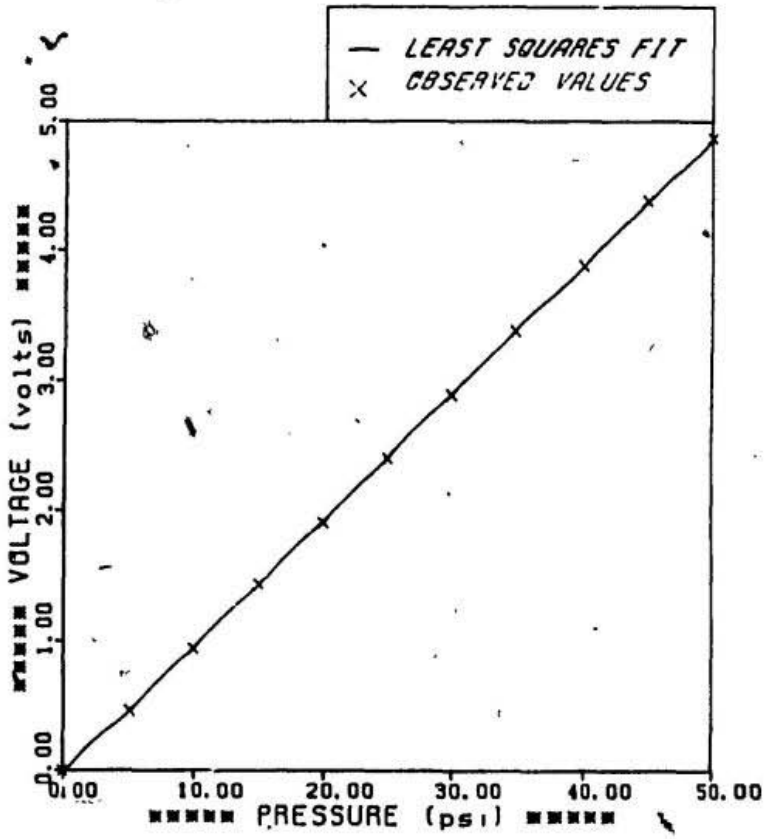

Calibration of Pressure Transducer [5020/5.17 : Range=10]

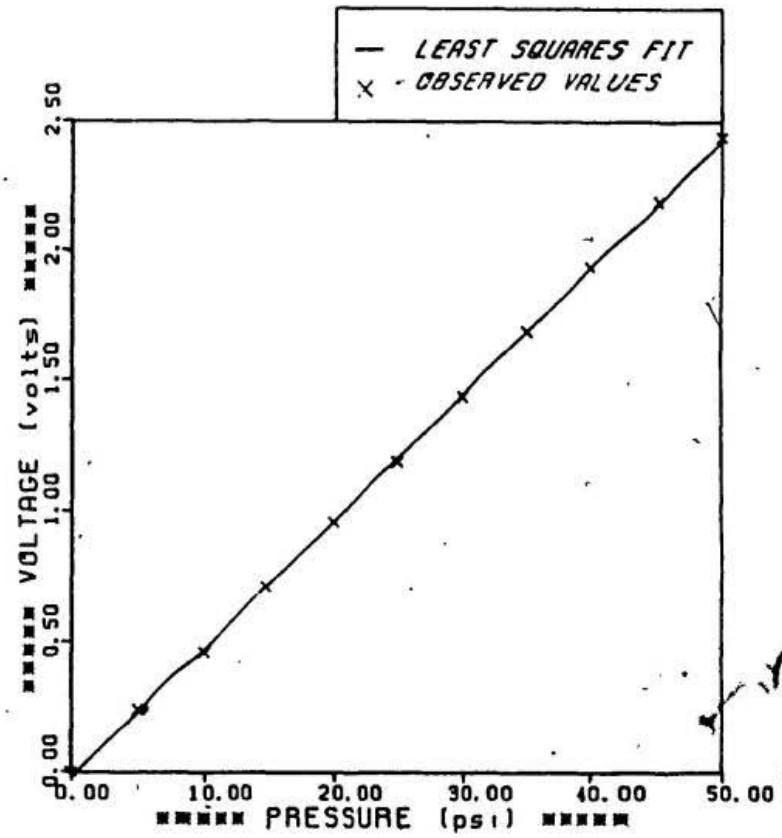

Calibration of Pressure Transducer [5020/5.17 : Range=20]

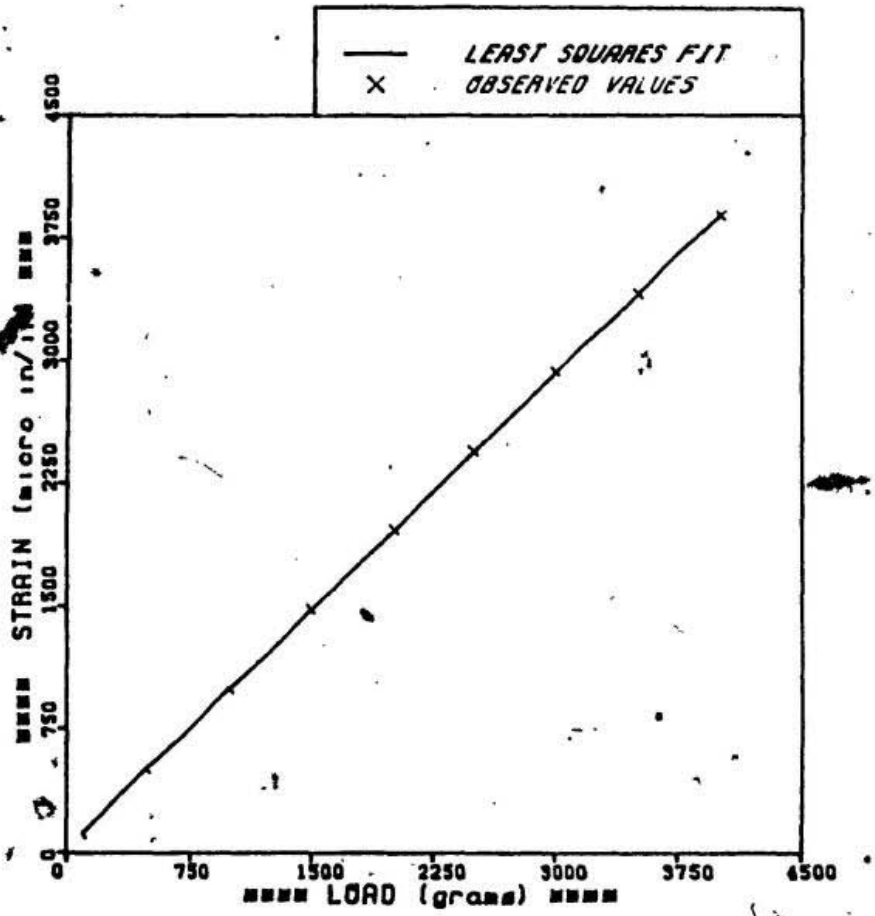

Calibration of Thrust Plate [Thin Plate]

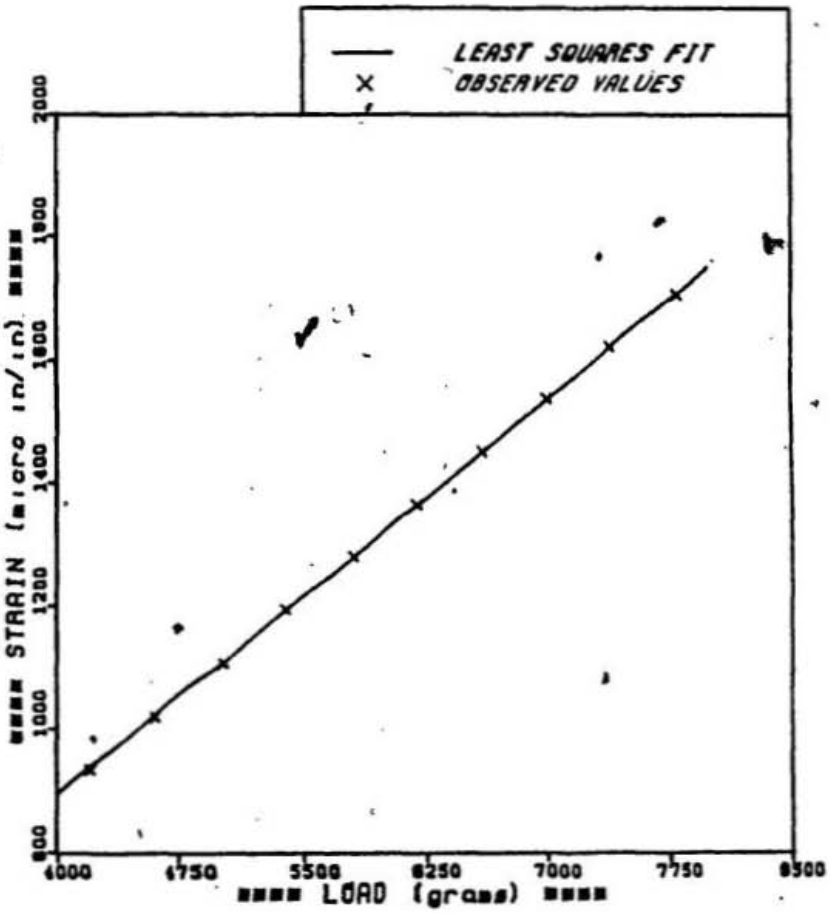

Calibration of Thrust Plate [Thick Plate]

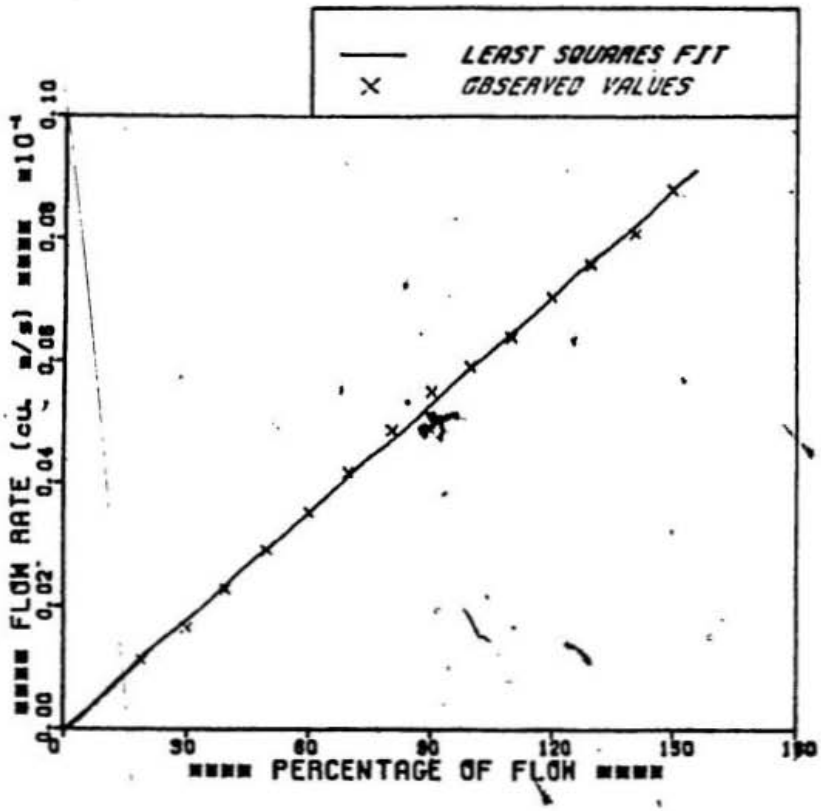

Calibration of Rotameter

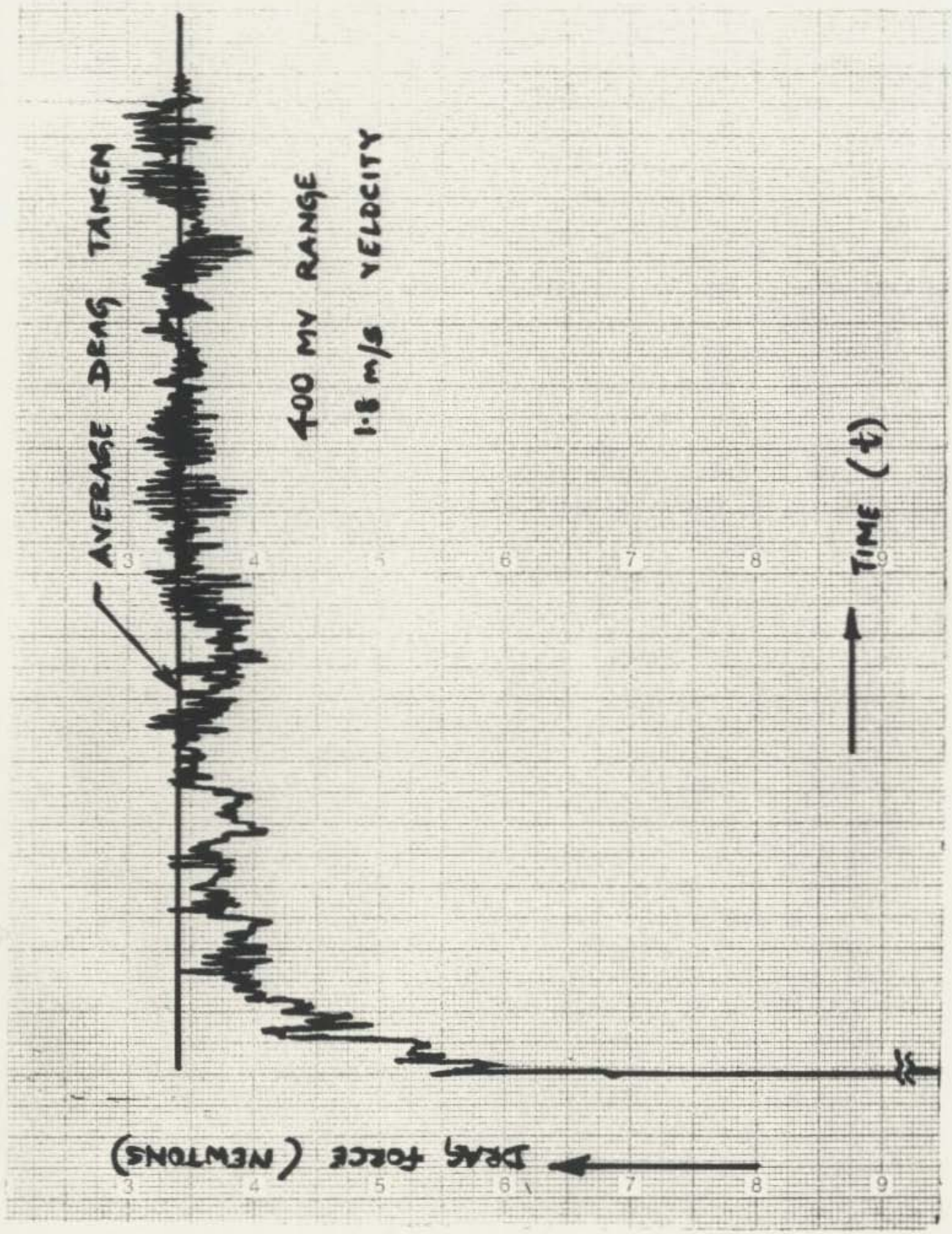

An example of the plotter output